

CHEMOSTRATIGRAPHY AND PALEOENVIRONMENT OF
THE SMITHWICK FORMATION, FORT WORTH
BASIN, SAN SABA COUNTY,
TEXAS

by

ELISHA NICHOLE HUGHES

Presented to the Faculty of the Graduate School of
The University of Texas at Arlington in Partial Fulfillment
of the Requirements
for the Degree of

MASTER OF SCIENCE IN GEOLOGY

THE UNIVERSITY OF TEXAS AT ARLINGTON

May 2011

Copyright © by Elisha Nichole Hughes 2011

All Rights Reserved

ACKNOWLEDGEMENTS

I would like to thank my loving and sympathetic family, including Della Dean Totty, Karen Hughes, Ed Hughes, and Kim Hughes. I would also like to thank Jason Berry for his support, the use of his desk, his excellent taste in music, and for putting up with retarded cat. Much thanks also to Summer Harrison for her support and superior editing skills.

Many thanks to my professors at the University of Texas during my undergraduate and graduate work: Dr. Gary Lowell, Dr. John Holbrook, Dr. John Wickham, Dr. Merlynd Nestell, Dr. Galina Nestell, Dr. Christopher Scotese, Dr. Larry Standlee, and Dr. Harold Rowe. I would like to thank Dr. Andrew Hunt for his time and help on the SEM. Much thanks to Dr. Galina Nestell and Dr. Merlynd Nestell for their help with the petrographic microscope and in trying to extract microfossils. I would like to thank Dr. Christopher Scotese for his paleogeographic insights and maps, as well as for briefly employing me. Many thanks also to my friends and colleagues who have assisted and entertained me: Pukar Mainali, James Hoelke, Jak Kearns, Ashley Wright, Krystin McAfee, Rolando Castilleja, Robert Nikirk, and Milton Cortez.

I would also like to thank everyone with the Bureau of Economic Geology, and the Mudrock System Research Laboratory (MSRL). This includes the BEG scientists Dr. Stephen Ruppel and Dr. Scott Hamlin. Thank you both for granting me access to core, working with me on sampling and thin sections, and discussing findings. Many thanks also to the hard-working core repository team: James Donnelly, Nathan Ivicic, and Kenneth Edwards.

I would like to sincerely thank the Geological Society of America Research Grants (Alexander & Geraldine Wanek Fund), the American Association of Petroleum Geology Grants-In-Aid Program (R. Dana Russell Memorial Grant), and the Gulf Coast Association of Geological Societies Student Research Grants for the financial support that has made this project possible. I would also like to thank the National Science Foundation and grant EAR-0841739 to HDR,

which funded the UIC, Inc. coulometer, permitting the in-house analysis of total inorganic carbon.

Lastly, much appreciation to my committee members: Dr. Harold Rowe, Dr. John Wickham, and Dr. Stephen Ruppel. To my committee chair, Dr. Rowe, thank you for guidance not only on my project, but also for encouraging me to take advantage of the various opportunities that led to my employment.

March 7, 2011

ABSTRACT

CHEMOSTRATIGRAPHY AND PALEOENVIRONMENT OF
THE SMITHWICK FORMATION, FORT WORTH
BASIN, SAN SABA COUNTY,
TEXAS

Elisha Nichole Hughes, M.S. Geology

The University of Texas at Arlington, 2011

Supervising Professor: Harold Rowe

The Early Pennsylvanian-Age Smithwick Formation was deposited in the tectonically active Fort Worth Basin in North Central Texas during a time of well-documented global climatic instability during the Late Paleozoic ice age. Geochemical and stable isotopic results from two cores recovered from the southwestern portion of the FWB provide paleoenvironmental insight into the conditions under which the Smithwick was deposited. Specifically, major element geochemistry and mineralogical results suggest a depositional setting grading from a carbonate-rich facies (Marble Falls and Big Saline) into a transgressive siliciclastic-dominated mudrock (Smithwick) that coarsens upward into a progradational mudrock and silt/sand sequence (Atoka and Strawn). While robust geochronological constraints are lacking for Middle Carboniferous strata, subtle oscillations in the detrital geochemical proxies (Si/Al, Ti/Al) may provide a temporal framework assuming they are a result of orbital forcing. Furthermore, thin siderite-rich intervals may indicate discrete periods of amplified eolian deposition due to the aridification associated with glaciation on Gondwana. Alternatively, the siderites may reflect a

more localized signature of changes in a tropical paleoclimate. Integration of trace metal, Fe-S-TOC relationships, and the overall lack of preserved fauna suggest largely suboxic bottom water conditions in the basin. Average TOC for the Smithwick is 1.5%, and the organic matter is dominantly marine algal based on C/N molar ratios of 6.6 to 17.5 and $\delta^{13}\text{C}$ values of -23.1 to -25.7 ‰. Integration and interpretation of the results suggest that the Smithwick represents a marginally productive environment that existed during the early stages of subsidence of the Fort Worth Basin.

TABLE OF CONTENTS

ACKNOWLEDGEMENTS	iii
ABSTRACT	v
LIST OF ILLUSTRATIONS.....	x
LIST OF TABLES	xii
Chapter	Page
1. INTRODUCTION.....	1
1.1 Project Outline and Study Area.....	1
1.2 Regional Geology.....	2
1.3 Tectonics and Paleogeography.....	4
1.4 Carboniferous Fort Worth Basin Stratigraphy	6
1.5 North American Carboniferous Glacioeustasy.....	8
1.6 Study Objective	10
2. METHODS	12
2.1 Drill Core Information	12
2.2 Energy-Dispersive X-Ray Fluorescence (ED-XRF)	12
2.2.1 ED-XRF Mudrock Calibration.....	15
2.2.2 ED-XRF Siderite Calibration	16
2.3 LECO-S, TIC, TOC, TN, $\delta^{13}\text{C}$, and $\delta^{15}\text{N}$ Analyses	16
2.4 Mineralogic and Petrographic Analyses.....	18
2.4.1 X-Ray Diffraction (XRD).....	18
2.4.2 Scanning Electron Microscopy (SEM)	20
2.4.3 Thin Section Preparation and Imaging.....	21
3. RESULTS.....	22

3.1 X-Ray Diffraction (XRD) Results	22
3.2 Core Chemostratigraphy and Inter-elemental Relationships	23
3.2.1 Geochemical Characterization of and Correlation between Cores	23
3.2.2 Fe and Carbonate Phases	29
3.2.3 Detrital Fraction	36
3.2.4 Trace Metals	44
3.2.5 Organic Carbon and Nitrogen	49
3.3 Petrographic Observations.....	51
3.4 Scanning Electron Microprobe (SEM) Images.....	60
4. DISCUSSION	64
4.1 Depositional Environment	64
4.1.1 Paleodepositional Setting.....	64
4.1.2 Productivity and Organic Matter.....	66
4.1.1 Paleoredox Conditions	68
4.2 Potential Linkages to Regional Tectonics	72
4.3 Potential Linkages to Regional and Global Paleoclimate	74
4.3.1 Potential Orbital Forcing and Glacioeustatic Changes	75
5. CONCLUSIONS	81
5.1 Summary of the Smithwick.....	81
5.2 Future Work.....	83
REFERENCES	86
BIOGRAPHICAL INFORMATION	93

LIST OF ILLUSTRATIONS

Figure	Page
1.1 Paleogeographic Maps of 320 Ma, Global View & FWB Location.....	3
1.2 Texas Map with Geologic Structures Surrounding the FWB.....	4
1.3 Generalized Stratigraphic Column for the Southwestern FWB.....	7
1.4 Sea-Level Curves and Glacial Records during the Carboniferous	9
1.5 Smithwick Study Area and Core Locations.....	11
2.1 ED-XRF Instrumentation Overview (a) sample setup, (b) instrument platform and vacuum pump, (c) filter, (d) beam area, (e) SiPIN detector.....	14
3.1 Al-Si-Ca Chemostratigraphy (Walker D-1-1).....	25
3.2 Al-Si-Ca Ternary Plot (Walker D-1-1).....	26
3.3 Al-Si-Ca Chemostratigraphy (Potter C-9-1)	27
3.4 Al-Si-Ca Ternary Plot (Potter C-9-1)	29
3.5 Correlation of the Walker D-1-1 and Potter C-9-1.....	31
3.6 Fe, Mn, Ca, and Mg Chemostratigraphy and Siderite Locations (Walker D-1-1)	33
3.7 Fe, Mn, Ca, and Mg Chemostratigraphy and Siderite Locations (Potter C-9-1)	34
3.8 Crossplots of Mn, Fe, Ca, and Mg and TIC (Walker D-1-1).....	35
3.9 Sulfur Crossplots (Walker D-1-1) (a) S/Fe, (b) S/TOC.....	37
3.10 Fe-S-TOC Ternary (Walker D-1-1).....	38
3.11 Crossplots of Detrital Associated Elements with Al (Walker D-1-1).....	39
3.12 Crossplots of Detrital Associated Elements with Al (Potter C-9-1)	40
3.13 Chemostratigraphy of Al, Si/Al, Ti/Al, Zr/Al, and Zr/Ti with highlighted Smithwick quasi-cycles (Walker D-1-1).....	42

3.14 Chemostratigraphy of Al, Si/Al, Ti/Al, Zr/Al, and Zr/Ti with highlighted Smithwick quasi-cycles (Potter C-9-1)	43
3.15 Chemostratigraphy of Enrichment Factors (V, Cr, Co, Ni, Cu, Zn, Mo, U) (Walker D-1-1)	45
3.16 Chemostratigraphy of Enrichment Factors (V, Cr, Co, Ni, Cu, Zn, Mo, U) (Potter C-9-1)	46
3.17 Crossplots of Trace Metals (V, Ni, Zn, U) with TOC and Al (Walker D-1-1)	48
3.18 Chemostratigraphy of TOC, N, C/N, $\delta^{15}\text{N}$, and $\delta^{13}\text{C}$ (Walker D-1-1)	50
3.19 SEM Images of pyrite (Walker D-1-1)	61
3.20 SEM Elemental Map of Zoned Pyrite (Walker D-1-1)	61
3.21 SEM Elemental Map of Zoned Siderite Grains (Walker D-1-1)	62
3.22 SEM Elemental Map of Siderite-Rich Sample (Walker D-1-1)	63
4.1 Crossplot of C/N and $\delta^{13}\text{C}$ for Organic Matter Typing (Walker D-1-1)	67
4.2 Fe-S-TOC Ternary Comparison of Pierre Shale and Equivalents with the Walker D-1-1 Core	70
4.3 Zonation of Bacterial Respiration and Trace Element Stabilities	72
4.4 Paleogeographic Map of 320 Ma with Climate Zones	74
4.5 Illustration of Depositional Duration Preserved in Drill Core	77
4.6 Paleogeographic Map of 300 Ma with FWB, Arrow Canyon, and Maritimes Basin Locations	78
4.7 Carboniferous Climatic Signatures for Arrow Canyon and Maritimes Basin	79

LIST OF TABLES

Table	Page
2.1 Drill Cores in Study.....	13
2.2 LDM by Element.....	17
2.3 XRD, Thin Section, and SEM Samples.....	19
3.1 Semi-Quantitative XRD Results from Walker D-1-1 Core.....	23
3.2 XRF-Generated Concentrations for Major (Al, Si, Ca), Carbonate (Ca, Mg, Mn, Fe), and Detrital (Ti,Zr) Elements	30
3.3 Quantified Enrichment Factors for Trace Metals	47
3.4 Quantified %TOC, %N, C/N, $\delta^{15}\text{N}$, and $\delta^{13}\text{C}$ for the Walker D-1-1 Core	51
3.5 Petrographic Observations and Images for the Walker D-1-1 Core	52
4.1 Average TOC Percentages for North American Hydrocarbon-Bearing Mudrocks	68

CHAPTER 1

INTRODUCTION

1.1 Project Outline and Study Area

It has been estimated that mudrocks constitute two thirds of the sedimentary record (Schieber and Zimmerle, 1998). As a consequence, they preserve significantly large intervals of Earth history, including the evolution of the ocean basins and continental margins. Organic-rich mudrocks are of academic interest because they possess unique sedimentological, geochemical, and paleontological archives that enhance the understanding of ancient water mass evolution, global carbon cycle, and the diverse paleoceanographic conditions leading to the oceanic response to, and control of, changes in the carbon cycle (Vine and Tourtellot, 1970; Dean and Arthur, 1989; Arthur and Sageman, 1994). In addition, organic-rich mudrocks are investigated by the energy industry for their potential to yield hydrocarbons.

Despite their often nondescript and/or spatially homogeneous, fine-grained appearance, mudrocks are deposited under a wide variety of conditions, making it important to define the subtle differences between various organic-rich mudrocks and shales for enhancing our ability to distinguish the sub-environments of deposition. Chemostratigraphy is an essential tool for distinguishing differences between, and controls upon, mudrock deposition. For instance, benthic redox and other hydrographic conditions can be inferred from analysis and interpretation of major and trace element geochemistry of mudrocks (e.g., Dean and Arthur, 1989; Piper, 1994; Algeo and Maynard, 2004; Piper and Perkins, 2004; Rimmer, 2004; Algeo and Maynard, 2008; Rowe et al, 2008). Integrated geochemical and sedimentological approaches have been used successfully to better define depositional conditions (e.g., Algeo and Heckel, 2008).

The investigation provides a stratigraphic evaluation of geochemical and stable isotopic changes of organic-rich mudrocks deposited in a foreland basin setting. Specifically, the project focuses on understanding the paleoenvironmental conditions responsible for organic-rich deposition of the early Pennsylvanian-age (Morrowan-Atokan; Bashkirian-Early Muscovian) Smithwick Formation in the Fort Worth Basin of equatorial Laurussia (**figure 1.1**), which is in present day North-Central Texas, USA. The Smithwick Formation is commonly referred to as a shale unit (McBride and Kimberly, 1963; Walper, 1982; Erlich and Coleman, 2005), but lacks fissility throughout and, therefore, fits into the overarching classification of mudrocks (Folk, 1980). A detailed investigation of these strata is important because the expanded section of mudrocks in the Walker D-1-1 core, potentially representing ~9.5-11.6 million years of deposition (based on Gradstein et al, 2004), may provide a highly-resolved record of Early Pennsylvanian eustatic and/or tectonic change from the paleoequatorial region, far away from the glacioeustatic controls of southern Gondwanan icecaps (Mii et al, 1999; Gradstein et al, 2004; Haq and Schutter, 2008; Heckel, 2008; Rygel et al, 2008; Bishop et al, 2010)

1.2 Regional Geology

The Smithwick Formation was deposited in the Fort Worth Basin (FWB) during Pennsylvanian time (Ng, 1979; Lovick et al, 1982; Walper, 1982; Grayson et al, 1990; Erlich and Coleman, 2005). Structural features formed during the collision of Gondwana and Laurussia bind the FWB. The Ouachita thrust belt borders it to the east; the northern edge of the basin is delimited by the Red River and Muenster Arches; the southern limit of the basin is the Precambrian- and Paleozoic-exposed Llano Uplift; and, the Bend Arch runs along the western boundary of the basin (**figure 1.2**) (Ng, 1979; Lovick et al, 1982; Thompson, 1982; Walper, 1983; Erlich and Coleman, 2005; Pollastro et al, 2007). The westward progression of the Ouachita thrust belt resulted in a foreland basin with a trough bordering the thrust belt, and shoaling out toward the Bend Arch and Concho platform (Walper, 1982; Grayson et al, 1990). The deepest part of the basin formed adjacent to the Muenster arch, with decreased subsidence toward the Llano uplift, to the south (Erlich and Coleman, 2005; Pollastro et al,

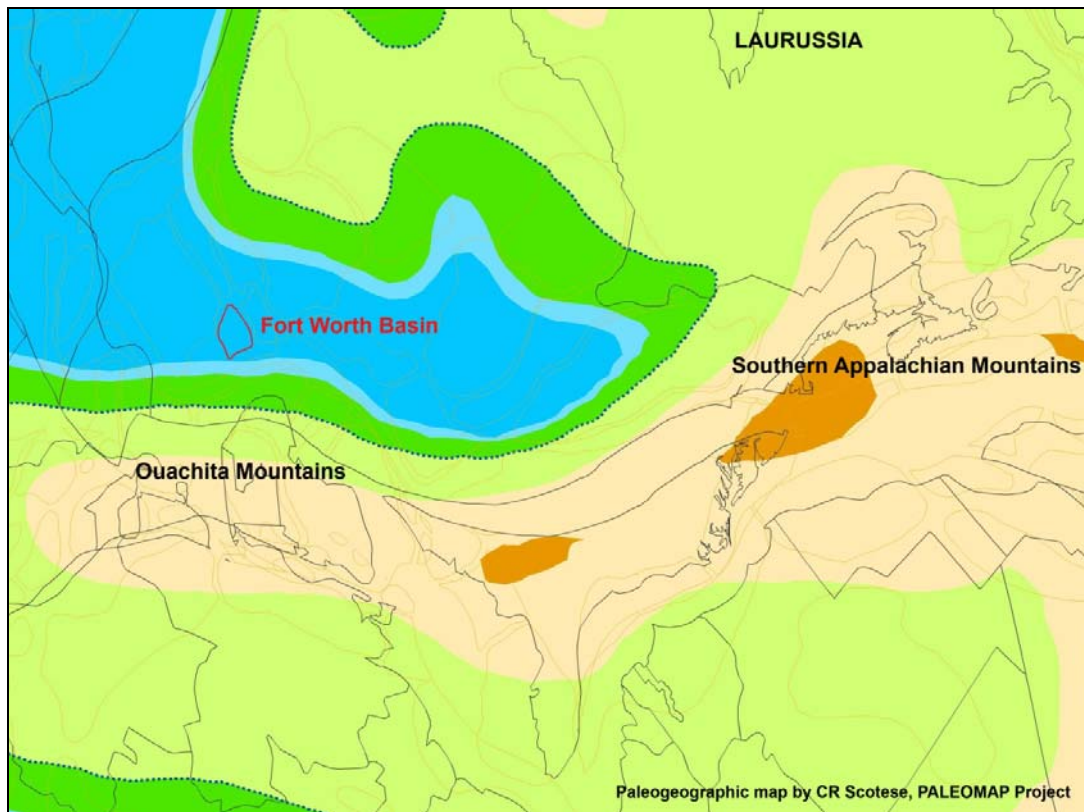
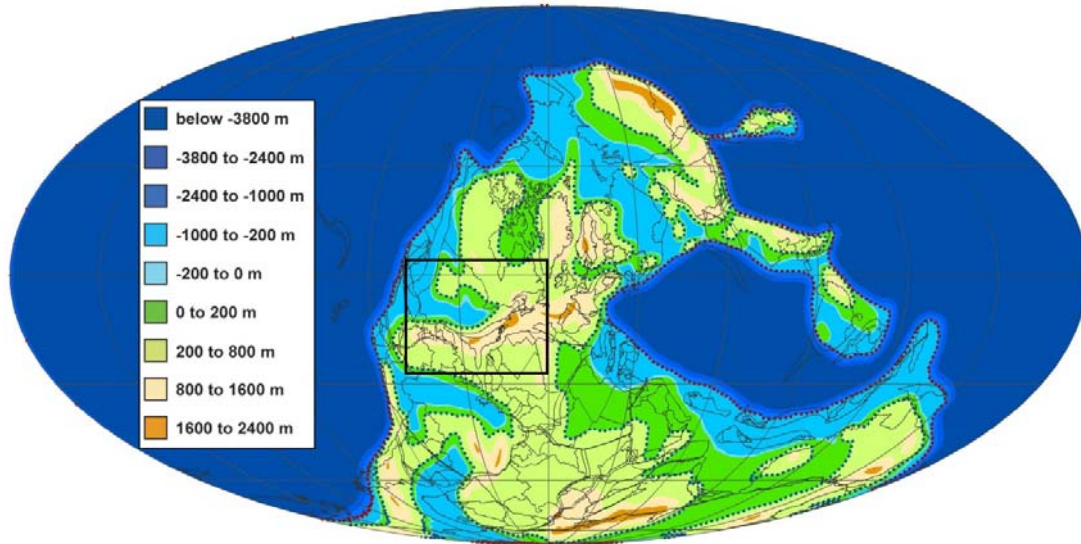


Figure 1.1 Paleogeographic maps of 320 Ma. (top) Global depiction illustrating the collision of Laurussia and Gondwana with the site of the developing Fort Worth Basin outlined. (bottom) Closer view of the Fort Worth Basin site showing the Fort Worth Basin in an emperic sea on the North American craton.

2007). The FWB is approximately 200 miles (322 km) in length along the presently buried Ouachita foldbelt, and its width ranges from more than 100 miles (161 km) in the north to less than 10 miles (16 km) in the south (Thompson, 1982; Walper, 1982).

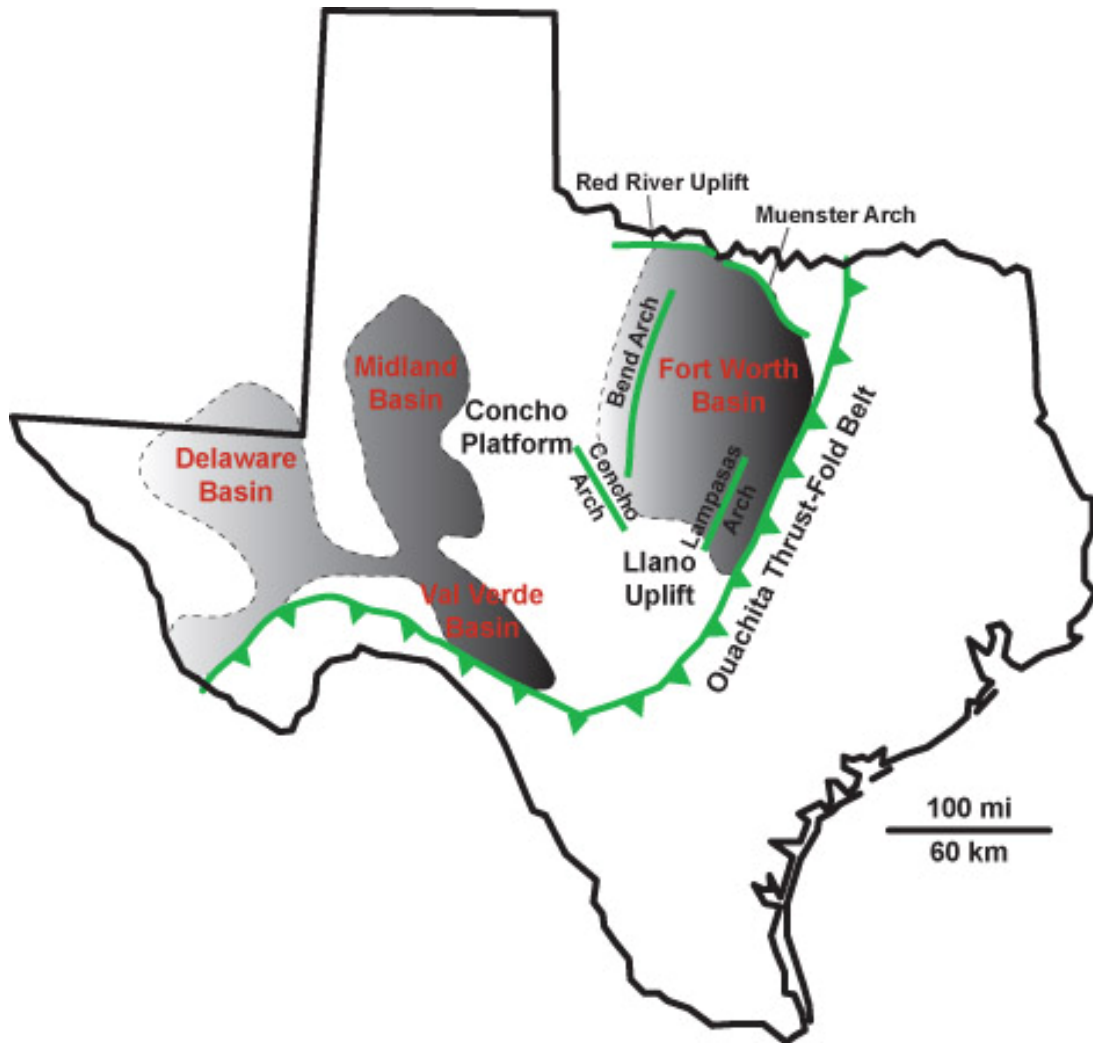


Figure 1.2 Map of Texas showing the generalized geologic structures including and surrounding the Fort Worth Basin. (Modified from Rowe et al, 2008).

1.3 Tectonics and Paleogeography

Continental rifting at the southern edge of the North American craton (Laurentia) formed the Iapetus Ocean in the Early Paleozoic (Blakey, 2008). The Taconic orogeny in Middle through Late Ordovician marked the final Iapetus subduction as Baltica and other

microcontinents collided with Laurentia, forming Laurussia (Murphy et al, 2010), and producing a cratonic disturbance that resulted in the uplift and formation of the Concho Platform that delimits the western margin of the Fort Worth Basin (Walper, 1982). Following the closure of the Iapetus, the Rheic Ocean expanded and subsequently occluded during the collisional events of Laurussia and Gondwana during the Devonian through the Early Carboniferous (Mississippian) (Walper, 1982; Viele and Thomas, 1989; Scotese, 2004; Blakey, 2008; Murphy et al, 2010). A subduction complex formed as the Rheic Ocean closed from strata that were scraped from the Laurussian oceanic lithosphere as it was subducted under a volcanic island arc that developed along the northern edge of Gondwana. Ultimately, the strata were thrust onto the North American craton during the Early Carboniferous (Early Mississippian) forming the Ouachita thrust belt (Lovick et al, 1982; Walper, 1982). Before the final collision of Laurussia and Gondwana, the FWB developed in the mid-Carboniferous between the Concho platform and the advancing Ouachita orogenic belt (Lovick et al, 1982; Grayson et al, 1990).

The Taconic orogeny in Middle Ordovician was synchronous with the closing of the Iapetus Ocean. The Alleghenian and Ouachita orogenies in the Carboniferous marked the closing of the Rheic Ocean and collision of the North American and South American plates (Blakey, 2008; Murphy et al, 2010). The combination of these paleogeographic reconstructions created continental-scale flexure of the southern and eastern Laurussian craton, resulting in the emergence of structural features that delimited the FWB (Walper, 1982; Murphy et al, 2010). The loading of the craton from the Ouachita complex resulted in subsidence proximal to the foldbelt (Lovick et al, 1982) and a northwestward-migrating upwarp of the craton, culminating in marine transgression and a shallow epicontinental sea (Adams, 1962; Ng, 1979; Walper, 1982). The Llano uplift obstructed the progression of the Ouachita fold-thrust belt, thereby limiting subsidence and dictating the geographic location of the Fort Worth Basin and other Late Paleozoic basins (Midland, Val Verde) (**figure 1.1**) (Lovick et al, 1982, Grayson et al, 1990). The present northern and northeastern boundaries of the Fort Worth basin, the Red River and Muenster arches, also developed during the cratonic bowing (Walper, 1982). As the cratonic

hinge line of the basin moved westward, contemporaneous transtensional faulting in the Early Pennsylvanian produced fault blocks that affected the lateral distribution of sediment (Kier, 1980; Grayson et al, 1990; Erlich and Coleman, 2005). The Bend Arch emerged as the final hinge line between the Fort Worth Basin and Concho platform, as Ouachita movement abated and the Midland basin subsided in the Permian. (Lovick et al, 1982; Thompson, 1982; Walper, 1982).

1.4 Carboniferous Fort Worth Basin Stratigraphy

The FWB developed alongside other foreland basins in southern and southwestern Laurussia, in front of the advancing Ouachita thrust belt. In the Late Mississippian (Serpukhovian), the North American plate was subducted beneath northern Gondwana, with Gondwana sufficiently proximal to provide sediment supply to the FWB (Wickham, 1976). The Barnett carbonate and shale and Comyn carbonate were deposited at this time (Walper, 1982). Beyond the carbonate shelf, eastward across the basin, marine muds graded into more coarse-grained siliciclastics adjacent to the Ouachita thrust belt (Walper, 1982). This trend continued in Early Pennsylvanian (Bashkirian) throughout the Morrowan and into the earliest Atokan, with the penecontemporaneous deposition of carbonate Marble Falls, Smithwick shale, and Atoka clastics (Lovick et al, 1982; Walper, 1982; Grayson et al, 1990; Erlich and Coleman, 2005). Faulting occurred in the FWB during the Early Pennsylvanian that led to the Smithwick being broken into fault blocks with thicker deposition in grabens (Grayson et al, 1990). The Smithwick formation is considered marine, based on the fauna preserved in the unit (Plummer, 1947; Grayson et al, 1990), and eventually grades into a prodeltaic environment, evidenced by the coarsening upward strata (McBride and Kimberly, 1963; Kier, 1980). The contact between the Smithwick and the underlying Marble Falls is conformable (Barnes, 1948; Kier, 1980). The Marble Falls hinge line gave way to the Big Saline hinge line further west during Atokan time and subsequently lead to the progradation of Smithwick over Marble Falls and Atokan over Smithwick (**figure 1.3**) (Kier, 1980; Walper, 1982). The continued westward shifting hinge line

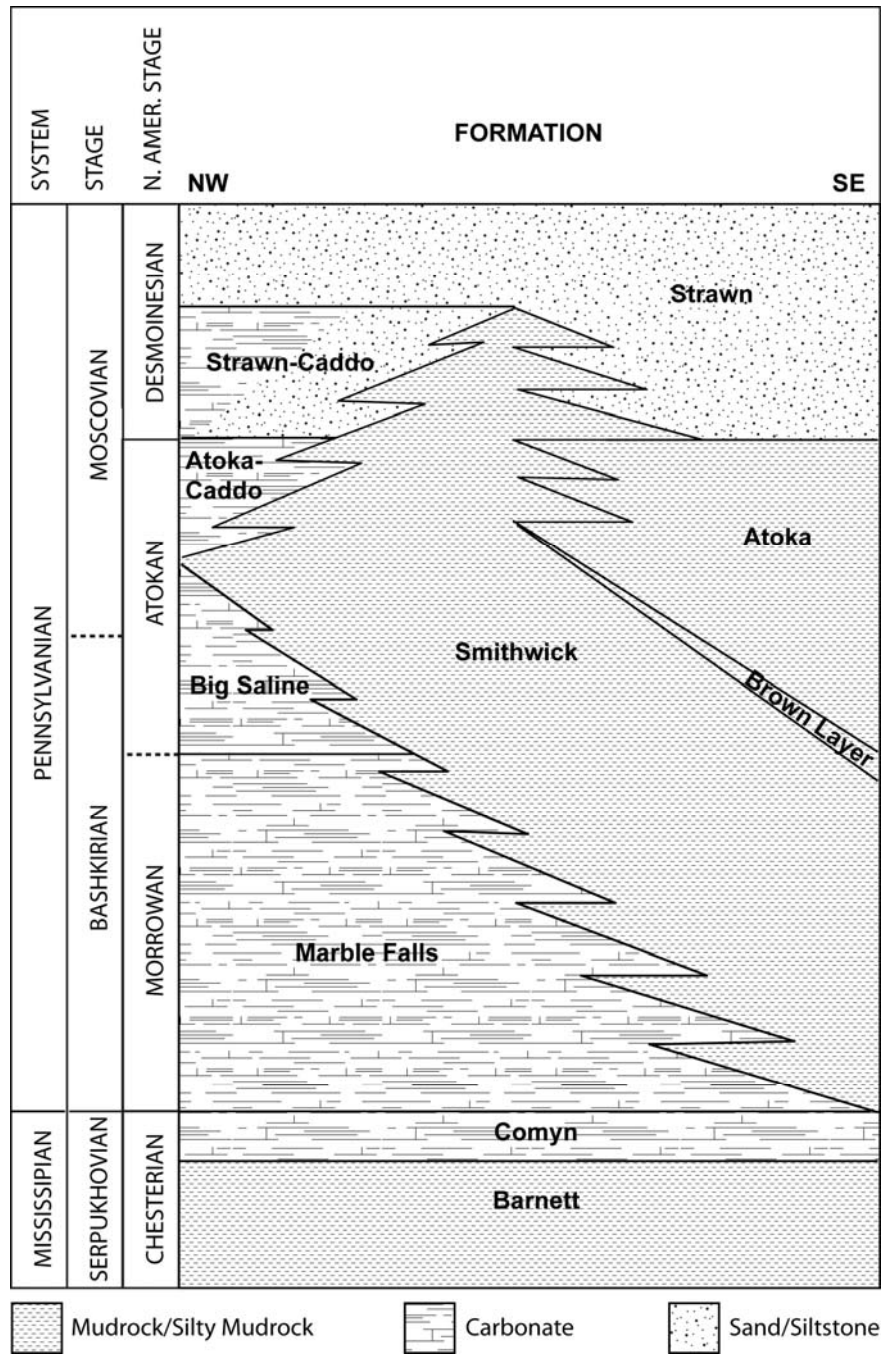


Figure 1.3 Generalization of the Fort Worth Basin stratigraphy going north to south along the western edge of the basin, north of the Llano Uplift (based on descriptions and illustrations from Kier et al, 1979; Lovick et al, 1982; Walper, 1982; Pollastro et al, 2003; Erlich and Coleman, 2005; Jarvie et al, 2007).

led to the deposition of Atokan and Smithwick strata over the Big Saline Limestone in late Atokan (Walper, 1982). In the central to northern part of the FWB the Big Saline clastic equivalent, the Bend Group, was deposited over the Marble Falls while still underlying the transgressive Smithwick (Lovick et al, 1982). The primary source of sediment supply in the Fort Worth Basin during the Pennsylvanian was derived from the Ouachita thrust belt (Kier, 1980; McKinzie and McLeod, 2003), but the Bend conglomerates of the north were supplied by the Muenster and Red River arches (Lovick et al, 1982). The hinge line reached the Concho platform in the Desmoinesian, and a new strata succession consisting of Strawn-Caddo Limestone, Smithwick Shale, and Strawn sands were deposited on the east margin of the basin (Walper, 1982). With the cessation of plate convergence, the Strawn deltas, consisting of both Ouachita thrust belt and Muenster arch sediments, prograded across the Fort Worth basin, and the contemporaneous subsidence of the Midland basin to the west activated the uplift of the Bend Arch (Walper, 1982).

1.5 North American Carboniferous Glacioeustasy

The Carboniferous was a time of significant glaciation in Gondwana coupled with marked eustatic changes (**figure 1.4**) (Mii et al, 1999; Gradstein et al, 2004; Haq and Schutter, 2008; Heckel, 2008; Rygel et al, 2008; Bishop et al, 2010). It has been determined that the glaciation was in fact dynamic and consisted of multiple ice sheets, as opposed to one large ice sheet over Gondwana (Isbell et, 2003; Blakey, 2008; Fielding et al, 2008; Rygel et al, 2008; Bishop et al, 2010). The onset of the late Paleozoic ice age began in the mid- to late-Mississippian (Garzanti and Sciunnach, 1997; Mii et al, 1999; Bishop, 2010). There is a lack of literature discussing Early Pennsylvanian sedimentation in North America as a response to paleoclimatic forces (Heckel, 2008, fig. 6). A global sea-level drop at the Mississippian-Pennsylvanian boundary (**figure 1.4**) (beginning of Bashkirian) created a massive unconformity in North America (Veevers and Powell, 1987; Gradstein, 2004; Blake and Beuthin, 2008; Rygel et al, 2008). However, Arrow Canyon, Nevada, in the Great Basin, contains cyclic strata through the Mississippian-Pennsylvanian boundary indicative of

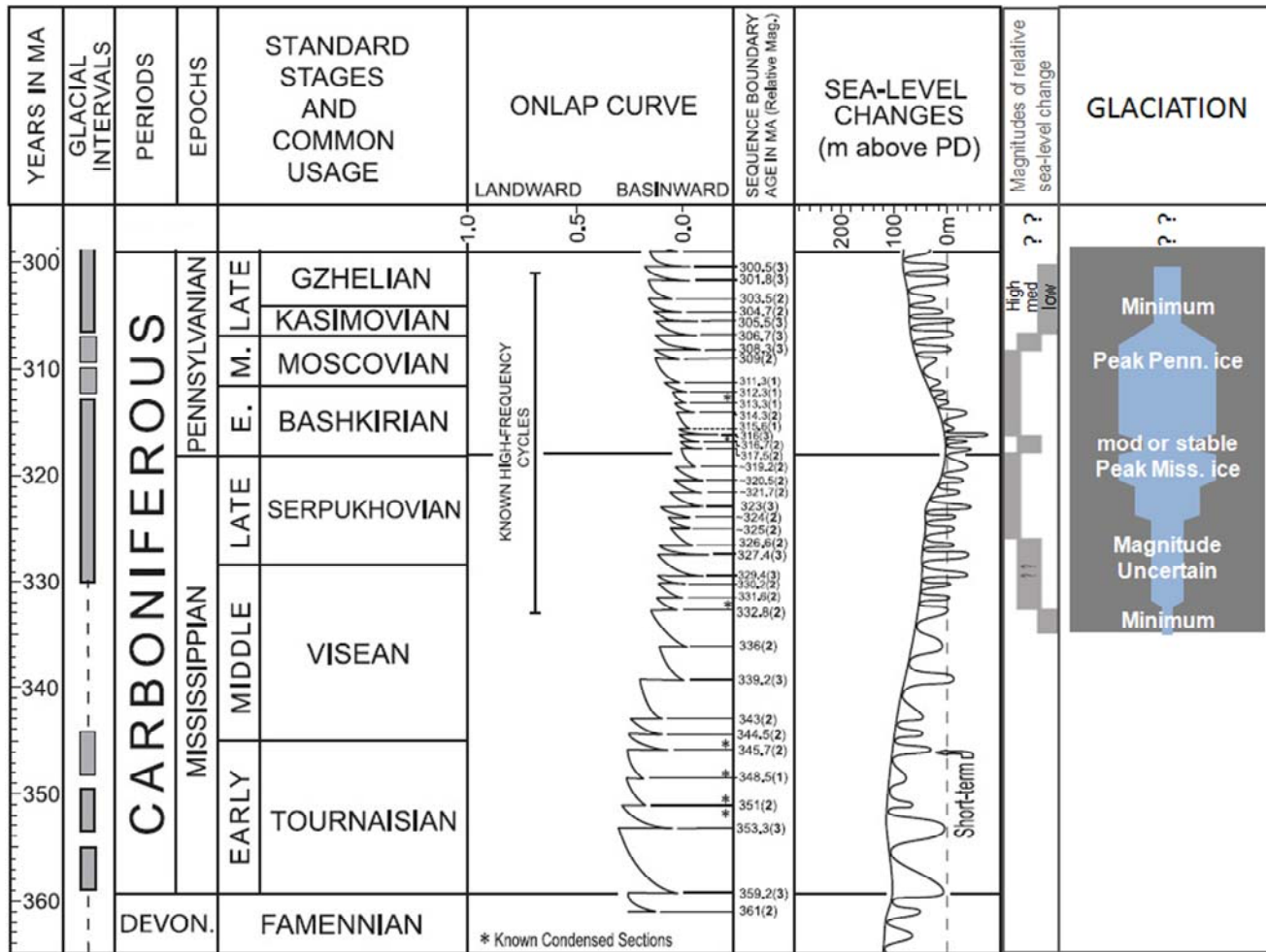


Figure 1.4 Time scale through sea-level curve from Haq and Schutter (2008). Magnitudes of relative sea level change and glaciation are redrawn from Bishop et al (2010) and represent the results of their study on the Arrow Canyon, Nevada successions. (Time scale after Gradstein et al (2004) and Ogg et al (2008).

glacioeustatic fluctuations (Gradstein et al, 2004; Bishop et al, 2010). Bishop et al (2010) determined, from a high resolution study of the Arrow Canyon successions, that the glacioeustatic record preserved in the strata affirms the concept of dynamic glaciation through alternations of eustatic amplitude. Glacial minima and a subsequent decrease in net eustatic changes occurred during early Morrowan (early Bashkirian) and late Desmoinesian (late Moscovian) at the paleoequatorial locale of Arrow Canyon (Bishop et al, 2010). In comparison, the North American midcontinental glacioeustatic record from Mid-Pennsylvanian cyclothems reflects the consistent and frequent transgressive-regressive cycles that resulted from the waxing and waning of Gondwanan ice sheets throughout the Pennsylvanian and into the Permian (Heckel, 1990, 1998, 2008; Sageman et al, 1998; Bishop et al, 2010). With regard to the FWB, the fact that the region was undergoing active tectonism contemporaneous with well-documented glacial activity associated with the late Paleozoic ice age is a complicating factor.

1.6 Study Objective

The objective of this study was to better constrain the depositional conditions of the Smithwick through the incorporation of geochemical and petrographic analyses. The utilization of these tools has provided insight into redox conditions in the basin, determined variations in elemental chemistry, and found potential paleoclimatic and tectonic implications. Two cores, the Walker D-1-1 from San Saba County, Texas, and the Potter C-9-1 from Brown County, Texas (**figure 1.5**), were investigated, with particular emphasis on the Walker D-1-1 core (~1029 ft/314 m). The upper section (~147 ft/45 m) of the core is dominated by course-grained siliciclastics while the lower portion is carbonate-rich (~61 ft/18 m). However, this study concentrated on the middle shale/mudrock portion of the core (~820 ft/250 m), including the Smithwick, a brown layer, and the overlying Atoka formations, with particular emphasis on the Smithwick.

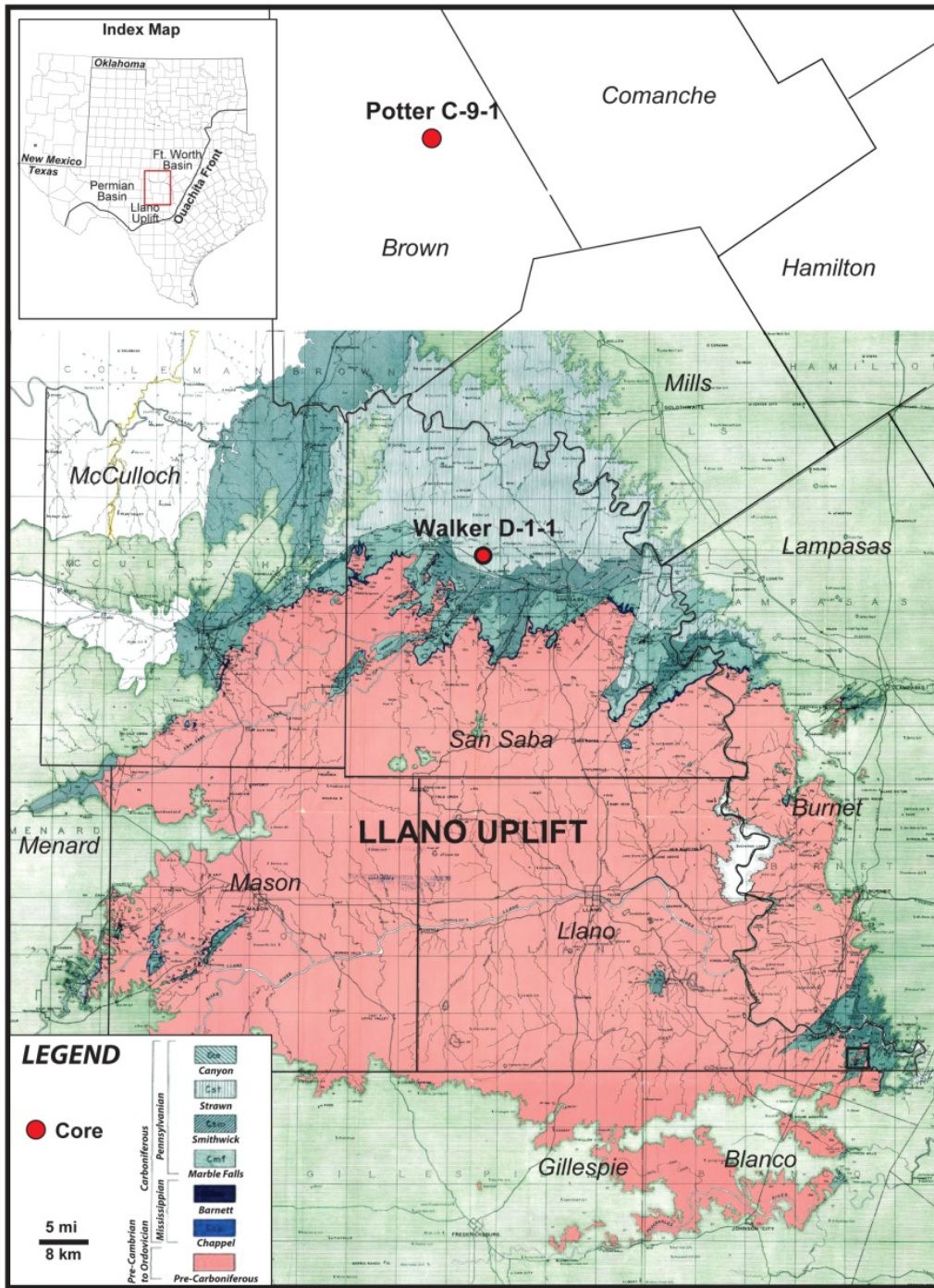


Figure 1.5 Smithwick study area and core locations in the southwestern Fort Worth Basin, Texas.

CHAPTER 2

METHODS

2.1 Drill Core Information

Two drill cores recovered from the southwestern Fort Worth Basin (FWB), in central Texas, preserve expanded sections of the Pennsylvanian-age Smithwick Formation along with sections from bounding formations (**table 2.1**). The Walker D-1-1 from San Saba County and the Potter C-9-1 from Brown County (**figure 1.5**) are currently being housed in the core repository of the Texas Bureau of Economic Geology (BEG) at the Pickle Research Center in Austin, TX. Access to analyze these cores was granted by research scientist and mudrock project activity coordinator for the BEG, Dr. Stephen Ruppel. The Walker D-1-1 and Potter C-9-1 were originally exploratory mineral test wells drilled by Houston Oil and Minerals Corporation in the late 1970's. The diameter of the Walker D-1-1 core is 2 inches (5 cm). The upper 47 feet of the Potter core has a diameter of 2 inches (5 cm), but the lower 560 feet have a 1.5-inch (3.8 cm) diameter. A geologist and research scientist for the BEG, Scott Hamlin, identified the stratigraphy of the Walker D-1-1 through observation, detailed core description, and geochemistry. The same approximate boundaries and formation names used in the study for the Walker D-1-1 are based on Dr. Hamlin's work.

2.2 Energy-Dispersive X-Ray Fluorescence (ED-XRF)

Both cores were analyzed for inorganic elemental chemistry using a Brüker Tracer III-V handheld energy-dispersive x-ray fluorescence (ED-XRF) instrument (BEG K0673). An approximately one-foot sampling interval was used. The instrument was kept stationary by use of a platform, and the samples were placed on the instrument nose, immediately above the 3 x 4 mm elliptical beam area (**figure 2.1A & D**).

Table 2.1 Drill Cores in Study

Core Name	Walker D-1-1		Potter C-9-1	
API	41130100		42049317690000	
Location	San Saba County, Texas		Brown County, Texas	
(Units)	(feet)	(meters)	(feet)	(meters)
Depth Interval for ED-XRF (for TOC, N, C/N, $\delta^{15}\text{N}$, $\delta^{13}\text{C}$)	195 – 1083 (54 – 1083)	59 – 330 (16 – 330)	1497 – 2104	456 – 641
Length	888 (1029)	271 (314)	607	185
Smithwick Interval	541 – 1022	165 – 311	1935 – 2071	590 – 631
Box Numbers	16-106 (1-106)		15-76	
Number of Samples	921 (235)		620	
Cut Condition	Uncut		Primarily uncut (3.5 boxes slabbed)	

Because the measurement sensitivity of the ED-XRF instrument decreases by the inverse square of the distance from the silicon detector (SiPIN), located directly beneath the sampling window (**figure 2.1D & E**), a flat sample surface is needed in order to optimize measurement consistency and accuracy. The Potter C-9-1 core was analyzed on the slabbed face when possible, whereas the cylindrical Potter C-9-1 and Walker D-1-1 samples were filed in order to create a flat surface using a Dremel and an aluminum oxide grinding stone (Dremel #932). The inorganic elemental suite was generated using two separate and distinct data acquisitions for each sample. Major element data acquisition, including V and Cr measurements, was undertaken using a low-energy, vacuum-pumped instrument setting; trace element data acquisition was undertaken using a filtered, high-energy instrument setting. Both low- and high-energy analyses were undertaken at the same location on the core face, marked by white correction fluid.

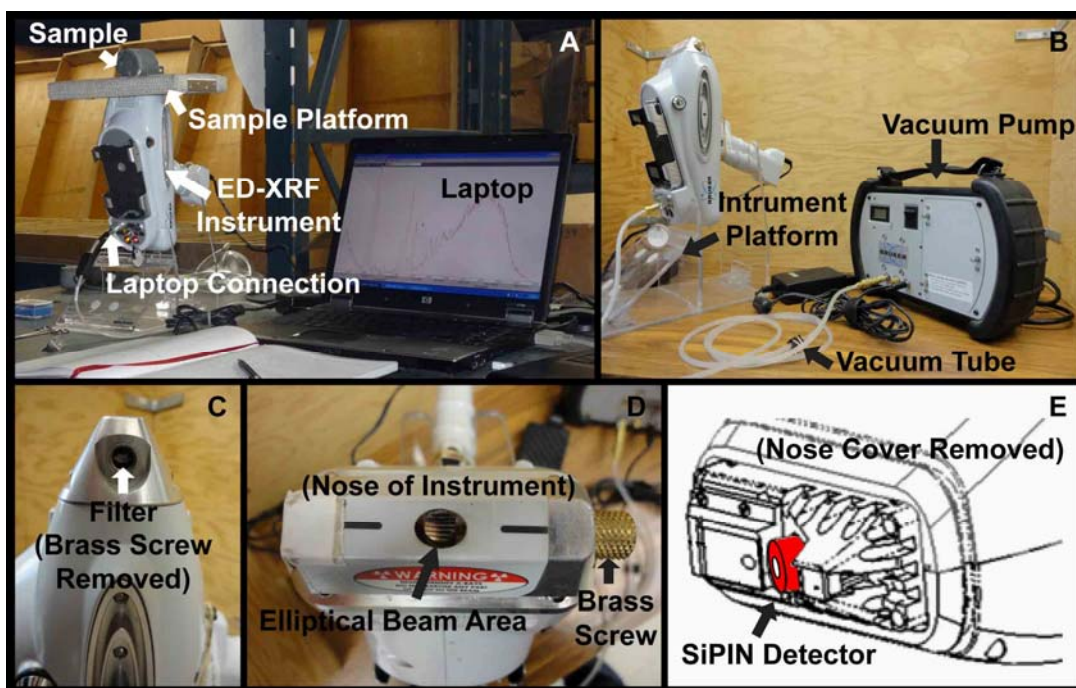


Figure 2.1 Overview of ED-XRF instrumentation illustrating A) core samples laid directly on nose of instrument with aid of a platform while data is recorded on a laptop, B) the instrument platform used in (A) to keep the instrument immobile and upright alongside the vacuum pump used in low-energy acquisitions, C) the filter used in high-energy acquisitions, D) the nose of the instrument where the beam is emitted, and E) the SiPIN detector below the beam area (drawn from Brüker manual, Kaiser, 2008).

Specifically, low-energy spectrum acquisition includes elements that emit characteristic x-rays between 1.25 to 7.06 kV. In order to obtain the elements in this range, and allow for backscatter that does not interfere with the peaks of interest, the voltage on the instrument was set to 15 kV. The instrument current was set to 42 μA ; however, while the voltage settings remain constant for this elemental range, regardless of the Tracer III-V used, the current settings vary between instruments due to the inter-instrument variability associated with the manufacture of the x-ray tube and electronics. In addition, instrument sensitivity to lighter elements (below and including Ca) was increased through the use of a vacuum pump, which removes the air between the sampling window and the detector. A vacuum pump operating at <3 torr was attached directly to the Tracer III-V (figure 2.1B).

The characteristic x-rays between 6.92 and 19.80 kV were measured in the high-energy acquisition mode (40 kV and 28 μ A). While a filter was used to prevent the low-energy x-rays from reaching the detector, a vacuum pump was not necessary because the energies of x-rays emitted from heavier elements are not attenuated in the short distance between the sample and the detector. The filter consists of 0.006" Cu, 0.001" Ti, and 0.012" Al and is inserted directly into the instrument (**figure 2.1C**). Both low- and high-energy acquisitions were taken for 3 minutes each.

2.2.1 ED-XRF Mudrock Calibration

The raw spectra obtained during the Tracer III-V acquisition is qualitative and requires a calibration to convert the data into quantified weight percentages. The calibration for the handheld ED-XRF unit is matrix-specific, so a calibration for major and trace elements of mudrocks was developed using a suite of 90 reference materials (Rowe and Hughes, 2010). The calibration includes the following 90 mudrock standards: 5 international, 7 Devonian-Mississippian Ohio Shale, 20 Pennsylvanian Smithwick Formation of Central Texas, 27 Devonian-Mississippian Woodford Formation of West Texas, 15 Late Cretaceous Eagle Ford Formation of South Texas, and 16 Mississippian Barnett Formation of North-Central Texas.

Each of the 90 reference materials were pulverized in a TM Engineering Pulverizer with trace-metal grade grinding barrels to 200 mesh. Approximately 8 grams of each of the powdered standards with a boric acid backing were pressed using a Carver press to 40 tons with a 40 mm die. The finished reference pellets were analyzed for major and trace elements using wavelength-dispersive x-ray fluorescence (WD-XRF) and inductively-coupled plasma mass spectrometry (ICP-MS), respectively.

The standard pellets were analyzed on the Bruker Tracer III-V for six minutes at three different locations on the pellet face under both low and high energy settings. All 270 raw x-ray spectra (90 references x 3 analyses) were loaded into Bruker's CalProcess software along with the accepted (WD-XRF & ICP-MS) elemental concentrations for all standards. Low energy and a high energy calibrations were developed by making inter-element corrections (slope and

background) for each element in each calibration. Certain standards were omitted after the implementation of the inter-element corrections using statistical analysis for each element to determine the outliers with a studentized value greater than 3.0 standard deviations from the mean.

The completed calibration yields quantified values using the raw ED-XRF spectra from unknown samples. The low energy calibration quantifies the following elements: Mg, Al, Si, P, S, K, Ca, Ba, Ti, V, Cr, Mn, and Fe. The high energy calibration quantifies the following elements: Ni, Cu, Zn, Th, Rb, U, Sr, Y, Zr, Nb, and Mo. The limits of determination of a method (LDM) for each element (**table 2.2**) (Rousseau, 2001) are provided.

2.2.2 ED-XRF Siderite Calibration

Because of a significant difference in matrix characteristics, a high and low energy siderite calibration was developed with a similar methodology to that of the mudrock calibration above. The primary difference is that 8 Pennsylvanian Smithwick siderite standards were used instead of the 90 mudrock references. The siderite reference pellets were prepared and analyzed in the same manner as the mudrock standards. The high energy settings were the same for both lithologies, but the low energy instrument settings were 15kV voltage and 15 μ A current for a siderite matrix. The lower amperage was used because of the high Fe content of siderite-bearing samples. Iron is a strong absorber and re-emitter of x-ray energy, thus lower amperage was used to avoid saturation of the x-ray detector.

2.3 LECO-S, TIC, TOC, TN, $\delta^{13}\text{C}$, and $\delta^{15}\text{N}$ Analyses

Samples for additional geochemical analyses were collected by cutting discrete samples from the Walker D-1-1 core at 4-foot intervals and subsequently pulverizing in a TM Engineering Pulverizer. The pulverized samples were stored in 120 mL specimen containers

Table 2.2 LDM by Element

Element	Accepted Value ^a	Instrument 1 (UTA-1)			Instrument 2 (1st UTA-2)		
		Measured Value ^b	σ (n=7) ^b	LDM ^c	Measured Value ^b	σ (n=7) ^b	LDM ^c
Mg (%)	0.67	0.80	0.09	0.17	0.85	0.14	0.28
Al (%)	4.96	5.39	0.14	0.28	5.32	0.11	0.22
Si (%)	32.6	33.7	0.2	0.5	33.1	0.4	0.8
P (%)	0.07	0.05	0.03	0.07	0.09	0.03	0.06
S (%)	3.34	2.18	0.10	0.20	2.27	0.09	0.18
K (%)	2.07	2.31	0.09	0.18	2.22	0.07	0.14
Ca (%)	0.13	0.23	0.03	0.06	0.24	0.02	0.04
Ti (%)	0.23	0.27	0.02	0.04	0.27	0.02	0.03
Mn (%)	0.015	0.012	0.001	0.002	0.013	0.001	0.003
Fe (%)	2.93	2.55	0.06	0.12	2.52	0.06	0.13
Ba (ppm)	2090	1884	376	753	1706	300	600
V (ppm)	928	1114	68	137	1110	80	159
Cr (ppm)	110	98	13	26	106	14	27
Ni (ppm)	130	153	26	52	150	20	40
Cu (ppm)	83	147	20	40	87	12	23
Zn (ppm)	823	844	96	191	880	74	147
Th (ppm)	8.4	9	1	2	9	1	2
Rb (ppm)	122	123	12	25	131	12	25
U (ppm)	18.1	17	6	11	22	4	8
Sr (ppm)	75.5	87	5	10	93	9	18
Y (ppm)	35.4	34	3	5	36	2	4
Zr (ppm)	80.3	95	7	13	96	6	13
Nb (ppm)	9	9	1	2	9	1	2
Mo (ppm)	79	83	4	9	82	3	6

^a Values for major elements from lithium borate-fused disc analysis by WD-XRF at SGS; values for trace elements (ppm) from sodium borate fusion dissolution and analysis by ICP-MS.

^b Average HH-ED-XRF measured values (n = 7) and standard deviations for reference material RTC-W-260, a black shale from the Devonian Woodford Formation of West Texas.

^c Limit of Determination of a Method (LDM) calculated according to Rousseau (2001).

(VWR part# 82030-366). Sulfur analyses were conducted using a LECO C-S analyzer, with a standard deviation of unknowns averaging less than 0.01% at the Kentucky Geological Survey. Total inorganic carbon (TIC) analyses were performed using a UIC, Inc. coulometer equipped

with a CM5230 acidification module (Engleman et al., 1985), with average unknown standard deviations of <0.5%. The TIC samples were weighed between 5 to 80 mg and acidified at 70°C with 10% phosphoric acid (H₃PO₄). Total organic carbon (TOC), total nitrogen (TN), and stable isotopic compositions of TOC ($\delta^{13}\text{C}$) and TN ($\delta^{15}\text{N}$) were performed on powdered samples that were weighed into silver capsules (Costech Analytical, Inc. #41067) and subsequently acidified repeatedly with 6% sulfurous acid (H₂SO₃) in order to remove carbonate phases (Verardo et al., 1990; Rowe et al., 2001). Samples were analyzed at the University of Texas at Arlington using a Costech 4010 elemental analyzer interfaced with a Thermo Finnigan ConFlo IV device to a Thermo Finnigan Delta V isotopic ratio mass spectrometer. Isotopic results are reported in per mil (‰) relative to V-PDB for $\delta^{13}\text{C}$ and air for $\delta^{15}\text{N}$. The average standard deviations of USGS-40 glutamic acid (IAEA-8573) were 0.11‰ and 0.07‰ for $\delta^{13}\text{C}$ and $\delta^{15}\text{N}$, respectively, 1.07% and 0.08% for the TOC and TN of USGS-40, respectively, and 0.13 for C/N. The average standard deviations for unknown samples analyzed in triplicate were 0.10‰ for $\delta^{13}\text{C}$, 0.12‰ $\delta^{15}\text{N}$, 0.02% for TOC, 0.01X% for TN, and 0.18 for C/N.

2.4 Mineralogic and Petrographic Analyses

A subset of samples was selected for mineralogic and petrographic study (**table 2.3**) based on stratigraphically-defined changes in bulk geochemistry. The samples were analyzed using x-ray diffraction, thin sections, and scanning electron microscopy (SEM).

2.4.1 X-Ray Diffraction (XRD)

Samples selected for XRD (Table 2.4) were analyzed by the powder x-ray diffraction method (Cu-K α radiation) at the Kentucky Geological Survey using a Bruker D8 X-Ray Diffraction Unit. Bulk powder spectra were analyzed from 2°-90° 2 θ . Both glycolated and unglycolated clay fractions were prepared and analyzed using a suspension and powder-peel method across a 2 θ angle range from 2°-22°.

Table 2.3 XRD, Thin Section, and SEM Samples

Sample Name	Depth		XRD	Thin Section	SEM
	(ft)	(m)			
Potter 29.2.7	1632.67	497.64	X		
Potter 35.2.6	1689.76	515.04	X		
Potter 42.4.8	1761.71	536.97	X		
Potter 58.5.2.5	1919.23	584.98	X		
Potter 63.3.5.5	1963.76	598.55	X		
Walker 4.3.4	94.89	28.92		X	
Walker 9.2.4	144.18	43.95		X	
Walker 16.4.4	201.25	61.34		X	
Walker 25.2.8	291.25	88.77		X	X
Walker 37.3.8	415.36	126.6	X	X	
Walker 40.5.4	445.03	135.64		X	
Walker 44.2.4	479.69	146.21		X	
Walker 46.5.4	504.03	153.63		X	
Walker 49.3.1	527.83	161.06		X	
Walker 50.2.8	536.58	163.55	X	X	
Walker 52.5.6	561.42	171.12	X	X	X
Walker 57.2.4	602.69	183.7		X	
Walker 62.3.4	651.36	198.53	X	X	
Walker 64.3.4	670.92	204.5		X	
Walker 66.1.6	686.42	209.22	X	X	X
Walker 75.2.4	770.92	234.98		X	
Walker 78.1.7	799.58	243.71	X	X	X
Walker 80.3.2	821.42	250.37	X	X	X

Table 2.3 – *Continued*

Sample Name	Depth		XRD	Thin Section	SEM
	(ft)	(m)			
Walker 83.2.8	852.92	259.97	X	X	
Walker 88.3.4	905.92	276.12		X	
Walker 93.2.4	953.69	290.69	X	X	
Walker 94.1.4	960.92	292.89	X		
Walker 97.5.8	997.92	304.17	X	X	
Walker 99.3.8	1012.92	308.74	X	X	
Walker 101.5.4	1035.81	315.71	X	X	
Walker 101.5.8	1036.92	316.05	X	X	X
Walker 102.1.8	1038.92	316.66	X	X	
Walker 102.4.8	1044.92	318.49	X	X	
Walker 103.2.4	1049.69	319.95		X	
Walker 104.1.8	1057.92	322.45		X	
Walker 106.5.4	1083.03	330.11	X		
Walker 106.5.8	1083.92	330.38	X	X	

2.4.2 Scanning Electron Microscopy (SEM)

Elemental x-ray maps for select samples (**table 2.3**) were obtained with an ASPEX Scanning Electron Microscope using a Peltier cooling system, silicon drift detector, and a 10mm² window. The SEM operated in a variable pressure mode (chamber pressure 0.2 torr) that allowed thin sections to be used without additional preparation. The SEM operated with an accelerating voltage of 25 kV, a beam current of approximately 1 nA, and a working distance of

approximately 15 mm. Backscattered electron images were collected with a solid state, four-quadrant detector.

2.4.3 Thin Section Preparation and Imaging

Samples selected for thin sections (**table 2.3**) were prepared by Spectrum Petrographics, Inc. on 27 x 46 mm uncovered glass slides at a 25-micron thickness, mounted with Loctite Impruv 363, and vacuum-impregnated with EPOTEK 301. Thin section descriptions were based on observation through a Meiji ML9000 Microscope under both plane-polarized and cross-polarized light, with a 30 watt light source and a zoom range of 4-40x. Petrographic images of a subset of the thin section samples were taken using a Petrographic Nikon microscope with a Polaroid Digital Microscope camera connected to an Apple G3 computer. Images, some in color and some in black and white, were taken under plane-polarized light at a magnification range of 4-20x.

CHAPTER 3

RESULTS

3.1 X-Ray Diffraction (XRD) Results

Thirty samples were selected from the Walker D-1-1 (Walker) core in order to 1) cover the elemental range of variability observed with the XRF, and 2) represent the majority of the studied formations. The samples were analyzed for mineralogy using semi-quantitative XRD. **Table 3.1** shows the percentages of minerals estimated by Dr. Necip Guven from analysis of the raw XRD patterns of the 30 samples. The results indicate that all formations except for the Marble Falls are dominantly clay and belong to the mudrock classification. Quartz content is highest in the Atoka formation, consistent with higher XRF-generated %Si values (**figures 3.1 and 3.3**) compared with the Smithwick. The Marble Falls strata included in the sampling are primarily carbonate, consisting of calcite and some secondary ankerite. The calcite content decreases stratigraphically upward from the Marble Falls into the Smithwick, and is below detection limits for much of the Smithwick, the Brown Layer, and the Atoka. The only significant occurrence of dolomite or apatite is associated with siderite-rich samples. Given the sporadic occurrence of dolomite, apatite and gypsum, the dominant Ca phase is calcite in the Walker core. Interestingly, the ankerite and siderite are separated; however, the siderite is diluted by clay. The presence of siderite, ankerite, and pyrite would normally indicate Fe-enrichment in the core; however, the pyrite observed in the samples is a relatively minor constituent ranging from 0-2% except for one 10% sample. In addition, ankerite is found primarily in the Marble Falls Formation associated with calcite. The high-Al brown layer has significant kaolinite, while the dominant clay is illite in the majority of the core. Traces of kaolinite occur in the Smithwick samples, but are completely absent in the Atoka.

Table 3.1 Semi-Quantitative XRD Results from Walker D-1-1 Core

Formations	sample ID	depth in feet	depth in meters	quartz	plagioclase	K-feldspar	carbonates				apatite	gypsum	pyrite	rutile	clay minerals					TOTAL	
							calcite	dolomite	ankerite	siderite					illite + mica I/S	mixed-layer	smectite	attapulgite	kaolinite		chlorite
Atoka	16.4.4	201.25	61.34	55	8							+	+	20	10					7	100
	17.1.8	205.81	62.73	42	4		3					+	1	25	15					10	100
	17.3.8	209.36	63.81	30	4							+	1	35	15					15	100
	17.5.8	212.92	64.90	32	3	1	1				2	+	1	30	15					15	100
	25.2.8	291.25	88.77	45	3	1	1				2	+	1	32	10					10	105
	37.3.8	415.36	126.60	7	3		10					+	+	10	5					5	100
	40.5.4	445.03	135.64	45	4							1	+	25	15					10	100
	44.2.4	479.69	146.21	30	8						+	2	+	30	15					15	100
Brown Layer	49.3.1	528.03	160.94	10								+	1	30	14				20	25	100
	50.1.4	533.92	162.74	25									+	25	10				10	30	100
	50.2.8	536.58	163.55	10	4				46				+	15	10					15	100
	50.3.4	537.47	163.82	30	4							+	1	30	10				10	15	100
Smithwick	52.5.4	560.92	170.97	35	4							+	1	30	15				5	10	100
	52.5.6	561.42	171.12	20					50	10				10	5				5		100
	62.3.4	651.36	198.53	10					67	2	1			5	5				5	5	100
	64.3.4	670.92	204.50	25	6		2		1			1		30	15				10	10	100
	66.1.6	686.42	209.22	15	5				35				+	20	10				5	10	100
	78.1.7	799.58	243.71	5	3			12	60	8		+	+	5	2					5	100
	80.3.2	821.42	250.37	4	2				7	80			+	4	3						100
	83.2.8	852.92	259.97	30	2							1	+	40	15				6	6	100
	93.2.4	953.69	290.69	15			30	4	20	1		10		10	5					5	100
	94.1.4	960.92	292.89	35	3		7		4			1	+	25	10				5	10	100
	97.5.8	997.92	304.17	35	5		13		1			1	+	22	10				5	8	100
99.3.8	1012.92	308.74	30	8		25					2	+	15	8				2	10	100	
Marble Falls	101.5.4	1035.81	315.71	25	1		33	10				1		15	5				2	8	100
	101.5.8	1036.92	316.05	15			70	8				+		3	2					2	100
	102.1.8	1038.92	316.66	25			40	10				+		10	5					10	100
	102.4.8	1044.92	318.49	25	4		35	10				1		10	5					10	100
	106.5.4	1083.03	330.11	6			87					1	2	2						2	100
	106.5.8	1083.92	330.38	5			87	5				+		2	1						100

* About 10% of Fe is probably substituted by Mn in these siderites or a poorly crystalline manganese carbonate (rhodochrosite) may be making 10% of carbonates.

3.2 Core Chemostratigraphy and Inter-elemental Relationships

3.2.1 Geochemical Characterization of and Correlation between Cores

Figure 3.1 shows the chemostratigraphic relationship of %Al, %Si, and %Ca in the Walker D-1-1 core, in the context of the main stratigraphic units. The oldest stratigraphic unit,

the Marble Falls Formation, is Ca-enriched and Al-depleted, as expected for limestone. The boundary between the Marble Falls and the overlying Smithwick Formation is drawn at 1022 ft (311 m), however, the true boundary is gradational, as evidenced by the oscillation of %Ca between <1% and 12% in the lowermost Smithwick (below 988 ft; 301 m). The top of the Smithwick Formation, hereafter termed the “Brown Layer,” is marked by a highly Al-enriched layer (%Al>10%) at 541 ft (165 m). The Brown Layer (520 ft - 541 ft.; 158 m - 165 m) is overlain by the Atoka section, which is geochemically and sedimentologically similar to the Smithwick, but with a slightly higher silica content. The decreasing spikes in %Al and %Si that occur throughout the core, but especially in the Smithwick Formation, indicate siderite-rich intervals.

Figure 3.2 is a ternary diagram depicting normalized weight percentages of SiO_2 , $\text{Al}_2\text{O}_3 \cdot 5$, and $\text{CaO} \cdot 2$. The ternary was developed by Brumsack (1989) to compare the major constituents of modern TOC-rich sediments to average shale, as defined by Wedepohl (1971). The SiO_2 end-member represents content both from quartz and clay mineralogies, assuming little influence from other minerals (e.g., feldspars). The $\text{Al}_2\text{O}_3 \cdot 5$ represent the claybound-%Al fraction, with the assumption of minimal feldspar and Al-oxide minerals. The $\text{CaO} \cdot 2$ end-member represents the Ca-rich carbonate constituents, assuming minimal Ca-phosphate. The diagram ignores other major constituents, but is useful for defining the clay-quartz-calcite variability within mudrock sequences. What can be observed in **Figure 3.2** is that the majority of the Smithwick, Brown Layer, and Atoka samples plot around the “average shale” value, reflecting a dominance of clay minerals and an overall lack of calcium carbonate content. Calcium-rich samples are largely restricted to the Marble Falls Formation, and samples collected from the gradational boundary between the Marble Falls and Smithwick Formations. These samples also tend to fall on the SiO_2 -rich side of the Ca-dilution line, reflecting an increase in quartz content, relative to stratigraphically higher samples. Samples high in siderite also have a higher affinity for Ca than the mudrock portion of the core, and thus plot further toward the $\text{CaO} \cdot 2$ end-member. It can also be observed that the Atokan samples plot slightly closer to the SiO_2 end member, reflecting their higher quartz content, while the

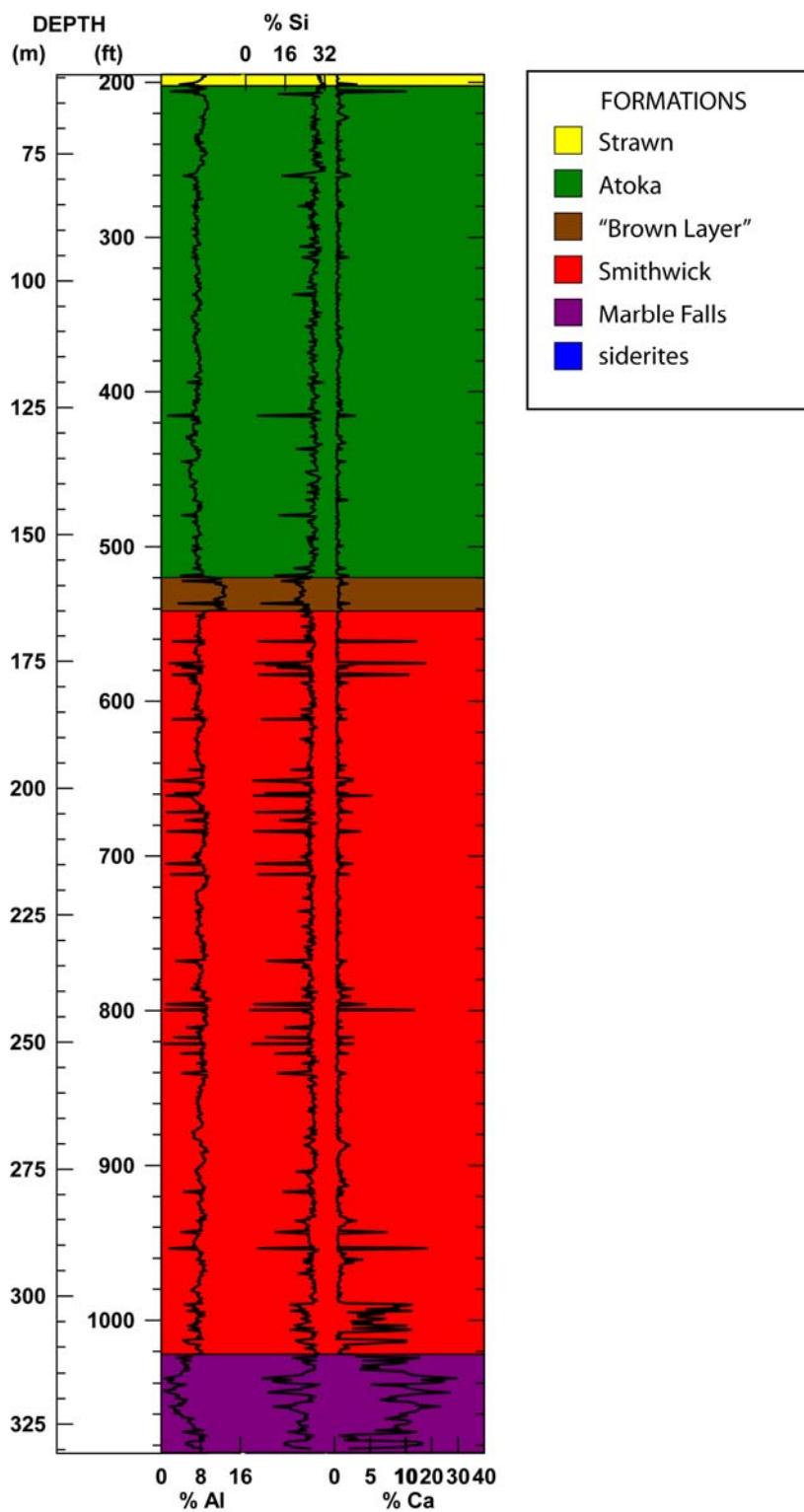


Figure 3.1 Major element (Al, Si, Ca) chemostratigraphy for the Walker D-1-1 core, along with the formations and units.

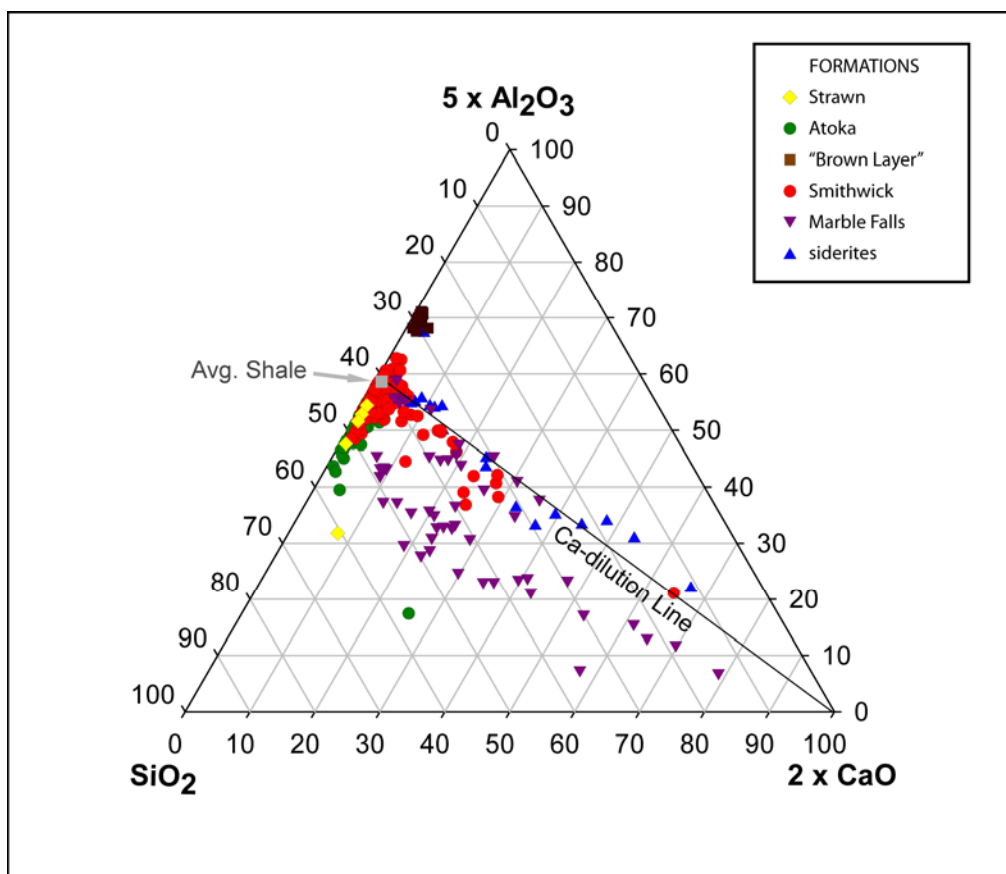


Figure 3.2 An Al-Si-Ca ternary plot, reflecting relative changes in the clay, quartz, and calcium carbonate fractions of samples from the Walker D-1-1 core (after Brumsack, 1989).

Brown Layer samples plot closer to the $\text{Al}_2\text{O}_3 \cdot 5$ end-member, reflecting relatively high clay content.

Figure 3.3 shows the major element chemostratigraphic relationships in the Potter C-9-1 (Potter) core. Unlike the gradational nature of the contact between the Marble Falls and Smithwick Formations in the Walker core, the contact between the Big Saline and Smithwick Formations in the Potter core is much sharper. However, the abrupt upper contact between the Smithwick and the Al-rich Brown Layer, and the slightly more silica-rich Atokan, are common between the two cores. Above the Atokan are three chemically-distinct units. Based on descriptions from Walper (1982), and Figure 1.4, the units have been identified as the Atoka-

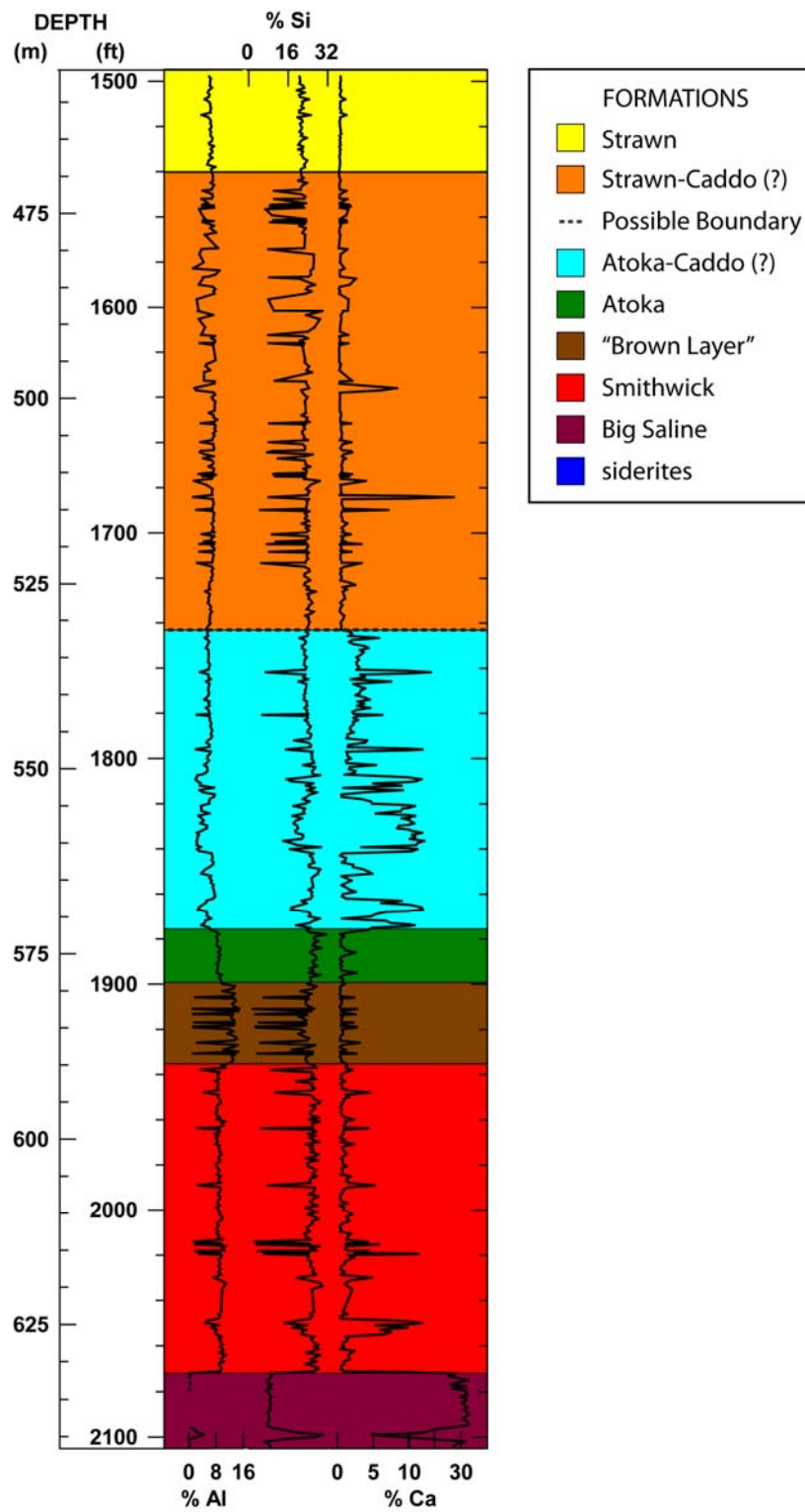


Figure 3.3 Major element (Al, Si, Ca) chemostratigraphy for the Potter C-9-1 core, along with the formations and units.

Caddo, Strawn-Caddo, and Strawn in ascending order. It is observed in **Figure 3.3** that the Atoka-Caddo unit shows substantial fluctuation in %Ca, but an overall increase from the underlying mudrock formations. The Strawn-Caddo has much more subdued stratigraphic fluctuations in %Ca, a slightly higher overall %Si content from proximity to the Atoka-Caddo, and a high occurrence of siderites. The lower %Ca content may indicate that the Strawn-Caddo is a transitional unit that is still part of the Strawn, but for geochemical comparison it will remain separated. The base of the Strawn is identified by a relatively stable stratigraphic pattern in %Al, %Si, and %Ca. The dominant constituent is silica, reflecting a high percentage of quartz.

The Al-Si-Ca ternary diagram for the Potter core (**figure 3.4**) illustrates the enrichment of Si in all formations overlying the Brown Layer. The carbonate Big Saline groups heavily toward CaO. The other heavily carbonate-influenced groups, Atoka-Caddo and siderites, follow the Ca-dilution line. In both the Walker and Potter cores, the Smithwick plots closely to the average shale value. **Table 3.2** quantifies the Ca-Al-Si relationships for both cores.

The Walker core is measured for elemental chemistry beginning at approximately 200 feet (60 m) below surface, and the Smithwick section top begins around 540 feet (165 m) below surface. The Potter core begins at approximately 1500 feet (455 m) subsurface, with the Smithwick top at approximately 1935 feet (590 m) subsurface. When scaled the same, as in **Figure 3.5**, there is a conspicuous difference in the thickness of the Smithwick and Atoka formations between the two cores. The Walker has a Smithwick section roughly 480 feet (145 m) thick, an Atoka section of nearly 320 feet (100 m) thick, and an intermediate brown layer around 20 feet (5 m) thick. Comparatively, the Potter core contains a Smithwick section of only 135 feet (40 m) and an Atoka section of a mere 22 feet (7 m), but has a thicker brown layer at 35 feet (9 m) and a higher occurrence of siderites compared to the Walker brown layer. In both cores, siderites are more abundant in the Smithwick section than in the Atoka. **Figure 3.5** also shows a correlation between the Walker and Potter cores given the chemostratigraphic results; however, the boundaries above the Atoka in the Potter core might change with a

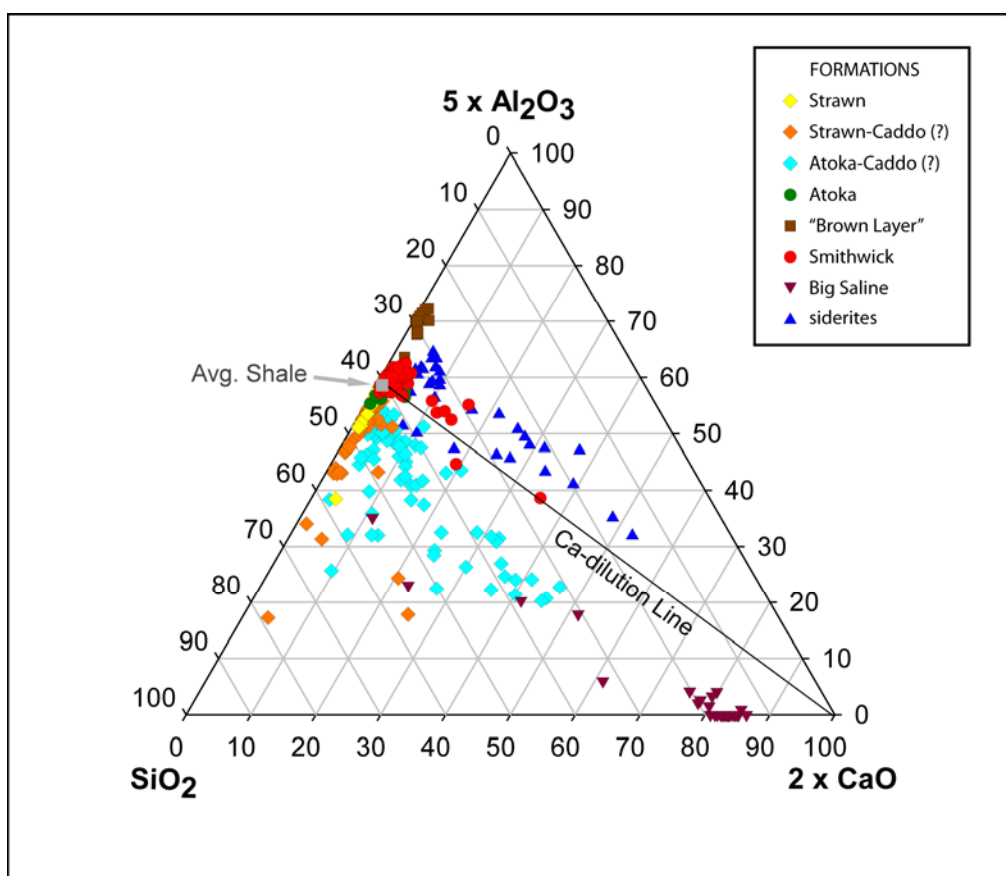


Figure 3.4 An Al-Si-Ca ternary plot, reflecting relative changes in the clay, quartz, and calcium carbonate fractions of samples from the Potter C-9-1 core (after Brumsack, 1989).

sedimentological evaluation. The concentration of Si is a particularly useful parameter for correlation, because it is present in all formations, easily differentiates the Smithwick and Atoka Formations, indirectly identifies the presence of siderites, and maintains a reasonable range for plotting across all formations.

3.2.2 Fe and Carbonate Phases

The XRD analysis (**table 3.1**) indicates the potential for Fe-enrichment in siderite, ankerite, and pyrite. Ankerite exists predominantly in the carbonate-rich Marble Falls strata and pyrite does not comprise a significant component, typically ranging from 0-2%. Therefore, stratigraphic spikes in the Fe concentration of mudrock strata (**figure 3.6**) indicate the location of siderite beds or nodules. The stratigraphic Fe concentration (excluding the siderite) (**figures**

Table 3.2 XRF-Generated Concentrations for Major (Al, Si, Ca), Carbonate (Ca, Mg, Mn, Fe), and Detrital (Ti,Zr) Elements
(Siderite-rich samples were separated and not included in whole core calculations)

	FORMATION	Strawn	Strawn-Caddo	Atoka-Caddo	Atoka		Brown Layer		Smithwick		Big Saline	Marble Falls	Whole Core		Siderite		
	CORE	Potter	Potter	Potter	Walker	Potter	Walker	Potter	Walker	Potter	Potter	Walker	Walker	Potter	Walker	Potter	
	n =	47	153	135-136	314	23	22	35	485	127-128	15-34	63	884	535-556	30	10-46	
% Al	MEAN	6.34	6.55	5.32	7.29	8.73	12.11	12.85	7.91	8.91	1.00	4.71	7.56	7.13	2.93	3.04	
	MEDIAN	6.40	7.01	5.76	7.26	8.62	12.37	13.05	7.96	8.93	0.43	4.59	7.61	7.06	2.75	3.22	
	RANGE	MIN	3.79	1.29	2.01	1.99	8.12	10.80	9.94	1.76	4.63	0.10	0.68	0.10	0.69	1.13	
		MAX	7.84	9.07	7.78	9.44	9.54	13.15	14.77	9.93	10.88	4.48	9.25	13.15	14.77	6.91	4.54
% Si	MEAN	21.57	23.46	23.33	27.58	26.53	22.87	23.46	26.16	25.40	10.24	22.06	26.29	23.03	8.35	7.33	
	MEDIAN	21.45	23.37	23.60	27.70	26.29	22.92	23.46	26.47	25.66	8.62	23.10	26.79	23.66	7.48	7.99	
	RANGE	MIN	19.54	8.13	14.09	13.73	24.32	20.04	17.56	5.22	10.72	6.57	7.04	5.22	6.57	2.01	1.68
		MAX	25.12	29.80	29.27	33.32	31.25	25.71	27.41	29.61	29.75	30.25	29.62	33.32	31.25	16.08	11.79
% Ca	MEAN	0.44	0.86	4.77	0.59	0.89	0.74	0.59	0.96	1.50	27.91	10.85	1.53	3.57	3.94	3.07	
	MEDIAN	0.41	0.52	3.09	0.47	0.66	0.63	0.55	0.50	1.00	30.79	10.10	0.52	0.84	2.30	2.01	
	RANGE	MIN	0.28	0.22	0.38	0.28	0.36	0.48	0.33	0.26	0.36	4.80	0.80	0.26	0.22	0.91	1.16
		MAX	1.28	27.15	16.07	9.96	2.70	1.84	1.17	18.23	15.28	33.04	29.37	29.37	33.04	17.54	18.48
% Mg	MEAN	0.74	0.82	1.13	0.97	1.30	0.71	0.94	1.08	1.34	2.02	1.06	1.03	1.11	3.20	4.09	
	MEDIAN	0.74	0.86	1.06	0.93	1.29	0.78	0.84	1.04	1.27	1.44	1.06	1.00	1.04	3.32	4.07	
	RANGE	MIN	0.02	0.01	0.34	0.24	0.93	0.24	0.37	0.45	0.79	0.47	0.36	0.24	0.01	1.84	3.39
		MAX	1.22	2.07	4.03	3.19	1.71	1.06	2.96	5.37	5.58	6.24	1.72	5.37	6.24	4.36	4.85
% Mn	MEAN	0.03	0.03	0.04	0.03	0.02	0.15	0.04	0.04	0.04	0.04	0.03	0.04	0.03	1.84	0.18	
	MEDIAN	0.03	0.03	0.03	0.02	0.02	0.11	0.04	0.03	0.02	0.03	0.03	0.03	0.03	1.71	0.11	
	RANGE	MIN	0.01	0.01	0.01	0.01	0.01	0.02	0.01	0.01	0.01	0.01	0.01	0.01	0.01	0.27	0.04
		MAX	0.06	0.07	0.15	0.23	0.05	0.88	0.12	0.58	0.32	0.10	0.06	0.88	0.32	10.49	0.82
% Fe	MEAN	3.62	3.36	3.06	3.97	3.77	4.92	4.47	4.14	4.11	0.85	2.42	3.98	3.41	21.84	20.30	
	MEDIAN	3.56	3.39	3.11	3.80	3.74	4.68	4.24	3.98	3.89	0.40	2.26	3.89	3.48	21.39	20.47	
	RANGE	MIN	1.68	1.01	1.31	1.27	3.08	2.94	2.72	2.92	2.78	0.25	1.25	1.25	0.25	9.23	9.19
		MAX	4.90	6.63	8.24	12.29	4.68	7.05	10.64	9.68	16.06	3.29	4.04	12.29	16.06	31.93	32.08
% Ti	MEAN	0.43	0.42	0.32	0.43	0.41	0.57	0.52	0.44	0.41	0.04	0.28	0.43	0.38	0.14	0.14	
	MEDIAN	0.44	0.44	0.35	0.44	0.41	0.56	0.52	0.45	0.42	0.02	0.27	0.44	0.41	0.15	0.15	
	RANGE	MIN	0.22	0.11	0.13	0.18	0.35	0.47	0.43	0.18	0.21	0.00	0.04	0.04	0.00	0.01	0.04
		MAX	0.49	0.62	0.44	0.64	0.46	0.62	0.70	0.54	0.47	0.24	0.58	0.64	0.70	0.28	0.22
ppm Zr	MEAN	215	197	143	134	136	127	149	118	145	76	98	123	160	56	71	
	MEDIAN	205	178	145	131	136	131	153	122	144	75	98	124	154	50	78	
	RANGE	MIN	175	95	86	66	122	107	28	26	60	29	38	26	28	15	33
		MAX	312	445	204	457	149	140	169	167	269	118	231	457	445	121	110

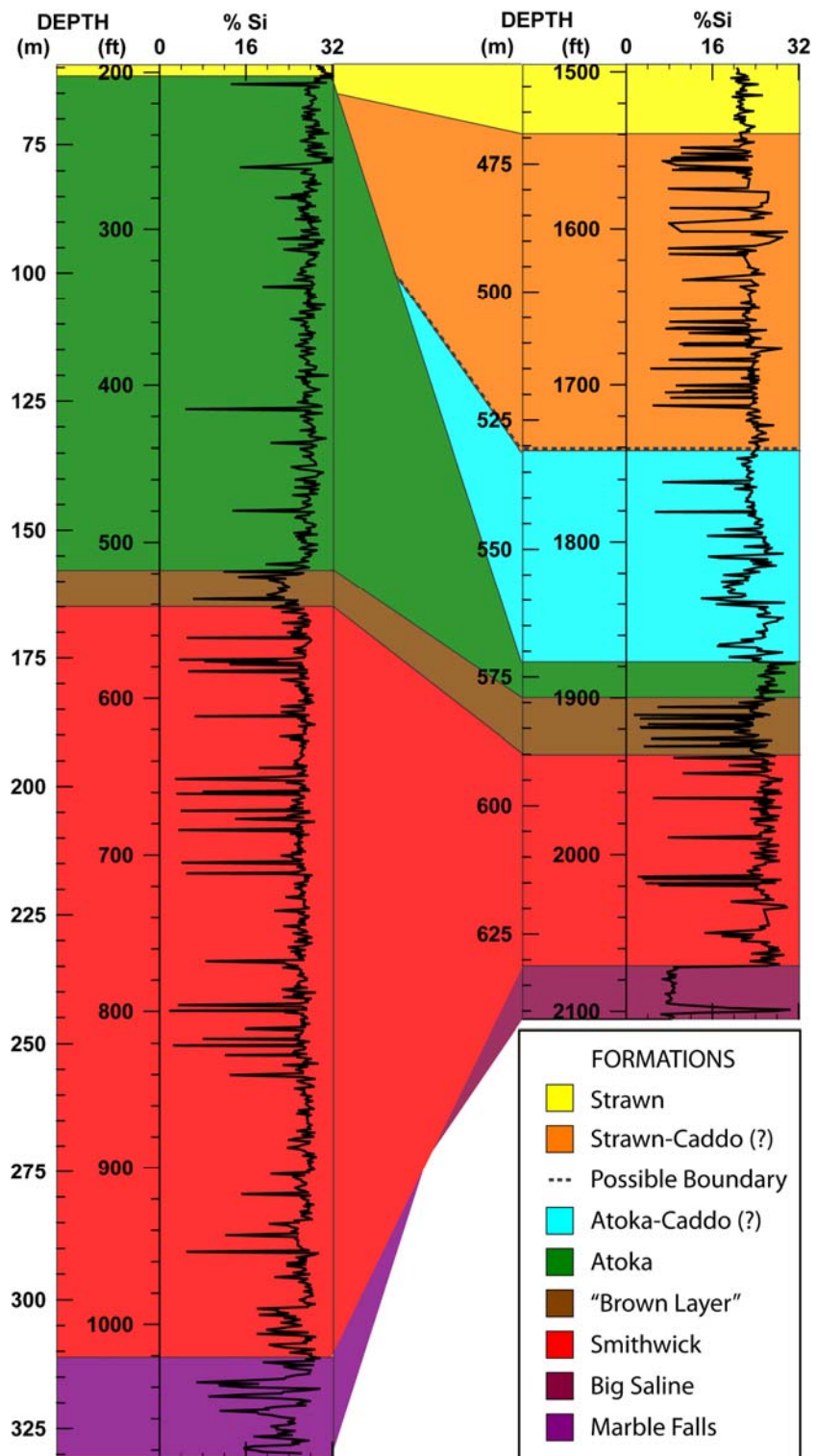


Figure 3.5 Correlation of the Walker D-1-1 (left) and Potter C-9-1 (right) cores using stratigraphic Si concentrations.

3.6 and 3.7) in the two dominant mudrock units, the Smithwick and Atoka, have ranges from 1-16%, but have mean values of approximately 4% in both cores (**table 3.2**), and modes of 3.77 and 3.43 in the Walker and Potter cores, respectively. The only other significant minerals present in the Walker core that could potentially contain iron, according to the XRD analysis, are the clay minerals. Thus, the Fe baseline around 4% illustrates the Fe associated with the clay-rich mudrock matrices. Iron occurs in three primary phases in the mudrock portions of the Walker core based on XRD and chemostratigraphic results. In order of abundance the phases are as follows: clay, siderite, and pyrite. Due to similar Fe chemostratigraphy, the Potter core (**figure 3.7**) most likely exhibits the same relative abundances of Fe phases throughout the mudrock strata.

The Walker core contains more siderite per length than the Potter core in the Smithwick Formation, but the opposite is true of the brown layer. The carbonate matrix of siderite is susceptible to the incorporation of other elements such as Mn, Ca, and Mg (**figures 3.6 and 3.7**). The Mn-enrichment in both cores is dominantly in siderite, but the associations of Mg and Ca with siderite, while present, are not as strong, suggesting the occurrence of other phases.

Total inorganic carbon (TIC) measurements were taken at intervals averaging 4-feet (225 samples) in the Walker core. TIC indicates the presence of carbonate phases. **Figure 3.8** shows that the majority of the Smithwick samples have low concentrations of TIC and related elements, causing most of the 225 samples to group near the origin in all crossplots. The two siderites within the discrete sampling subset are the only samples enriched in Mn, and fall near the FeCO_3 line in the Fe plot (**figures 3.8C & D**). The Ca-enriched samples in the Smithwick and Marble Falls formations are dominantly calcite based on the correlation with stoichiometric calcite line (**figure 3.8B**), as well as the XRD analysis. High-Mg samples do not fall on the stoichiometric dolomite line (**figure 3.8A**). The association of dolomite and siderite in the XRD analysis (**table 3.1**) suggests the potential for ferroan dolomite. In addition, Mg could easily be incorporated into the clay fraction similar to Fe.

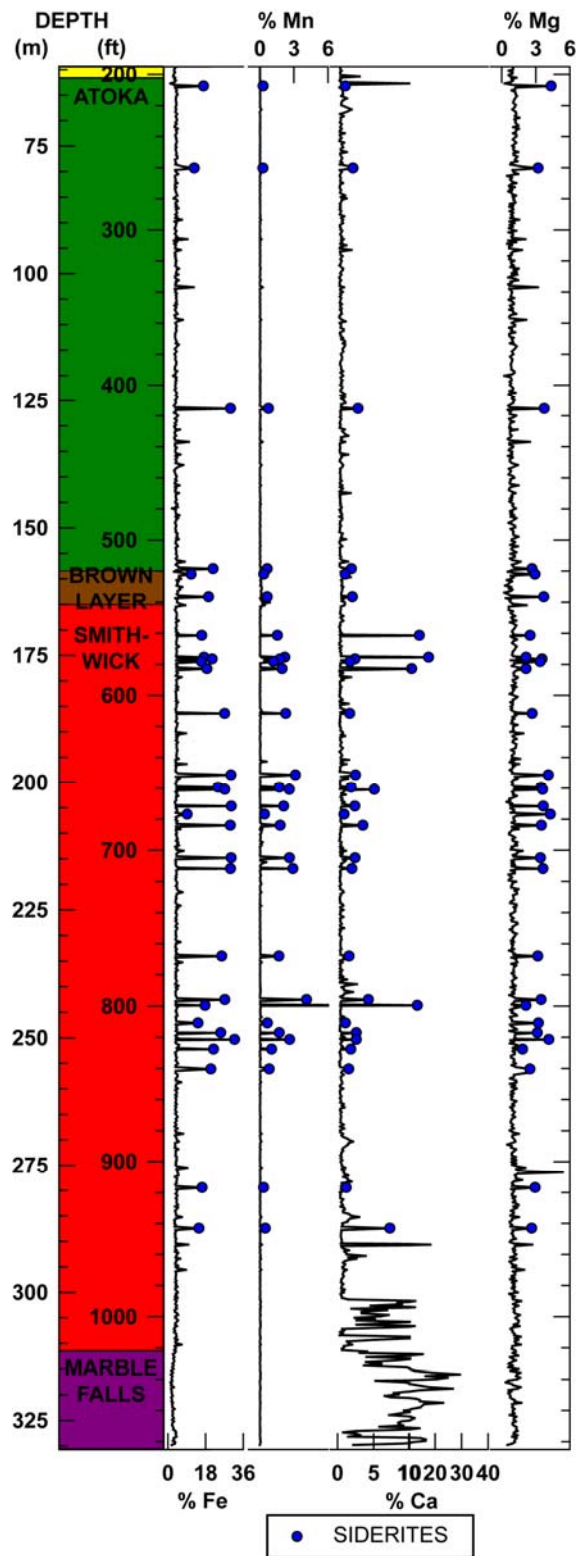


Figure 3.6 Fe, Mn, Ca, and Mg chemostratigraphy in the Walker D-1-1 core.

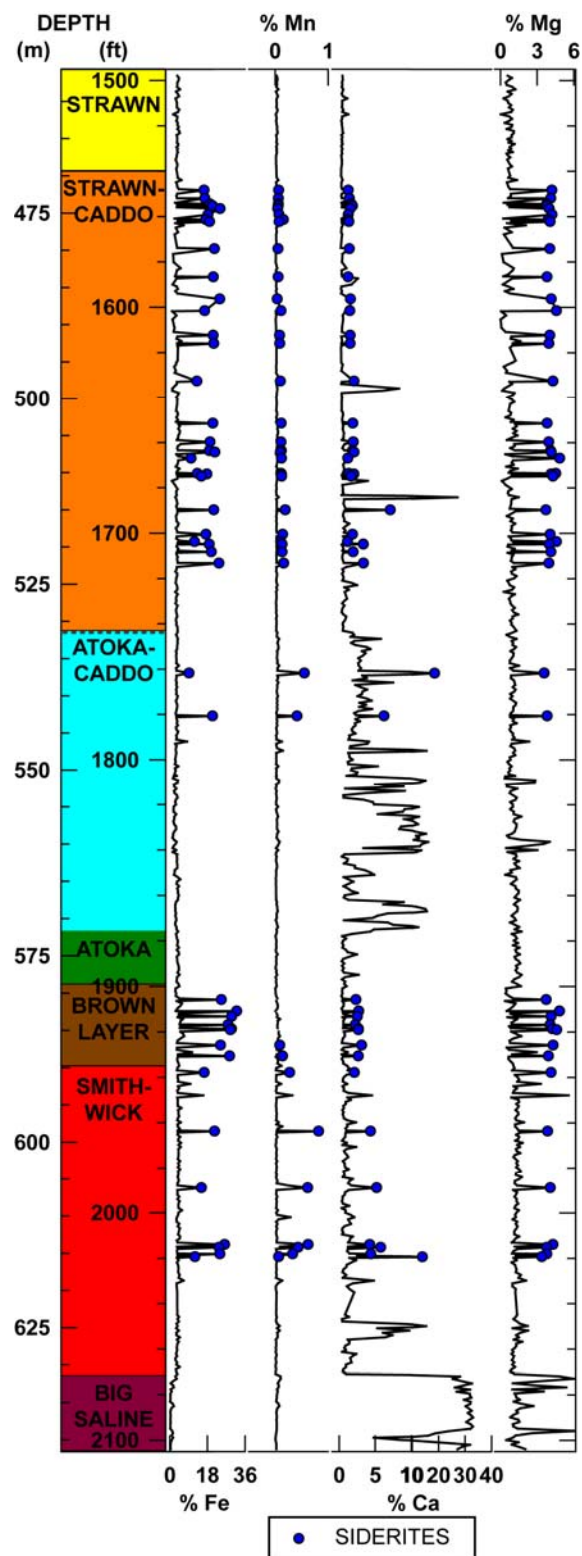


Figure 3.7 Fe, Mn, Ca, and Mg chemostratigraphy in the Potter C-9-1 core.

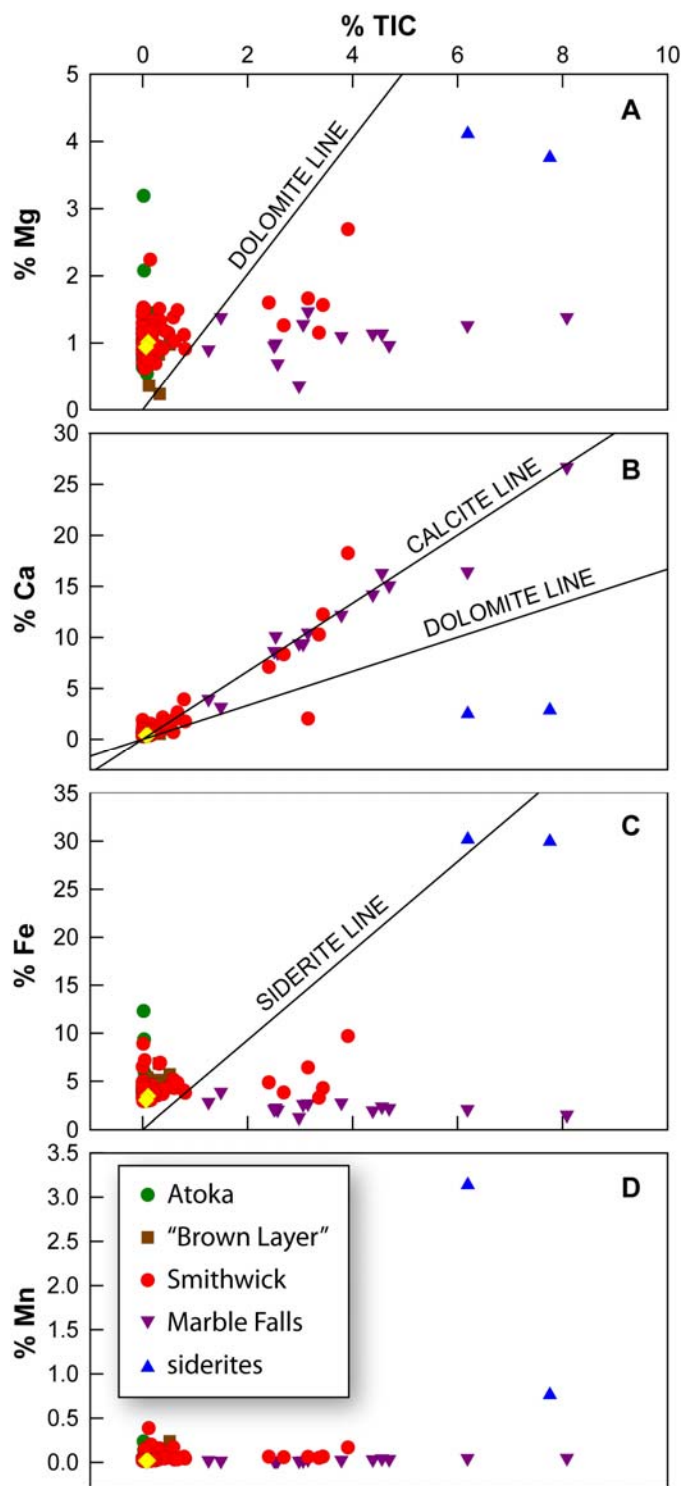


Figure 3.8 A subset of 225 samples from the Walker D-1-1 at ~4-foot intervals used to measure total inorganic carbon (TIC) and plotted against the weight percent concentrations of Mn, Fe, Ca, and Mg.

As previously discussed, minor amounts of Fe are fixed in pyrite. Analyzing relationships between iron, sulfur, and total organic carbon (TOC) can provide insight into depositional conditions (Dean and Arthur, 1989; Rowe et al, 2008). Pyrite is visible in the core both macro- and microscopically, but relatively infrequent. Plotting the weight percent of sulfur measured in a subset of 245 (225+20 additional samples used as standards) samples against the weight percent of Fe in the samples reveals an Fe-excess relative to pyrite (**figure 3.9A**). The degree of pyritization (DOP) provides insight into the redox conditions during deposition (Raiswell et al, 1988). DOP values are calculated from the ratio of pyritic Fe/total reactive Fe, but can be approximated using the ratio of pyritic Fe/total Fe (DOP_T) (Raiswell and Berner, 1986). Excluding the siderite-rich samples, and assuming that all S is in pyrite, the average DOP_T values for the Atoka and Smithwick formations are 0.14. **Figure 3.9B** shows the relationship between %S and %TOC. The majority of the samples have a positive correlation and fall close to the “normal marine” line as defined by Berner and Raiswell, 1983. Plotting the elements (Fe-S-TOC) en masse (Dean and Arthur, 1989) affirms the high percentage of Fe compared to pyrite, and the lack of correlation between the samples and pyrite formation (**figure 3.10**).

3.2.3 Detrital Fraction

The aluminum content of marine sediments is usually considered to be associated with the detrital fraction, due to its general immobility and aluminosilicate affiliation (Tribovillard et al, 2006). Elements like Ti and Zr, which generally occur at much lower concentrations than Al, are certainly reflective of detrital inputs due to their ultra-low seawater abundance (Li, 1982), and their lack of participation in biological cycling. Therefore, a dominantly linear relationship between Ti (or Zr) and another element in mudrocks reflects that the element in question is largely of detrital origin. Elements of similar detrital affinity are Th, Nb, Y, and very often, Si, although many mudrocks contain Si of biogenic origin.

The linear relationship between %Al and %Ti in both the Walker and Potter cores (**figures 3.11 and 3.12**) would suggest that Al is associated with the detrital clay fraction.

Crossplotting, potentially detrital, or more specifically, clay-associated elements to Al, can help determine if a relationship exists and how it varies stratigraphically. Ratioing an elemental concentration to the concentration of Al will hypothetically yield a “detrital clay normalized” value (Tribovillard et al, 2006).

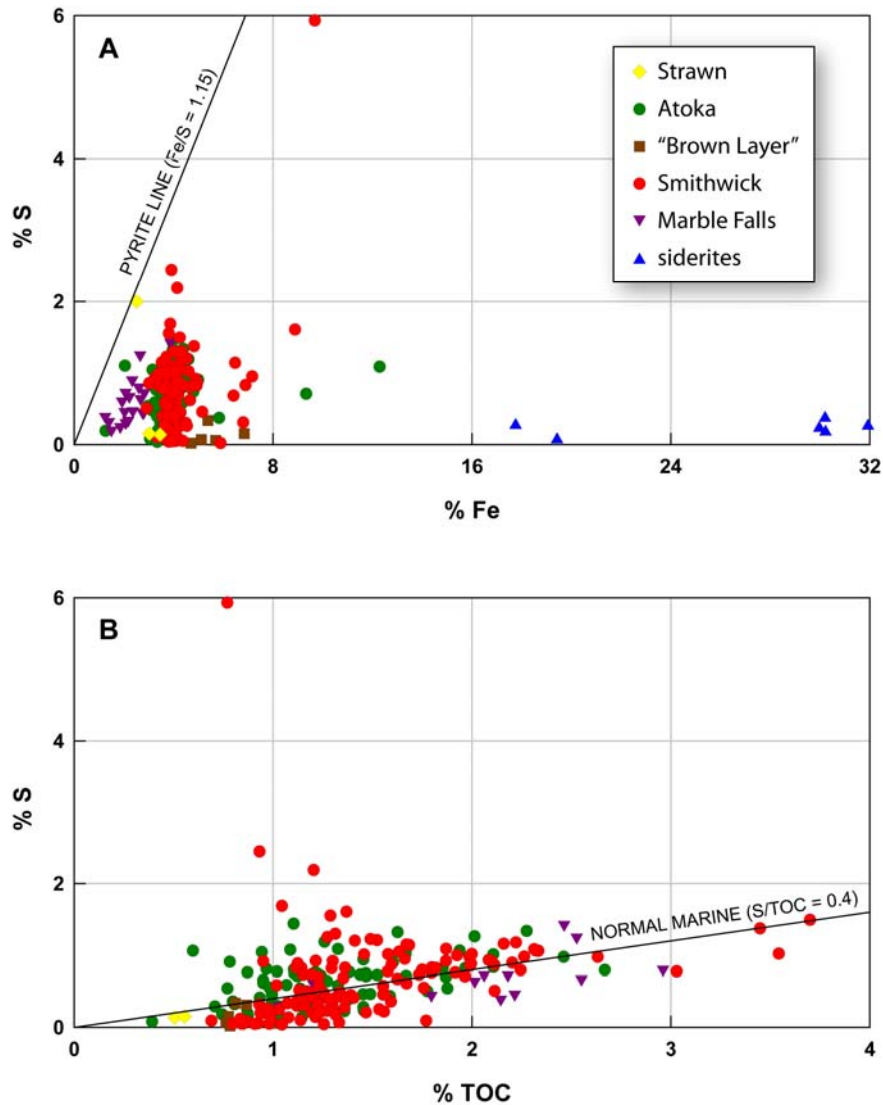


Figure 3.9 Two crossplots of A) weight percentages of Fe and S, and B) weight percentages of S and TOC from a subset of 245 samples from the Walker D-1-1 core. Normal marine line as defined by Berner and Raiswell, 1983.

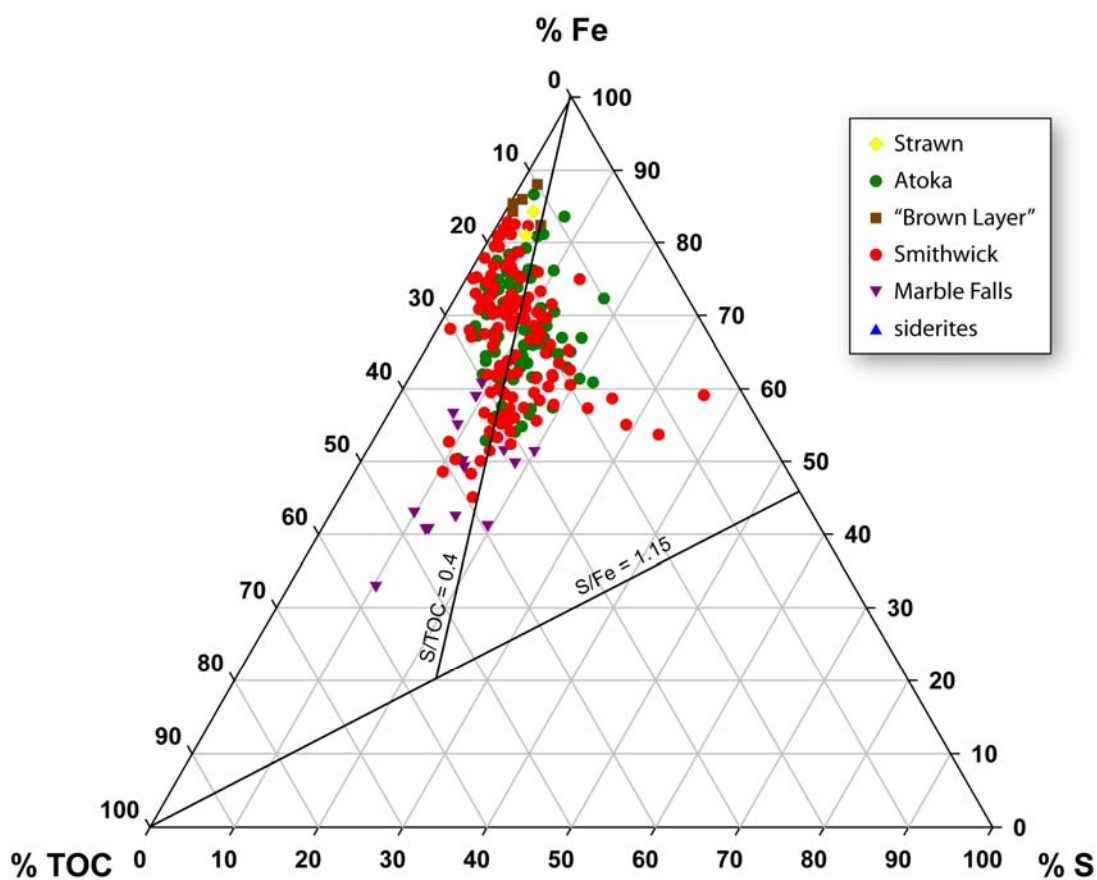


Figure 3.10 Ternary diagram depicting Fe-S-TOC relationships from a 225 subset of samples from the Walker D-1-1 core (after Dean and Arthur, 1989).

In both drill cores there is an indiscriminate affiliation between Mg and Al, suggesting that the majority of Mg is not clay-bound (**figures 3.11 and 3.12**). Iron is inversely related to Al in the siderite-rich samples, but is positively related to Al in most other samples from all formations, indicating a large Fe-bearing, detrital clay fraction. When samples from the Walker core are evaluated as one group, an overall positive linear relationship is evident between most elements (Fe, Si, K, Ti, and trace elements) and Al (**figure 3.11**). However, this relationship breaks down when the results are evaluated based on formation or unit, and it can be observed in **Figure 3.11** that much of the linearity of the inter-elemental plots is due to samples with variable Ca- and/or Fe-dilution. Samples from the brown layer fall off and to the right of most of

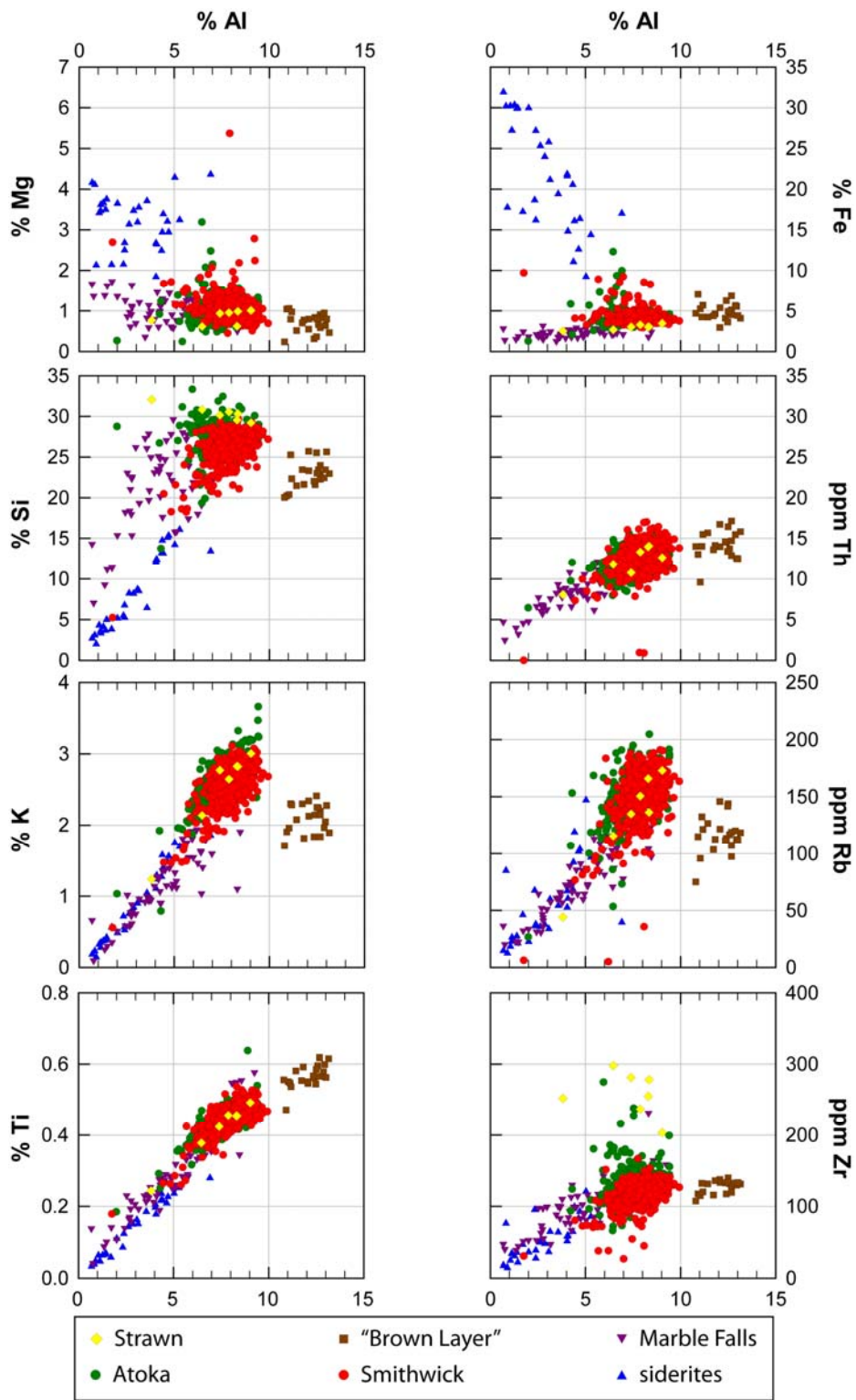


Figure 3.11 Crossplots of potentially terrigenous elements against Al by formation from the Walker D-1-1 core. (Thorium was not measured on siderite samples).

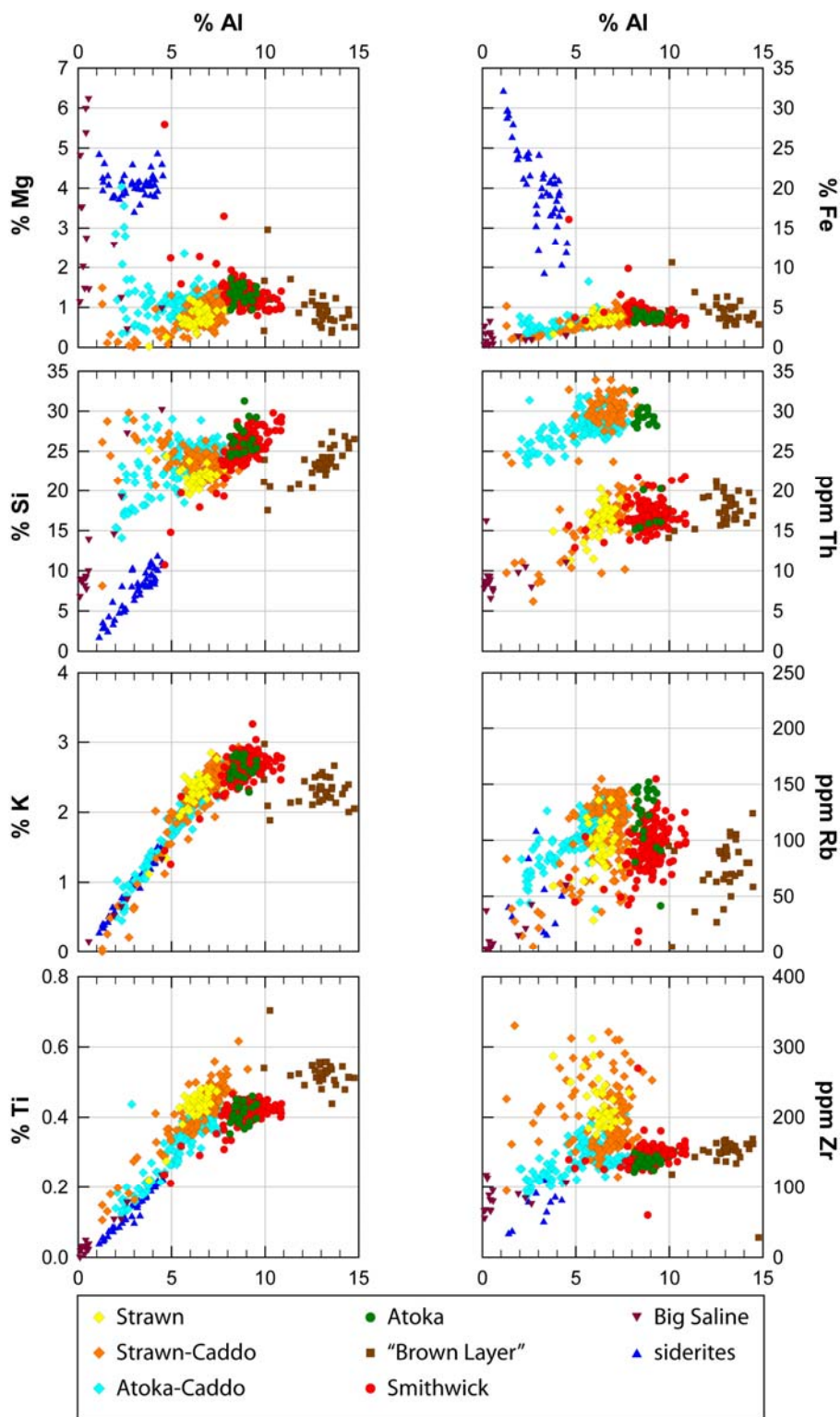


Figure 3.12 Crossplots of potentially terrigenous elements against Al by formation from the Potter C-9-1 core. (Thorium was not measured on siderite samples).

the X versus %Al biplots because of their high and largely invariant Al concentration relative to other elemental concentrations.

Figure 3.12 reveals that samples from the Potter core define similar chemostratigraphic trends to those observed in the Walker core. Nonetheless, a higher degree of elemental variability is evident because of the additional formations. Specifically, the Atoka and underlying Smithwick mudrocks possess similar chemical characteristics in both drill cores; however, Th concentrations in samples from the Potter core differ notably from those in the Walker core (**figures 3.11 and 3.12**). The average Th concentration in the Smithwick and Atoka formations of the Walker core is 12 ppm, but in the Potter core, the Smithwick averages 17 ppm Th and the Atoka averages 25 ppm Th. Rubidium concentrations in both the Smithwick and Atoka formations average approximately 50 ppm less in the Potter core when compared with the Walker core. The Smithwick has comparable Ti concentrations, averaging ~0.4% in both cores, but a slightly higher average Zr concentration (145 ppm Zr compared to 118 ppm Zr) is observed in the Potter core (**table 3.2**).

Stratigraphic plots of typically terrigenous elements (e.g., Al, Si, Ti, and Zr) (**figures 3.13 and 3.14**), reveal fluctuations in the amount and characteristics of detrital material inputs. The ratioed plots mirror Al with varying degrees, depending on their enrichments above the clay fraction. The Smithwick formation preserved in both cores displays well-defined, quasi-cyclical shifts in detrital input (horizontal grey highlights in **Figures 3.13 and 3.14**). This pattern is best observed in the stratigraphic changes in Si/Al of the Walker core (**figure 3.13**) and the down-core shifts in Ti/Al of the Potter core (**figure 3.14**). The observed oscillations are diminished to non-existent in Zr/Al and Zr/Ti of either core. The stratigraphic changes in Zr/Ti and Zr/Al are similar because of the linear relationship between Ti and Al observed in **Figures 3.8 and 3.9**. The strong correlation between Ti and Al is responsible for the more subdued stratigraphic fluctuations in Ti/Al relative to the other element/Al trends in the Potter core overall; however, the Ti/Al has the most pronounced oscillations in the Smithwick section compared to the other chemostratigraphic ratios (**figure 3.14**).

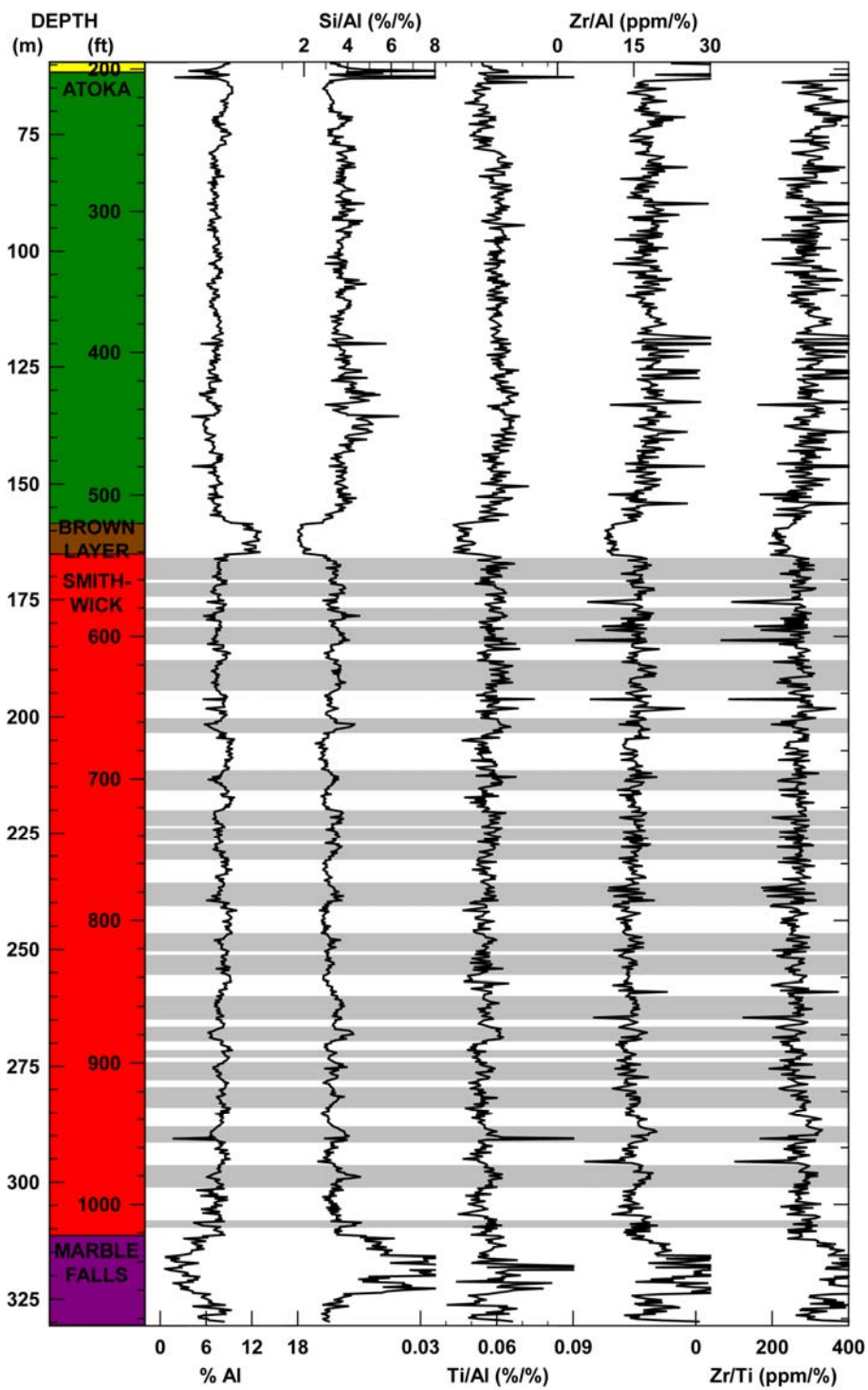


Figure 3.13 Stratigraphic plots of Al, Si/Al, Ti/Al, Zr/Al, and Zr/Ti for the Walker D-1-1 core. Grey bars in the Smithwick section highlight cyclical sedimentation. In the interest of scaling, so that detrital variability can be evaluated, siderite-rich samples are not plotted.

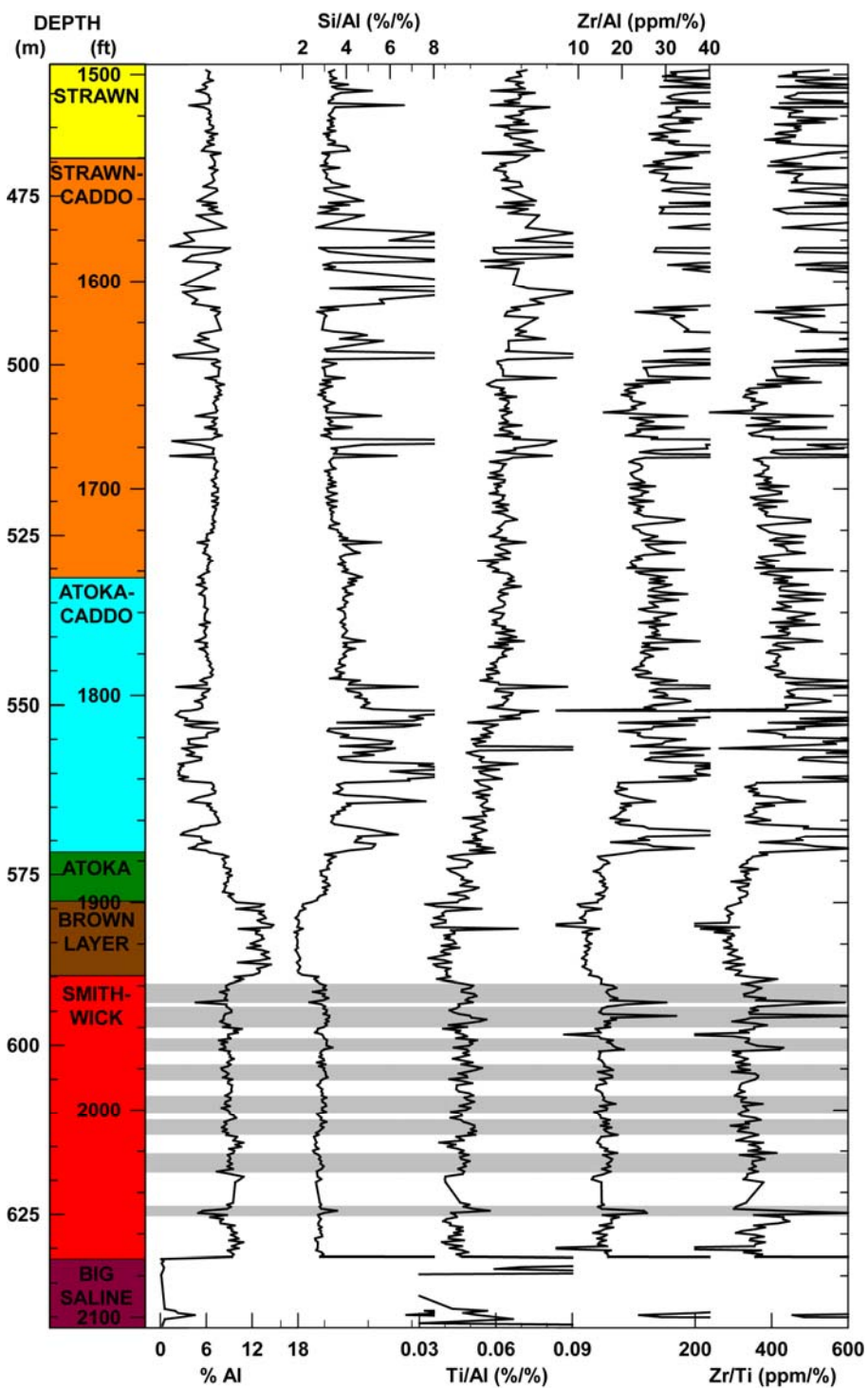


Figure 3.14 Stratigraphic plots of Al, Si/Al, Ti/Al, Zr/Al, and Zr/Ti for the Potter C-9-1 core. Grey bars in the Smithwick section highlight cyclical sedimentation. In the interest of scaling, so that detrital variability can be evaluated, siderite-rich samples are not plotted.

The Atoka section in the Walker core shows a slight increase in Si/Al and Zr/Al compared to the Smithwick section (**figure 3.13**). This indicates a change in the characteristics of the detritus from the Smithwick to the Atoka. In the Potter core, the Si/Al is higher in the Atoka, relative to the Smithwick, but this is not the case for Zr/Al. Ti/Al is consistent in the Atoka and Smithwick for both cores. Progressing upward from the Atoka in the Potter core, there is a substantial increase in Si and Zr relative to Al. Across the Atoka-Caddo/Strawn-Caddo and the Strawn-Caddo/Strawn boundaries there are zones of relatively stable Al. The stratigraphically lower Atoka-Caddo/Strawn-Caddo stable Al zone is expressed in Si/Al, Ti/Al, Zr/Al, and Zr/Ti with a decrease in the range of values compared to the lower Atoka-Caddo. The heightened variability expressed in Ti/Al, Zr/Al, and Zr/Ti above the lower stable Al zone continues through the upper stable Al zone. However, the Si/Al chemostratigraphy, except for two substantial spikes decreases again at the Strawn section in conjunction with the upper stable Al zone.

3.2.4 Trace Metals

Trace elements are often used as proxies to infer information about paleoenvironments (e.g. Brumsack, 1989; Dean and Arthur, 1989; Rimmer, 2004; Cruse and Lyons, 2004; Tribovillard et al, 2006; Algeo et al, 2007; Algeo and Maynard, 2008; Algeo and Tribovillard, 2009; Piper and Calvert, 2009). Enrichment factors are frequently used to standardize trace metal concentrations for analysis (Tribovillard et al, 2006). Using Wedepohl, 1971, average shale values enrichment factors are calculated as follows:

$$EF_{\text{element X}} = (X/Al)_{\text{sample}} / (X/Al)_{\text{average shale}}, \text{ where } EF_X > 1 = \text{enriched and } EF_X < 1 = \text{depleted}$$

Figures 3.15 and 3.16 reveal that the overall trace element EFs are relatively low, typical of an average shale (EF=1). In most cases, samples from the Smithwick and Atoka formations are only slightly enriched in both cores (**table 3.3**). The Cr concentration straddles the average shale value for both formations in both cores. The Co concentration is close to unity for the Atoka and Smithwick samples in the Walker core; however, in the Smithwick

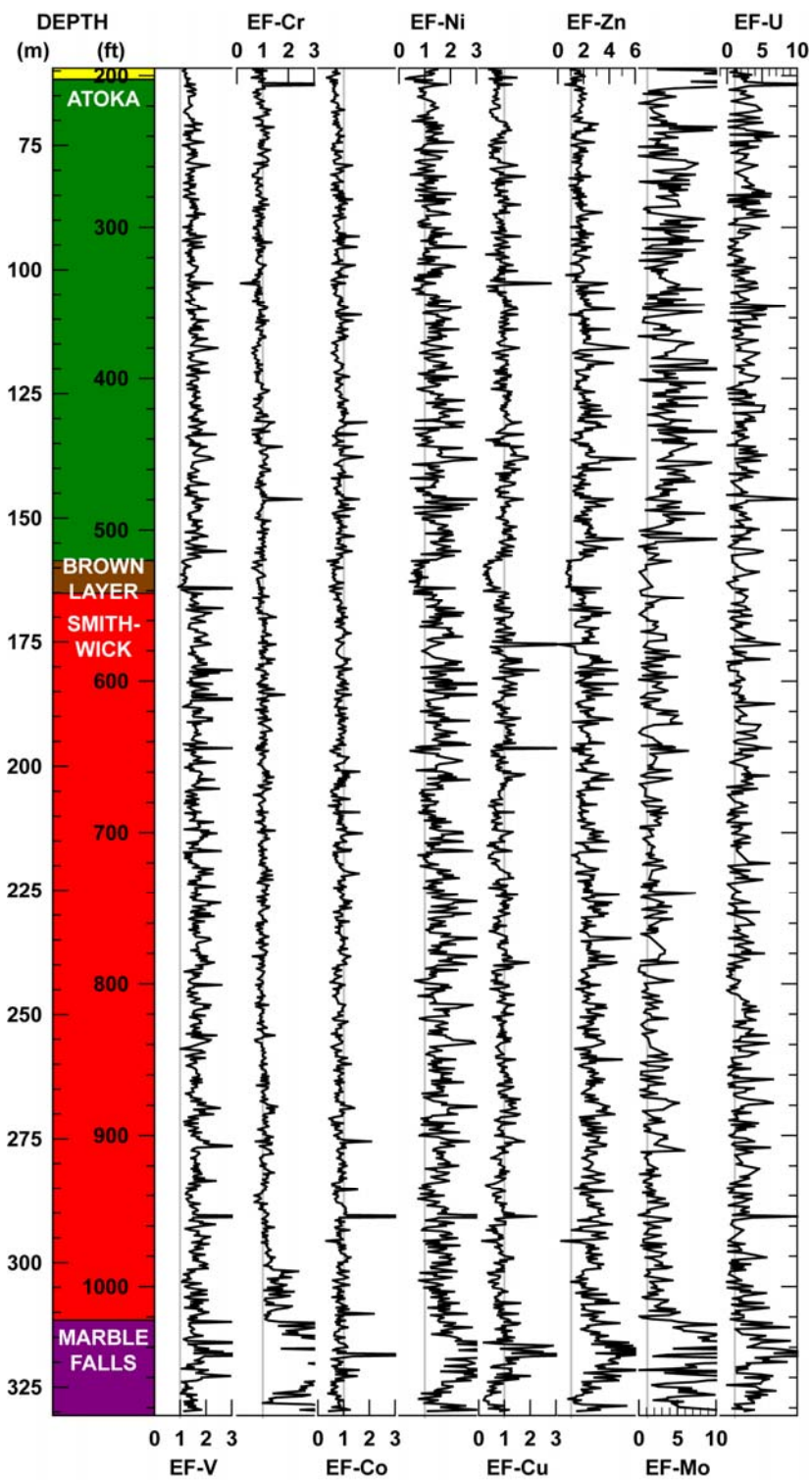


Figure 3.15 Chemostratigraphy of trace metal enrichment factors for the Walker D-1-1 core. Grey lines indicate $EF_x=1$. EFs cannot be calculated for siderite-rich samples.

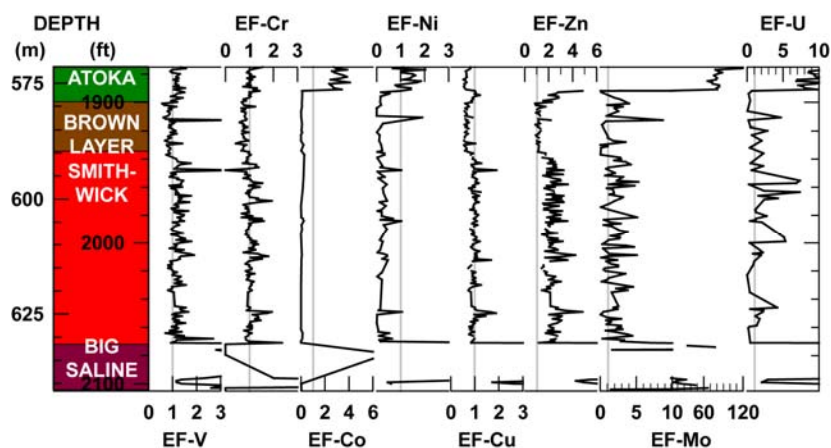


Figure 3.16 Chemostratigraphy of trace metal enrichment factors for the Potter C-9-1 core. Grey lines indicate $EF_x=1$. EFs cannot be calculated for siderite-rich samples or carbonate samples of the Big Saline.

section of the Potter core the Co is depleted throughout, but becomes enriched in the Atoka. A similar pattern of higher values in the Atoka samples compared to the Smithwick samples exists in the Potter core for Ni, Mo, and U. In the Walker core, Mo and U have higher enrichments in the Atoka samples as well; however, the difference in the Walker core is much less significant than in the Potter (**table 3.3**). Molybdenum and uranium fluctuate across unity in both cores, but have average values ranging from 1.3 to 62.5 (**table 3.3**); however, some samples were not included in the calculations since they were below detection limits. Copper is generally depleted throughout both cores. The Zn in both cores is slightly enriched in the Atoka and Smithwick samples with values averaging 2.0 to 2.7; however, the average Zn value for the Potter does not include the upper portion of the Atoka because the samples are below the lower threshold of calibration. The values are absent in the EF-Zn chemostratigraphy (**figure 3.16**) because they cannot be obtained, and therefore result in an erroneously high EF-Zn average for the Atoka samples of the Potter (**table 3.3**).

The mild enrichments in the trace metals found in both the Smithwick and Atoka formations has the potential to be part of the hydrogenous (seawater origin), biogenous (biological origin), or terrigenous (detrital origin) fraction. Crossplotting TOC and Al with the

Table 3.3 Quantified Enrichment Factors for Trace Metals
(The number of samples (n) vary within a formation when samples fell below the lower threshold of calibration and were subsequently omitted.)

FORMATION	Atoka		Brown Layer		Smithwick		Marble Falls		Whole Core			
	Walker	Potter	Walker	Potter	Walker	Potter	Walker	Potter	Walker	Potter		
EF-V	n =	314	23	22	35	485	128	63	-	884	186	
	MEAN	1.53	1.16	1.29	0.96	1.67	1.23	1.68	-	1.61	1.17	
	MEDIAN	1.49	1.15	1.18	0.87	1.60	1.18	1.52	-	1.54	1.13	
	RANGE	MIN	1.11	0.91	0.93	0.57	1.02	0.70	1.03	-	0.93	0.57
		MAX	2.77	1.52	3.89	3.23	5.25	3.46	6.62	-	6.62	3.46
EF-Cr	n =	314	23	22	35	484	127	63	-	883	185	
	MEAN	0.96	1.02	0.87	0.78	1.08	1.07	3.58	-	1.21	1.01	
	MEDIAN	0.93	1.04	0.86	0.76	1.05	1.00	3.16	-	1.02	0.98	
	RANGE	MIN	0.16	0.74	0.61	0.44	0.63	0.68	1.02	-	0.16	0.44
		MAX	6.47	1.42	1.10	1.24	2.38	2.36	14.30	-	14.30	2.36
EF-Co	n =	314	17	22	12	483	18	63	-	882	47	
	MEAN	0.86	2.75	0.66	0.06	0.90	0.09	0.90	-	0.88	1.05	
	MEDIAN	0.83	2.79	0.64	0.06	0.87	0.06	0.78	-	0.84	0.11	
	RANGE	MIN	0.50	0.09	0.38	0.00	0.34	0.00	0.41	-	0.34	0.00
		MAX	1.89	4.08	0.98	0.21	6.58	0.28	5.35	-	6.58	4.08
EF-Ni	n =	314	20	22	13	483	50	63	-	882	83	
	MEAN	1.36	1.13	0.84	0.25	1.61	0.29	2.43	-	1.56	0.48	
	MEDIAN	1.31	1.17	0.78	0.12	1.54	0.23	2.15	-	1.46	0.25	
	RANGE	MIN	0.27	0.16	0.42	0.00	0.45	0.01	0.78	-	0.27	0.00
		MAX	3.37	2.04	2.16	1.91	17.19	1.07	11.17	-	17.19	2.04
EF-Cu	n =	314	23	22	35	485	127	63	-	884	185	
	MEAN	0.97	0.75	0.43	0.66	0.93	0.99	1.07	-	0.94	0.90	
	MEDIAN	0.96	0.65	0.39	0.64	0.90	0.96	0.97	-	0.91	0.91	
	RANGE	MIN	0.30	0.53	0.20	0.54	0.15	0.72	0.20	-	0.15	0.53
		MAX	2.80	1.21	1.03	1.02	3.69	1.91	5.40	-	5.40	1.91
EF-Zn	n =	314	8	22	34	484	126	63	-	883	168	
	MEAN	2.04	2.72	1.09	1.21	2.48	2.34	3.34	-	2.35	2.13	
	MEDIAN	1.90	2.69	0.93	1.17	2.38	2.25	3.07	-	2.20	2.09	
	RANGE	MIN	0.58	1.56	0.67	0.87	0.04	1.16	0.82	-	0.04	0.87
		MAX	6.22	4.84	3.33	2.29	5.64	4.83	8.75	-	8.75	4.84
EF-Mo	n =	264	19	6	16	333	88	59	-	662	123	
	MEAN	4.52	62.51	1.34	1.99	1.99	2.10	8.24	-	3.55	11.42	
	MEDIAN	3.66	78.22	0.94	1.06	1.68	1.93	7.27	-	2.60	2.06	
	RANGE	MIN	0.02	0.07	0.11	0.04	0.01	0.04	0.09	-	0.01	0.04
		MAX	142.13	88.24	4.13	8.73	7.27	6.98	23.96	-	142.13	88.24
EF-U	n =	246	18	12	9	337	41	53	-	648	68	
	MEAN	2.53	7.51	1.63	1.41	2.05	2.03	4.80	-	2.45	3.40	
	MEDIAN	2.30	8.61	1.39	0.68	1.78	1.35	4.07	-	2.07	2.01	
	RANGE	MIN	0.04	0.24	0.02	0.07	0.00	0.03	0.04	-	0.00	0.03
		MAX	15.24	11.33	4.53	4.72	10.73	7.37	30.56	-	30.56	11.33

trace metals that showed some enrichment provides some indication of their associations, and hence, their origins. A strong linear relationship does not exist with any of the elements in **Figure 3.17**. However, Ni, Zn, and U show a positive correlation with TOC. Vanadium, Ni, and Zn display the same dilution effect as the major element *versus* Al plots (**figures 3.11 and 3.12**)

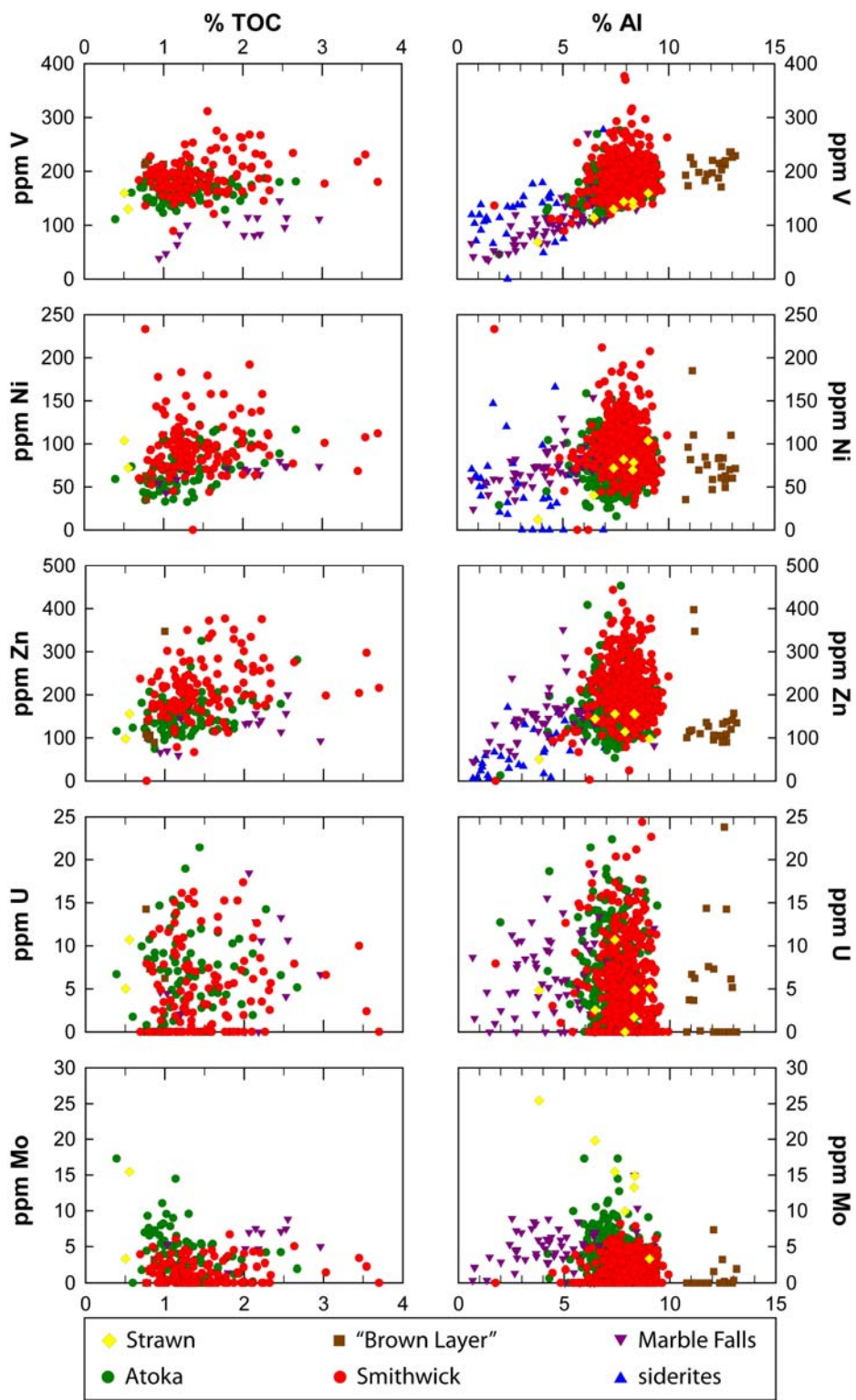


Figure 3.17 Trace metal concentrations plotted against %TOC (225 sample subset) and %Al (923 samples) for the Walker D-1-1 core.

due to Ca and Fe-dilution, giving the misconception that there is a definitive association. There is not an observable trend in the Smithwick samples alone, because the formation is very chemically and mineralogically invariant with the exception of intermittent siderite bed/nodules.

3.2.5 Organic Carbon and Nitrogen

Figure 3.18 displays the chemostratigraphy of %TOC, %N, C/N, $\delta^{15}\text{N}$, and $\delta^{13}\text{C}$ through the Walker core. Similar to the trace element stratigraphy, the Smithwick isotopes, TOC, and N have relatively small ranges. The differences between the maximum and minimum values of %TOC, %N, C/N, $\delta^{15}\text{N}$, and $\delta^{13}\text{C}$ for the Smithwick are 3.0, 0.2, 10.9, 3.2, and 2.6, respectively (**table 3.4**). While the stratigraphic fluctuations in the Smithwick samples of the aforementioned parameters have limited amplitudes, the average values for %TOC, %N, and C/N are higher in the lower Smithwick (**figure 3.18**). In addition, the frequency of the oscillations varies through the Smithwick. The lower Smithwick (950-1021 ft/290-311 m), containing the Ca-diluted samples, has high frequency oscillations in %TOC, %N, and $\delta^{13}\text{C}$ averaging 0.11 peaks/ft. The frequency decreases by ~50% in middle Smithwick samples (810-950 ft/247-290m) to 0.05 peaks/ft in %TOC and %N, and 0.06 peaks/ft in $\delta^{13}\text{C}$. The frequency increases again slightly in %TOC and %N to 0.07 peaks/ft in the upper Smithwick samples (542-810 ft/165-247 m), but the $\delta^{13}\text{C}$ maintains 0.06 peaks/ft. $\delta^{15}\text{N}$ has a consistent frequency of 0.06 peaks/ft through the entire Smithwick sampling interval. The C/N ratio has slightly less infrequent oscillations in the middle Smithwick samples.

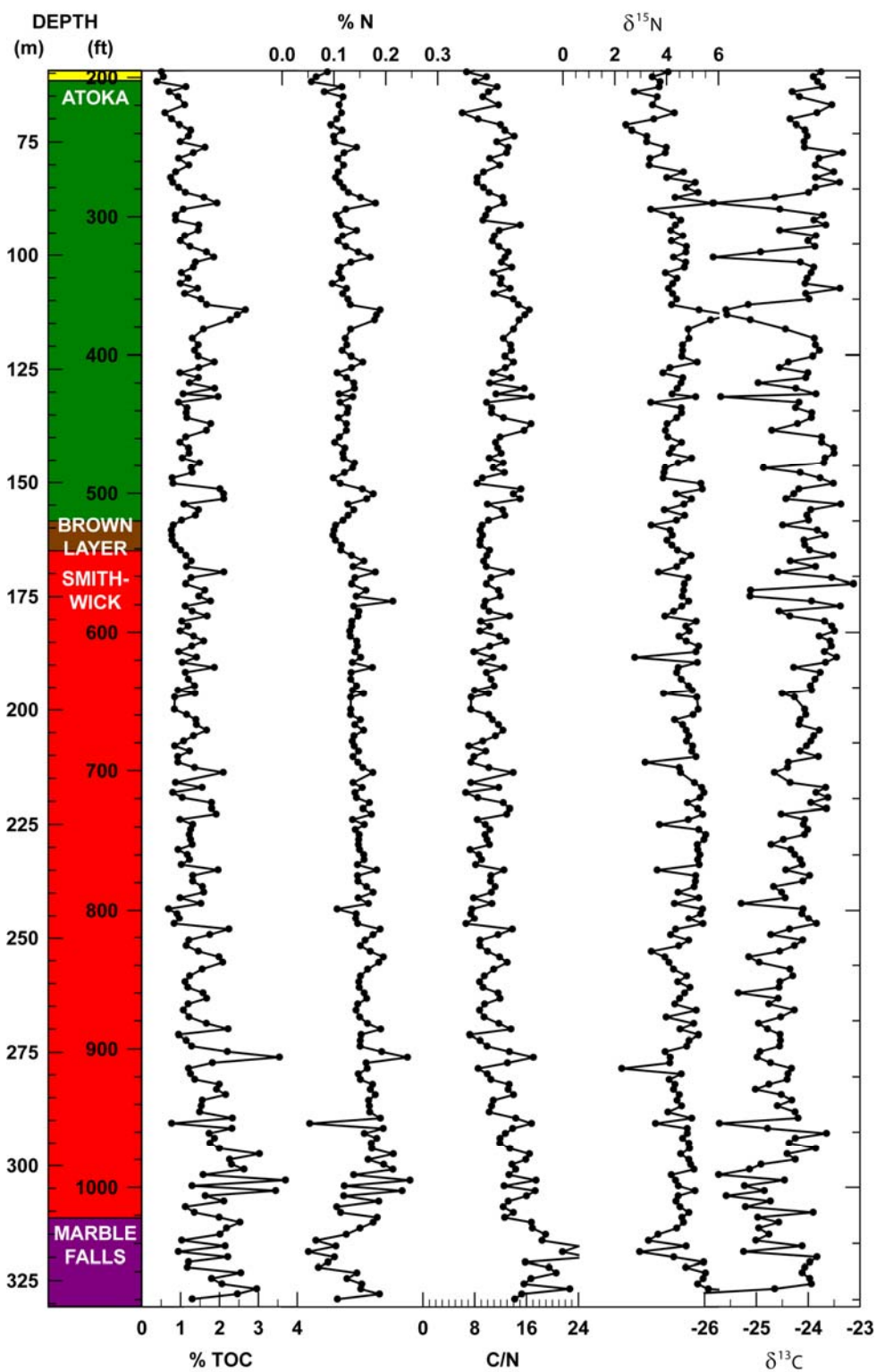


Figure 3.18 Values of TOC, N, C/N, $\delta^{15}\text{N}$, and $\delta^{13}\text{C}$ for a subset of 235 samples from the Walker D-1-1 core.

Table 3.4 Quantified %TOC, %N, C/N, $\delta^{15}\text{N}$, and $\delta^{13}\text{C}$ for the Walker D-1-1 Core

	FORMATION	Atoka	Brown Layer	Smithwick	Marble Falls	Whole Core	
	n =	80	6	122	15	223	
% TOC	MEAN	1.30	0.83	1.49	1.90	1.44	
	MEDIAN	1.22	0.80	1.33	2.06	1.30	
	RANGE	MIN	0.39	0.76	0.69	0.94	0.39
		MAX	2.67	1.00	3.70	2.96	3.70
% N	MEAN	0.12	0.11	0.16	0.12	0.14	
	MEDIAN	0.12	0.10	0.15	0.12	0.14	
	RANGE	MIN	0.06	0.10	0.05	0.05	0.05
		MAX	0.19	0.11	0.25	0.19	0.25
C/N	MEAN	11.98	9.20	10.94	18.84	11.80	
	MEDIAN	11.98	9.00	10.52	18.41	11.47	
	RANGE	MIN	6.08	8.83	6.63	14.19	6.08
		MAX	16.80	10.30	17.48	25.51	25.51
$\delta^{15}\text{N}$	MEAN	4.3	4.1	4.7	5.1	4.5	
	MEDIAN	4.3	4.2	4.8	4.8	4.6	
	RANGE	MIN	2.4	3.4	2.3	3.0	2.3
		MAX	6.4	4.4	5.5	9.3	9.3
$\delta^{13}\text{C}$	MEAN	-24.1	-24.0	-24.3	-24.7	-24.3	
	MEDIAN	-24.0	-24.0	-24.3	-24.6	-24.2	
	RANGE	MIN	-25.8	-24.5	-25.7	-26.6	-26.6
		MAX	-23.3	-23.7	-23.1	-23.8	-23.1

3.3 Petrographic Observations

Samples that represent all formations within the sampling interval (55-1083 ft/17-330 m below surface) were selected from the Walker D-1-1 core for petrographic observation. **Table 3.5** displays scanned images of the thin sections for all samples along with brief petrographic descriptions, and select petrographic images taken of the thin sections (4x-20x magnification). Overall, the thin sections reveal a coarsening upward sequence, with increasing quartz content beginning in the Smithwick and extending into the Strawn formation, with the brown layer being the exception. The Strawn-age grains are slightly mature and the samples possess considerable plant debris. Oscillation between mudrock and siltstone lithologies occurs at the boundary between the Atoka and Strawn Formations. In addition to being slightly siltier than the Smithwick, the Atoka has a marginal increase in detrital grains. The Smithwick is commonly fissile, while the Atoka is more indurated. Shell material is present in the Smithwick toward the

Table 3.5 Petrographic Observations and Images for the Walker D-1-1 Core

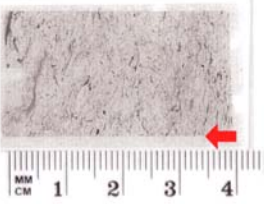
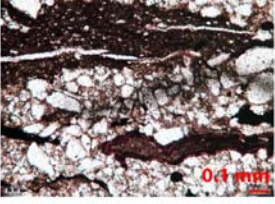
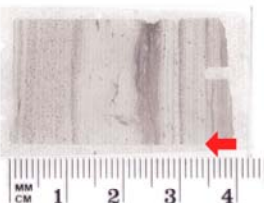
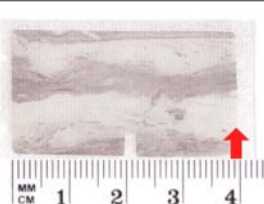
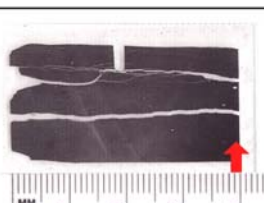
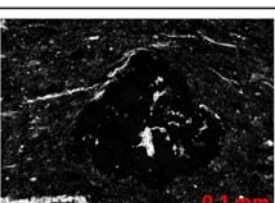
SMP #	DEPTH	(FT) (M)	PETROGRAPHIC NOTES	SCANNED THIN SECTION	PETROGRAPHIC IMAGES	
					A	B (when applicable)
4.3.4	94.89 28.92		Dominantly silt to fine sand-size subrounded moderately to well sorted quartz grains, some polycrystalline quartz grains, rich in organic matter (primarily plant debris) generally elongate parallel to compaction direction, some mica flakes, some plagioclase, and clay-size cement.			
9.2.4	144.18 43.95		Dominantly laminated subangular silt- and sand-size quartz grains with other sand-size extrabasinal grains and plant debris seams.			
16.4.4	201.25 61.34		Silty/muddy alternating irregular laminations (possibly from soft sediment deformation) with dominantly quartz silt, some organic particulate, and silty grains included in clay matrix layers.			
25.2.8	291.25 88.77		Dominantly clay-size particles with strong preferred orientation and significant pyrite (some framboidal).			

Table 3.5 - Continued

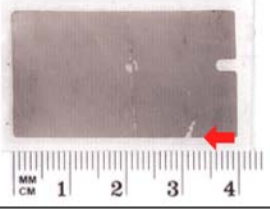
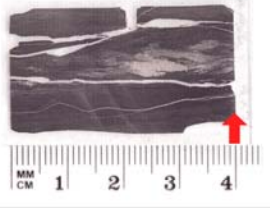
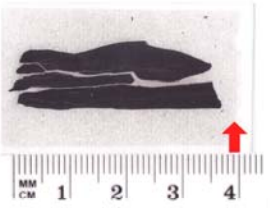
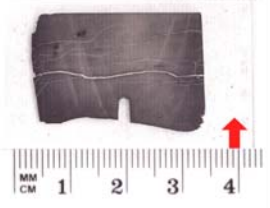
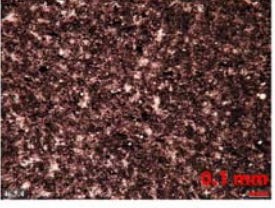
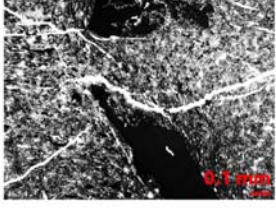
SMP #	DEPTH	(FT) (M)	PETROGRAPHIC NOTES	SCANNED THIN SECTION	PETROGRAPHIC IMAGES	
					A	B (when applicable)
37.3.8	415.36 126.60		Strongly homogeneous siderite matrix with some silt-size calcite and pyrite crystals.			
40.5.4	445.03 135.64		Primarily dark grey mudrock with wavy laminated bedding with silt-size quartz particles in the mudstone matrix and a very thin and wavy intrusive silty layer possibly a fine-scale flow-type structure.			
44.2.4	479.69 146.21		Dark grey to black fissile mudrock with interspersed silt-size quartz crystals and some microscopic fossils showing evidence of compaction.			
46.5.4	504.03 153.63		Dark grey to black mudrock with preferred orientation and occasional silt-size quartz, compaction features in microfossils, and some larger pyrite crystals.			

Table 3.5 - Continued

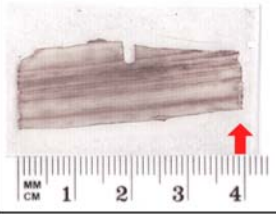
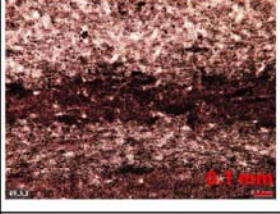
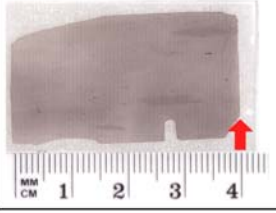
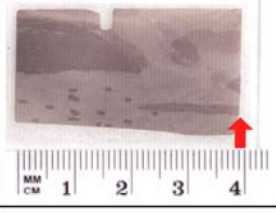
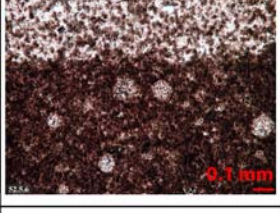
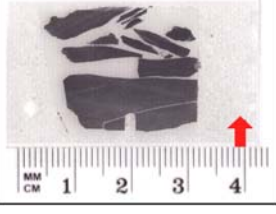
SMP #	DEPTH	(FT) (M)	PETROGRAPHIC NOTES	SCANNED THIN SECTION	PETROGRAPHIC IMAGES	
					A	B (when applicable)
49.3.1	527.83 161.06		Laminated brown and light brown clay layers with very dark brown-black clay- to silt-size minerals in the dark brown layers.			
50.2.8	536.58 163.55		Very fine-grained siderite matrix with siderite nodules elongated in the compaction direction, some clay- to silt-size calcite, and very few pyrite crystals.			
52.5.6	561.42 171.12		Calcitic matrix with dense zoned silt-size siderite grains and macroscopic brown siderite nodules comprised of amalgamated siderite grains with some silt- to very fine sand-size calcite concretions.			
57.2.4	602.69 183.70		Fissile dark grey mudrock with some silt-sized quartz grains and very few compacted microscopic fossils, microscopic linear black minerals with some rounded silt-size detrital grains.			

Table 3.5 - Continued

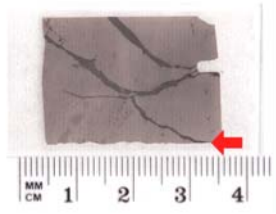
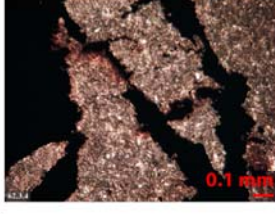
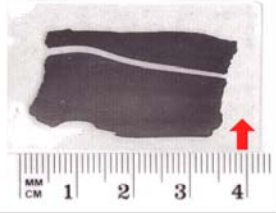

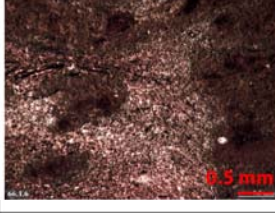
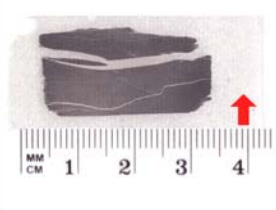
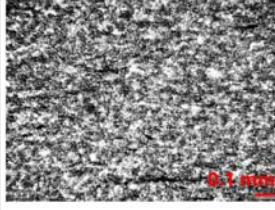
SMP #	DEPTH	(FT) (M)	PETROGRAPHIC NOTES	SCANNED THIN SECTION	PETROGRAPHIC IMAGES	
					A	B (when applicable)
62.3.4	651.36 198.53		Very fine-grained brown siderite with sponge spicules, some radiolarians, calcitic microscopic nodules, and pyrite-filled fractures.			
64.3.4	670.92 204.50		Fissile dark grey mudrock with microcrystalline quartz-replaced compacted microfossils, a few silt-size quartz grains and microscopic linear black minerals.			
66.1.6	686.42 209.22		Laminated dark grey mudrock matrix with some fissility and coalescing nodular siderite.			
75.2.4	770.92 234.98		Very fissile dark grey mudrock with both framboidal pyrite and some larger pyrite crystals.			

Table 3.5 - Continued

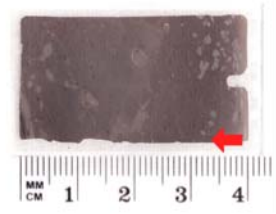

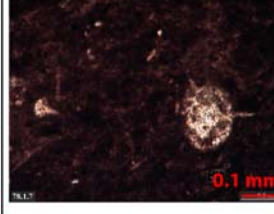
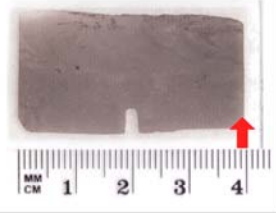

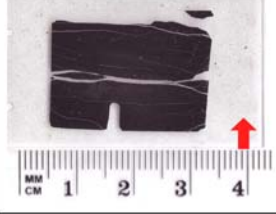

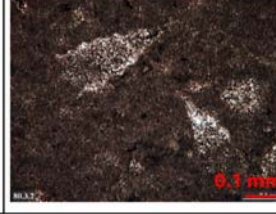
SMP #	DEPTH	(FT) (M)	PETROGRAPHIC NOTES	SCANNED THIN SECTION	PETROGRAPHIC IMAGES	
					A	B (when applicable)
78.1.7	799.58 243.71		Very fossiliferous (sponge spicules, radiolarians, shells) dark brown siderite with macroscopic but small darker and lighter brown nodules, some framboidal pyrite.			
80.3.2	821.42 250.37		Siderite with microfossils (primarily radiolarians and sponge spicules) and silt-size calcitic nodules, and haloed aggregates of framboidal pyrite.			
83.2.8	852.92 259.97		Fissile dark grey mudrock with sparse clay- to silt-size quartz grains and black grains, and a zone of framboidal pyrite.			
88.3.4	905.92 276.12		Fissile dark grey to black mudrock with abundant compacted microscopic shell material and framboidal pyrite, and some silt-size reddish-brown organic material.			

Table 3.5 - Continued


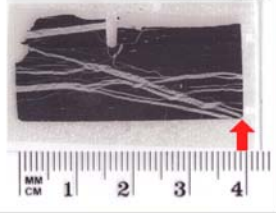

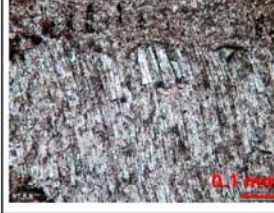
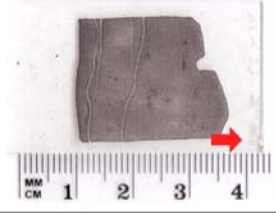
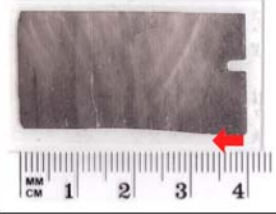
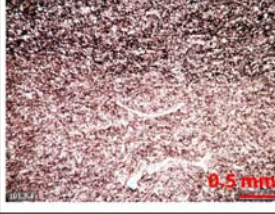
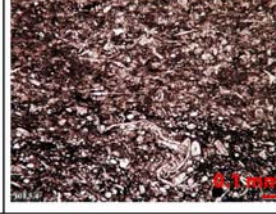
SMP #	DEPTH	(FT) (M)	PETROGRAPHIC NOTES	SCANNED THIN SECTION	PETROGRAPHIC IMAGES	
					A	B (when applicable)
93.2.4	953.69 290.69		Grain-supported carbonate with siderite cement, increasing abundance of framboidal pyrite to dominantly pyrite surrounding calcite/siderite grains upsection.			
97.5.8	997.92 304.17		Dark grey to black mudrock with abundant shell material, subhorizontal calcite-filled fractures primarily consisting of vertically aligned crystals, and some framboidal pyrite.			
99.3.8	1012.92 308.74		Dark grey calcareous mudrock with silt-size quartz and calcite grains, abundant broken shell material, and framboidal pyrite.			
101.5.4	1035.81 315.71		Argillaceous dark grey mudrock, alternating lighter and darker wavy laminations in clay matrix, abundant shell material, and pyrite framboids.			

Table 3.5 - Continued

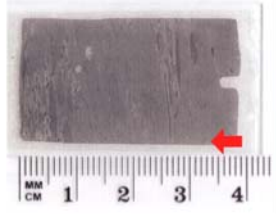

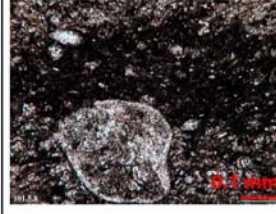
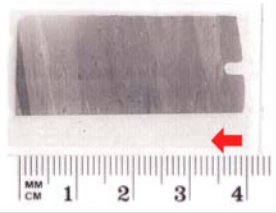
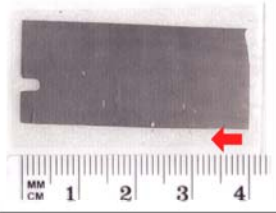
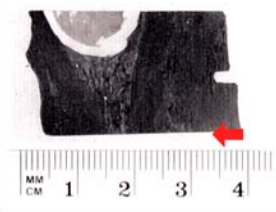
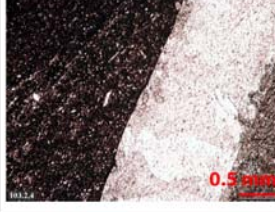

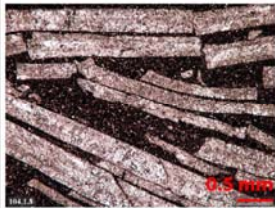
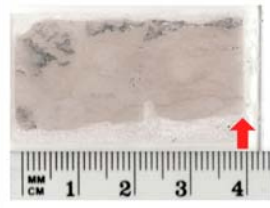
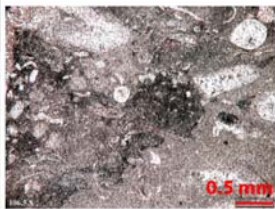
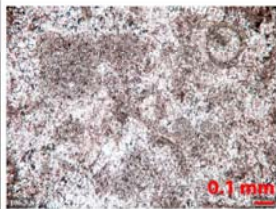
SMP #	DEPTH	(FT) (M)	PETROGRAPHIC NOTES	SCANNED THIN SECTION	PETROGRAPHIC IMAGES	
					A	B (when applicable)
101.5.8	1036.92 316.05		Argillaceous grey mudrock with darker clay-rich lenticular spots surrounded by lighter Ca-rich matrix, shell fragments, and detrital grains.			
102.1.8	1038.92 316.66		Argillaceous mudrock with light and dark grey fine-scale interfingering in matrix from increasing Ca-dilution, shell fragments parallel to bedding, and some detrital grains.			
102.4.8	1044.92 318.49		Grey calcareous mudrock with shell material and some pyrite.			
103.2.4	1049.69 319.95		Dark grey calcareous mudrock with brachiopod.			

Table 3.5 - Continued

SMP #	DEPTH	(FT) (M)	PETROGRAPHIC NOTES	SCANNED THIN SECTION	PETROGRAPHIC IMAGES	
					A	B (when applicable)
104.1.8	1057.92 322.45		Dark grey calcareous mudrock with thin-walled mollusks.			
106.5.8	1083.92 330.38		Fossiliferous limestone.			

Marble Falls boundary, but otherwise the mudrock portion is generally devoid of fossils. Many of the siderites, however, are quite fossiliferous. The dominant fossils in the samples consist of radiolarians and sponge spicules. The carbonate-rich Marble Falls contains considerable shell material. The samples directly below the Smithwick boundary represent a combination of calcareous and argillaceous mudrocks that eventually grades into fossiliferous limestone after ~60 ft (18 m) into the Marble Falls.

3.4 Scanning Electron Microprobe (SEM) Images

The SEM images are taken using thin sections from the Walker D-1-1 core. **Figures 3.19-3.22** represent highlights from the preliminary SEM study of four samples. The focus will be on displaying the pyrite observed in two samples and an elemental segregation of two siderite-rich samples. Backscattered electron images illustrate two different forms of pyrite present in the core (**figure 3.19**). Both are pyrite framboids, but have very different characteristics. The first image depicts a mudrock sample from the Atoka, and shows displacement in the clay matrix and coalescing of the pyrite. In addition, many of the remaining framboids are star-shaped and haloed (**figure 3.20**). The elemental mapping reveals Fe surrounding the amalgamated and individual framboids, but S is absent except in the cores. The second pyrite framboid (**figure 3.19**) is from a siderite in the Smithwick formation. This pyrite is comprised of framboids within framboids, showing no evidence of displacement in the surrounding sediment.

Smithwick strata in both cores possess intermittent siderite-rich intervals (**figures 3.6 and 3.7**). **Figure 3.21** shows elemental maps of zoned siderite grains comprising the siderite matrix of a sample from the Smithwick section of the Walker core. The clay-associated elements, Al and Si, are present in between the zoned siderite grains along with Ca. The siderite grains consist of primarily of Fe and Mn with Ba, Mn and Ca cores. **Figure 3.22** shows another siderite-rich sample with considerable Fe, Mn, Ca, and Ba throughout the matrix. The tiny Si grains and ring may be attributable to siliceous fossils.

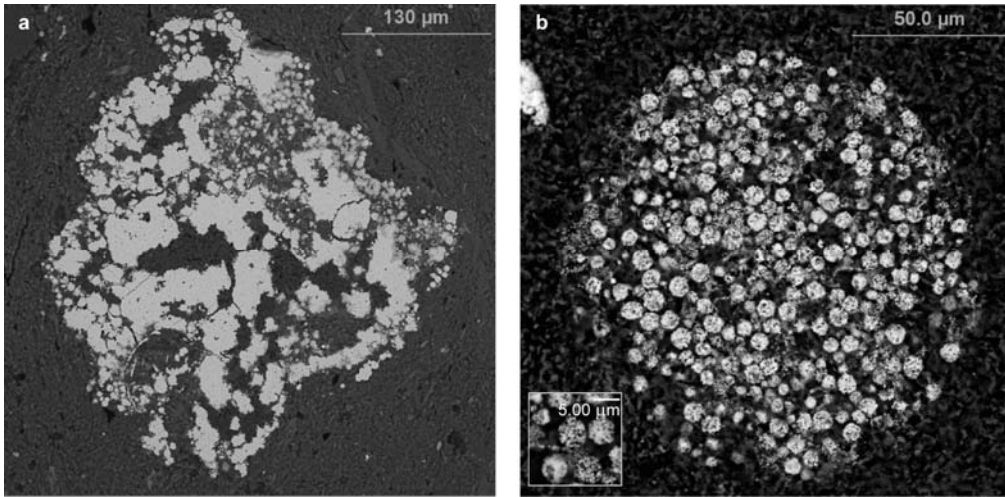


Figure 3.19 Backscatter electron images of pyrite from a) an Atoka mudrock (25.2.8) and b) a Smithwick siderite (80.3.2) in the Walker D-1-1 core.

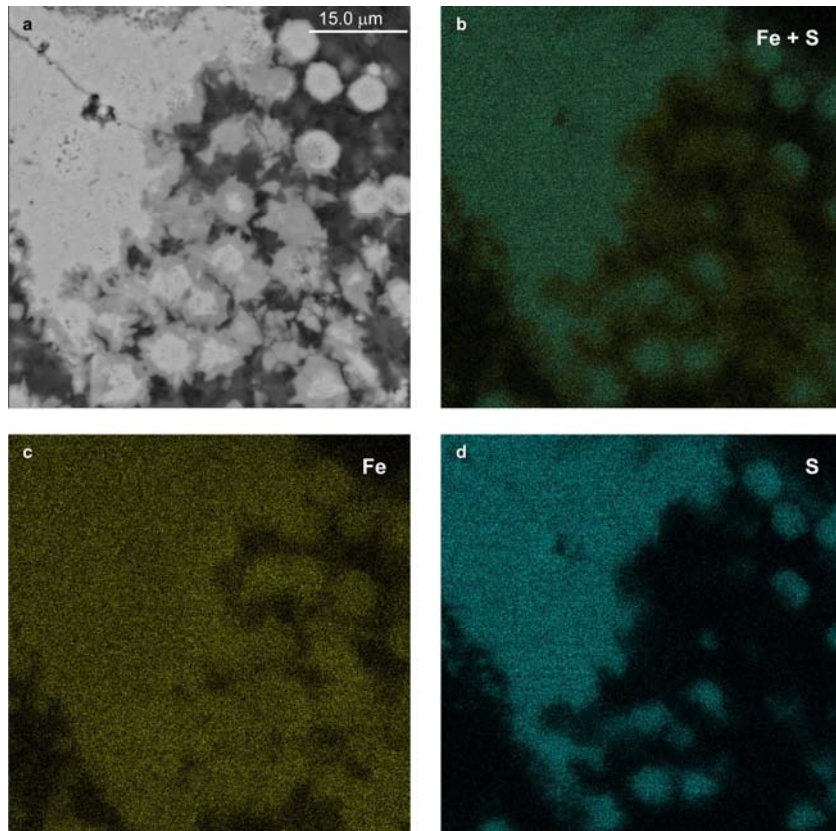


Figure 3.20 Higher magnification backscatter electron image of 3.19a with iron and sulfur elemental mapping.

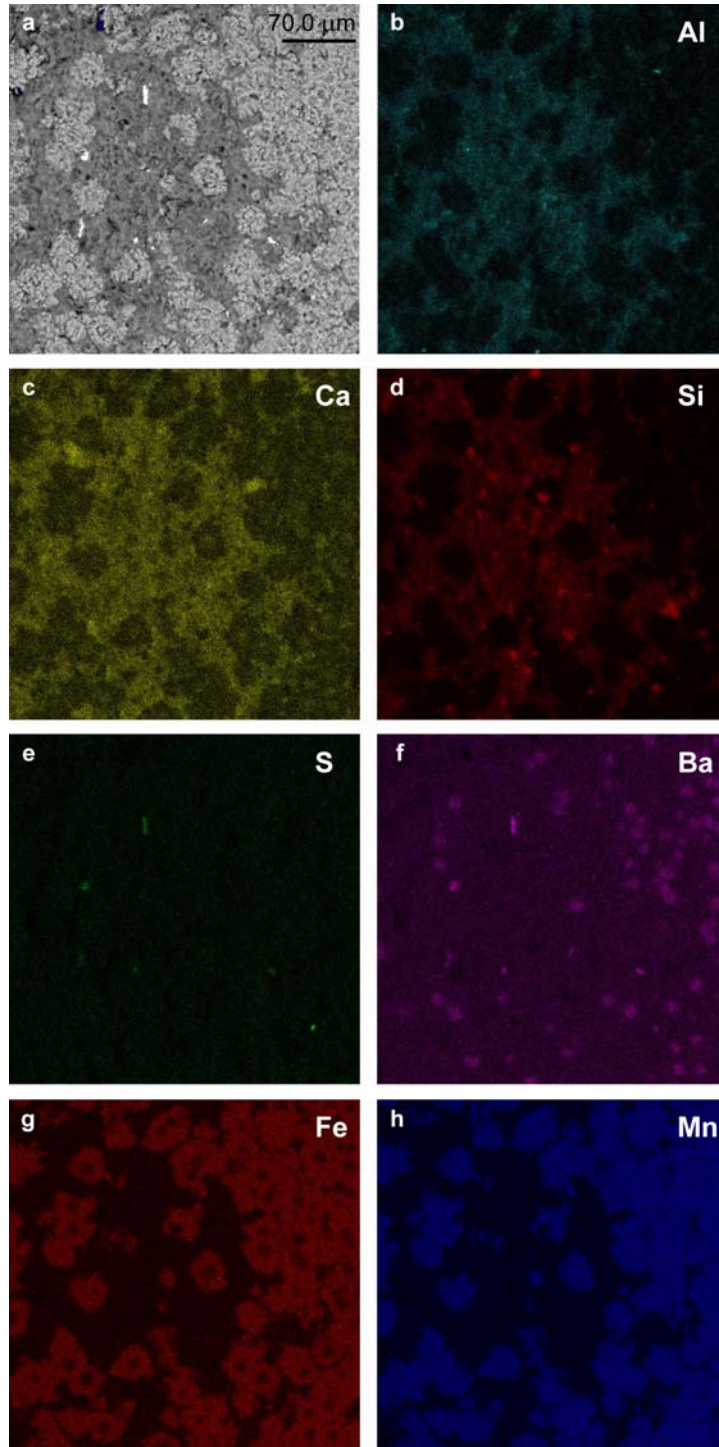


Figure 3.21 Backscatter electron image and elemental maps of a siderite-rich sample (52.5.6) from the Smithwick section of the Walker D-1-1 core.

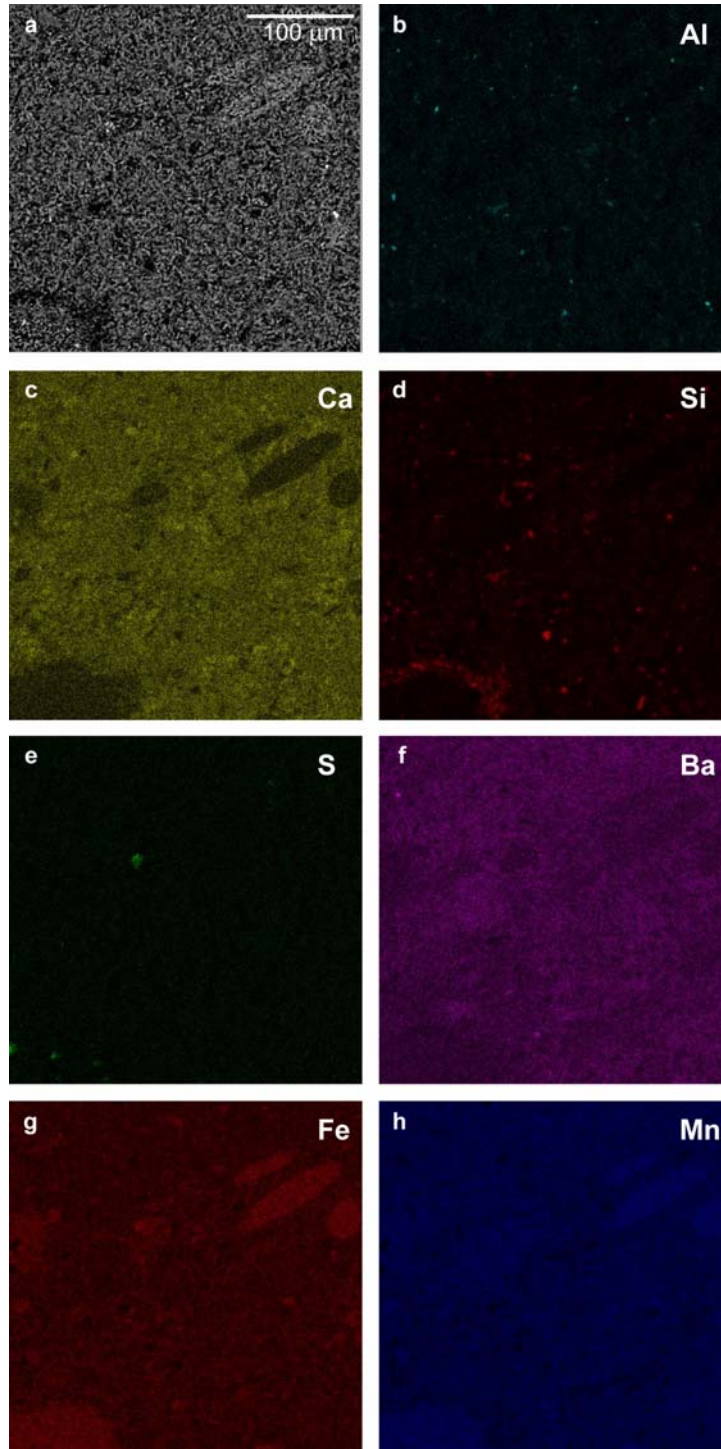


Figure 3.22 Backscatter electron image and elemental maps of a siderite-rich sample (78.1.7) from the Smithwick section of the Walker D-1-1 core.

CHAPTER 4

DISCUSSION

The following discussion will focus on the Smithwick Formation; however, results from other formations presented in the previous section are used for comparison and aid in stratigraphic reference to the Smithwick. From stratigraphic studies of a large suite of cores, it is apparent that Smithwick deposition is not age-specific, thereby impeding the use of definitive age constraints (Scott Hamlin and Steve Ruppel, pers. comm.; Walper, 1982; Erlich and Coleman, 2005). Moreover, and more importantly, a general range of absolute ages has yet to be determined for Smithwick-style deposition, further confounding the ability to define and refine sedimentation rates and the overall depositional characteristics of the Smithwick. Consequently, the timing of Smithwick-style deposition is based on inferences established by previous studies (Plummer, 1947; McBride and Kimberly, 1963; Kier et al, 1979; Ng, 1979; Lovick et al 1982; Thompson, 1982; Walper, 1982; Grayson et al, 1990; Pollastro et al, 2003; Erlich and Coleman, 2005), and the boundaries of Smithwick deposition are approximated in the cores based on relationships to the geochemistry of the vertically confining units.

4.1 Depositional Environment

4.1.1 Paleodepositional Setting

The Al-Si-Ca chemostratigraphy in **Figures 3.1 and 3.3** shows a Ca-rich base, grading into the Si-rich, Ca-poor Smithwick. Immediately above the Smithwick is the Al-rich brown layer, which grades into the slightly Si-enriched Atoka. Ca is generally precipitated as a carbonate, and is dominantly calcite in the Marble Falls samples of the Walker core, according to the XRD analysis (**table 3.1**). The Big Saline samples from the Potter core possess low to undetectable amounts of Al (**figure 3.4**). Both of these formations represent deposition on a carbonate shelf, but the boundary between the Smithwick and the Marble Falls is more gradational than the

boundary between the Smithwick and the Big Saline. The higher Al concentration in the uppermost Marble Falls compared to the Big Saline is due to the presence of argillaceous mudrock (**table 3.5**), while the Big Saline lacks a substantial clay component.

The Smithwick is a relatively homogenous mudrock with the exception of the siderite-rich intervals (**figures 3.11 and 3.12**). The siderite contains sponge spicules and radiolarians (**table 3.5**). Sponge spicules can occur in deep basin facies (Cavaroc and Ferm, 1968). The Smithwick is clay-dominated, mostly consisting of illite (**table 3.1**). There are minor amounts of shelly material near the Smithwick base (**table 3.5**), but in general, fossil content is lacking. The transitional zone between the Marble Falls and the Smithwick, consisting of argillaceous and carbonate-rich mudrock with some macrofossil fauna, marks the onset of basin subsidence and an associated increase in sea-level. The Smithwick shows evidence of significant fissility in portions of the strata (**table 3.5**), which would classify the formation as an alternating mudstone and shale (Folk, 1980). Fine-scale laminations in thin sections and the general lack of other sedimentary features would indicate a low energy environment. In addition, the average $\delta^{15}\text{N}$ value of 4.7 for the Smithwick (**table 3.4**) falls into the deep ocean range of +4 to +6‰ (Sigman et al, 1999; Algeo et al, 2008). The Smithwick mudrock represents a transgressive basin facies with deep basin characteristics in the FWB during Early Pennsylvanian.

Samples from the brown layer from the Walker core consist of 25-30% illite+mica, 10-14% mixed illite/smectite, 15-30% chlorite, and 10-20% kaolinite (**table 3.1**). The clay composition is comparable to both the Smithwick and Atoka samples except for the higher concentration of chlorite and kaolinite. The brown layer exhibits light and dark laminations in thin sections of the mudrock portion (**table 3.5**) and also contains siderite-rich intervals similar to the Smithwick. The brown layer is clay-rich and lacks fossils. It is potentially part of the basin facies and represents a shift in source or sea level just after the Smithwick deposition.

Overlying the brown layer is the Atoka formation. The Atoka is very chemically and mineralogically similar to the Smithwick. Two of the only differences include 1) the 5.4% and

4.4% increase in %Si compared to the Smithwick in the Walker and Potter cores, respectively, and 2) the decrease in abundance of siderite-rich intervals (**table 3.2**). The %Si difference is due to a greater abundance of quartz in the Atoka compared to the Smithwick and the brown layer (**table 3.1**). The slightly siltier sediment of the Atoka marks the beginning of the gradual decrease in accommodation space of the basin. The Atoka mudrock is a progradational basin facies, and marks the point where the basin begins to infill.

Samples from the overlying Caddo and Strawn formations in the Potter core are characterized by lower average %Si relative to the Atoka and Smithwick samples; however, the average ppm Zr increases with each successive formation (**table 3.2**). It is possible that the Si content is primarily quartz, but some biogenic silica may have been part of the %Si in the Atoka and Smithwick formations. The increase of Zr concentration has been linked to increases in silt particles (Taboada et al, 2006). The brown layer also has a higher Zr concentration than the Smithwick. The sedimentation gradually became siltier with the deposition of subsequent formations, indicating that subsidence had decreased and the basin was shallowing.

4.1.2 Productivity and Organic Matter

The Smithwick has an average TOC of 1.5%, comparable to the worldwide average for shales between 0.20 and 1.65% (Tissot and Welte, 1984; Passey et al, 1990). Using C-N proxies developed by Meyers (1997), the organic matter present in the Smithwick was determined to be dominantly marine algal with a possible minor terrigenous component (**figure 4.1**). The hydrogen indices were not analyzed for any of the Walker or Potter samples, but according to Jarvie (2007) and others, the Smithwick falls into the type III category with low hydrogen indices (HI) based on S₂ hydrogen of <200 mg HC/g rock and TOC values from 1 to 3%. The HI data does not correlate with the C/N and $\delta^{13}\text{C}$ data; however, the HI results could be from samples further north in the basin that have a greater terrigenous influx and possible sourcing from the Meunster Arch during late Smithwick deposition. The siderite-rich intervals in the Smithwick have not been analyzed for TOC; however, the increased influx of Fe created

radiolarian and sponge blooms that are not preserved in the mudrock portions of the core (**table 3.5**). Based on the potential compacted sedimentation rates calculated from the quasi-cyclical detrital sedimentation through the Smithwick, the uncompacted (shale is compacted to 1/6 of its original sedimentation according to Potter et al, 1984) sedimentation rates would be 340 ft/m.y. (100 m/m.y.) and 250 ft/m.y. (77 m/m.y) for the Walker and Potter cores, respectively. The possible moderate to high sedimentation rates would be ideal to preserve organic matter. While the %TOC is relatively average for mudrocks worldwide, it falls on the low end of the spectrum for the majority of hydrocarbon-bearing mudrocks (**table 4.1**). The lack of heightened TOC preservation during the Smithwick could be the result of siliciclastic dilution from a high sedimentation rate, or it could be the result of increased degradation of organic matter due to oxic/suboxic water column conditions.

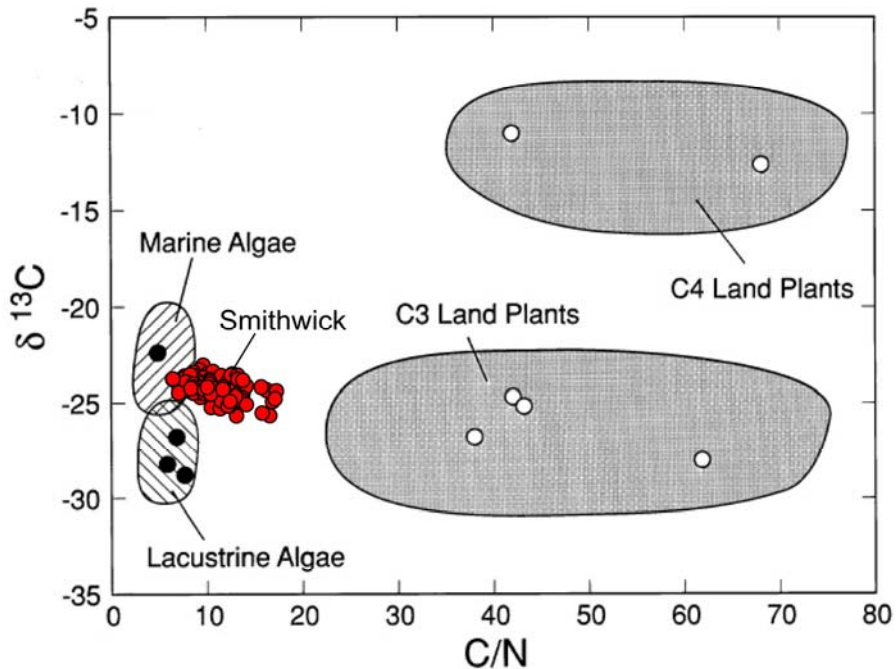


Figure 4.1 Diagram from Meyers (1997) showing the relationship between organic matter type using $\delta^{13}\text{C}$ and C/N proxies. Smithwick samples were added to the plot.

Table 4.1 Average TOC Percentages for North American Hydrocarbon-Bearing Mudrocks

Formation	Age	Location	Avg. TOC (wt%)	Max TOC (wt%)
Eagle Ford Shale	Cretaceous	Gulf Coast, TX	^a 3.6	6.4
Pearsall Shale	Cretaceous	Maverick Basin	^a 1.5	5.0
Haynesville Shale	Jurassic	East Texas Basin	^a 2.7	6.6
Smithwick	Early Pennsylvanian	Fort Worth Basin	^d 1.5	3.7
Barnett Shale	Late Mississippian	Fort Worth Basin	^b 4.1	8.9
Woodford Shale	Devonian-Mississippian	Permian Basin	^a 5.2	8.7
New Albany Shale	Late Devonian	Illinois Basin	^c 7.4	13.1

^aRowe, unpublished

^bJarvie et al, 2005

^cStrapoć et al, 2010

^dThis study

4.1.2 Paleoredox conditions

The three classes of conditions under which marine sedimentation occurs, as defined by Raiswell et al (1988), consist of: 1) aerobic, 2) restricted, and 3) inhospitable. These classes are defined by the activities of dissolved oxygen and free sulfide, which are directly associated with the redox state of the system in question. Because there is no direct method to evaluate the activities of these components for paleosystems, relationships between organic carbon, sulfur, and iron in rocks and sediments are often used to interpret bottom water redox conditions during deposition (e.g. Raiswell et al, 1988; Dean and Arthur, 1989; Rimmer, 2004; Lyons and Severman, 2006; Rowe et al, 2008).

The S/TOC ratio in the Smithwick is very close to the normal marine value of 0.4, indicating aerobic conditions (Berner, 1970; Dean and Arthur, 1989) (**figure 3.9B**). The S/Fe plot (**figure 3.9A**) shows a high enrichment of Fe relative to pyrite, but the total Fe/Al averages 0.5 (%/%), close to the shale average (0.55 ppm/ppm) (Wedepohl, 1971). Lyons and

Severmann (2006) use a combination of Fe proxies to determine redox conditions, showing that total Fe/Al is enriched relative to the average shale in euxinic, or inhospitable, environments.. An additional Fe proxy, the average DOP_T (pyritic Fe/total Fe), is 0.14 for both the Smithwick and Atoka formations. According to Raiswell (1988) and others, DOP values <0.42 were considered to have oxic bottom waters, reinforcing the classification of the Early Pennsylvanian as aerobic. However, the occasional finely laminated sediment, general lack of bioturbation, and lack of preserved fossils (except for radiolarians and sponge spicules in siderite-rich intervals) of the Smithwick is consistent with the sedimentological description of inhospitable conditions.. The low DOP_T is not necessarily a faithful indicator of the bottom water redox conditions of the Smithwick, due to the relatively minor concentration of pyrite. The pyritic Fe could have been diluted by Fe migration from diagenesis of the siderite-rich intervals, or limited by some factor during formation.

To distinguish the seemingly contradictory geochemical and sedimentological evidence for bottom water redox conditions, Fe-S-TOC relationships need to be analyzed simultaneously. The Fe-S-TOC ternary of the Walker core demonstrates the similarity of the Smithwick to the Pierre Shale and equivalents (Dean and Arthur, 1989) (**figure 4.2**). The Pierre shale equivalents represent Cretaceous-age marine mudrocks that were deposited at high sedimentation rates, and low DOP_T values in the Pierre shale equivalents resulted from the absence of hydrogen-rich organic matter that can be metabolized by sulfate-reducing bacteria to limit the amount of sulfide generated (Berner, 1970; Dean and Arthur, 1989). In contrast, the Smithwick samples from the Walker and Potter cores indicate a significant hydrogen-rich marine algal organic contribution (**figure 4.1**). Yet the limited formation of pyrite in the Smithwick occurred below the sediment-water interface as indicated by the SEM images in **Figure 3.19**. **Figure 3.19a** shows a displacive texture in the surrounding matrix, indicating that the pyrite is the result of diagenesis. Furthermore, **figure 3.19b** shows multiple framboids comprising a larger framboid, without displacive texture, indicating that the pyrite grew *in situ*. Sulfate-reduction that occurred in pore

waters is consistent with normal marine conditions (Raiswell et al, 1988). Based on the Fe-S-TOC and DOP_T proxies, the Smithwick was not deposited in a euxinic basin; however, there is still a discrepancy between the implied oxic bottom waters from S/TOC and DOP_T proxies and the preserved fossil assemblage (or lack thereof).

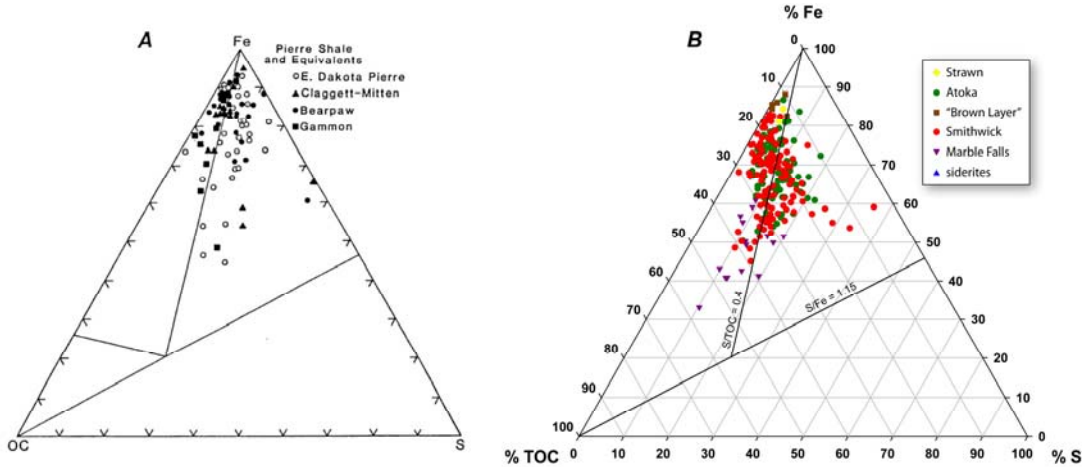


Figure 4.2 Comparison of Fe-S-TOC ternary diagrams from A) Dean and Arthur (1988) study of Pierre Shale and equivalents and B) the Walker D-1-1 core (see Figure 3.10).

Trace element enrichments are often used as paleoproxies for defining bottom water redox conditions (Piper, 1994; Cruse and Lyons, 2004; Piper and Perkins, 2004; Rimmer, 2004; Rowe et al, 2008; Piper and Calvert, 2009; Algeo and Maynard, 2010). The typical organic-rich mudrock is enriched in trace metals, but the amounts and relative concentrations can differ substantially in different formations (Algeo and Maynard, 2010). The average TOC for the Smithwick is 1.49% (table 3.4), and it is not notably enriched in trace metals compared to the average shale (table 3.3) as defined by Wedepohl (1971). Figure 4.3 shows the relative stabilities of trace-element compounds from Piper and Calvert (2009). Manganese enrichment factors are depleted in the Smithwick, with an average enrichment factor of 0.4. The relative enrichments of trace metals in the Smithwick indicate that the bottom water was not oxic (depleted Mn), but it is uncertain whether the Smithwick is suboxic or anoxic (in the absence of

euxinia). Interestingly, the Smithwick samples show the highest enrichment factors in both the Walker and Potter cores in Zn, U, and Mo, and close to average shale enrichment factors for V and Cr (**table 3.3**). Zn, Mo, and U are enriched in anoxic/euxinic environments (Cruse and Lyons, 2004; Piper and Perkins, 2004; Lyons and Severmann, 2006; Piper and Calvert, 2009), and the relative enrichments of V and Cr would be expected to be higher since they are the first to be enriched in suboxic conditions. It is possible that the Zn, Mo, and U enrichment values are higher than what is actually present in the core considering the omission of samples from enrichment calculations that fell below the threshold of calibration. Another possibility is that the rising sea-level associated with deglaciation during this time period, or a tortuous path over the sills of other nearby Late Paleozoic basins, preconditioned the water mass entering the FWB through denitrification, thus removing some of the V and Cr before reaching the basin. Algeo and Heckel (2008) discuss the idea of “preconditioned” waters reaching basins in southwestern Laurentia during the Late Pennsylvanian. The Zn, Mo, and U enrichments most likely occurred below the sediment-water interface in the sulfate-reducing zone in conjunction with limited pyrite. The enrichment of V and Cr and the depletion of Mn indicate suboxic bottom waters contributing to both insufficient O₂ necessary for a prolific macrofaunal community and increased degradation of organic matter facilitating sulphate reduction above the sediment.

Bottom waters in the FWB during Smithwick deposition were not oxic, evidenced by the lack of Mn, even though this contradicts the DOP_T value. There are rare exceptions where DOP ranges are not applicable (Raiswell et al, 1988; Lyons and Severmann, 2006), and the Smithwick appears to be one of those exceptions. Some pyrite is present in the Smithwick, but it is insignificant. This indicates that sulfate-reducing conditions occurred at least in the pore waters. The Fe-S-TOC ternary indicates that metabolizable organic matter was most likely the limiting factor in extensive sulfate-reduction above the sediment-water interface. The lack of sulfide in the bottom waters also helped facilitate the formation of siderite because reduced Fe preferentially forms pyrite (Ellwood et al, 1988; Middleton and Nelson, 1996). The FWB, during

the deposition of the Smithwick, had bottom water redox conditions that were dominantly suboxic.

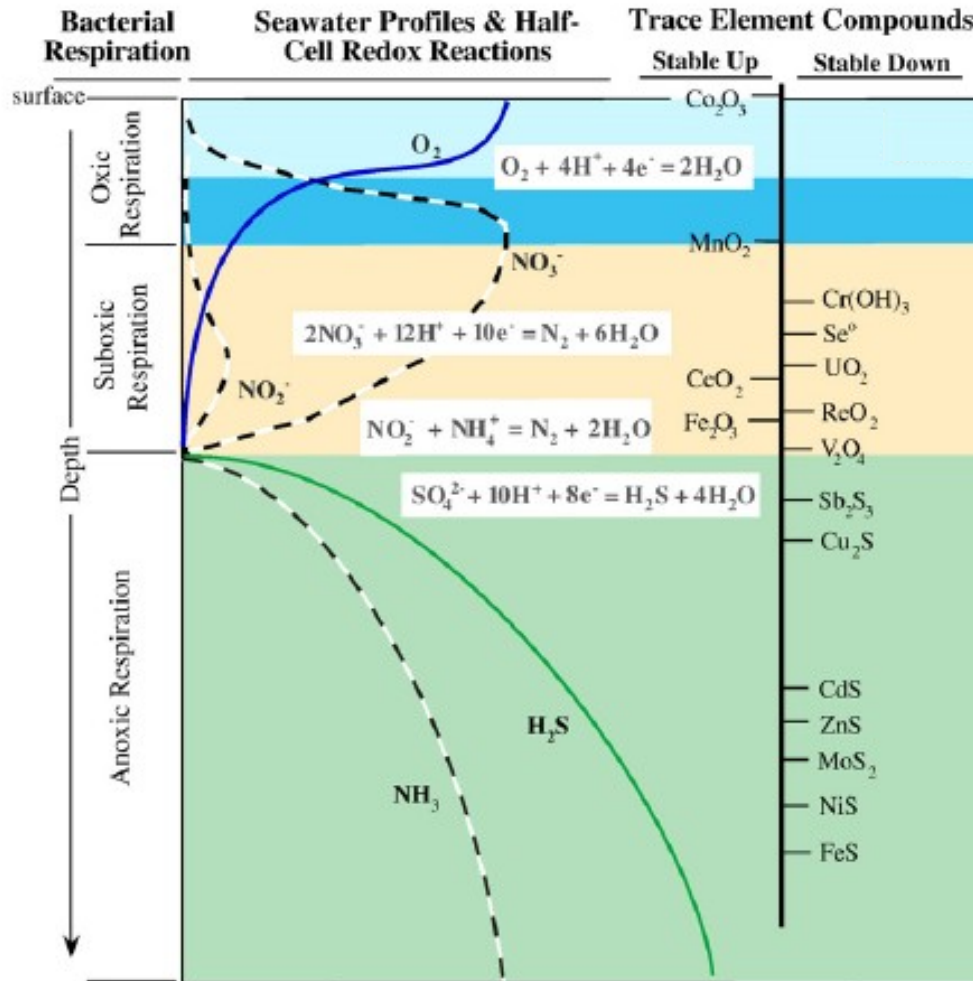


Figure 4.3 Illustration from Piper and Calvert (2009) showing the bacterial respiration and relative stabilities of trace-element compounds relative to water-column depth.

4.2 Potential Linkages to Regional Tectonics

The initial collision of Laurussia and Northern Gondwana during the Late Mississippian/Early Pennsylvanian, which subsequently formed the Ouachita thrust belt,

stimulated localized basin faulting contemporaneous with Smithwick deposition (Lovick et al, 1982; Walper, 1982; Denison, 1989; Grayson et al, 1990). The difference in thickness of the Smithwick preserved in the Walker (480 ft/145 m.) and Potter (135 ft/ 40 m) cores in **Figure 3.5** is hypothesized to be the result of the formation of intrabasinal faulting. Deposition in the vicinity of the Walker core potentially occurred in a graben setting, thereby accounting for the 345 ft (105 m) difference in thickness between the two cores. However, the variation in thickness could also be related to the difference in core positions relative to the basin geometry, or to a combination of geography and tectonics. An approximately 10% decrease in the %Si occurs between the base and the top of the Smithwick in both cores, potentially a response to the westward migration of the western edge of the basin and the relative deepening, or increased subsidence, at the core sites. Because the loading of the North American craton by the Ouachita thrust belt was responsible for forming the FWB, it is assumed to be the primary sediment source for the basin (Kier, 1980; Walper, 1982; McKinzie and McLeod, 2003). In addition to the Ouachita belt, other positive features surrounded the basin: the Concho Platform to the east, the Red River and Muenster arches to the northeast, and the Llano uplift to the southwest. However, the relative invariance of Smithwick chemistry and mineralogy (**figures 3.1, 3.3, 3.11, and 3.12**) (**table 3.1**) reinforces the interpretation that one sediment source dominated throughout its deposition. The Muenster arch would later become a sediment source (Lovick et al, 1982) for the Strawn group (Walper, 1982). The punctuation of siderite-rich intervals (**figures 3.6 & 3.7**), however, indicates brief changes in the sedimentation. If tectonic activity was the dominant control on sedimentation (Lovick et al, 1982), then it is possible that localized sea-level changes caused by episodic uplift of the advancing Ouachita front could simultaneously facilitate increased carbonate precipitation and erosion to supply Fe. The siderite-rich beds/nodules could also be related to eustatic changes brought on by changing paleoclimate conditions.

4.3 Potential Linkages to Regional and Global Paleoclimate

As previously mentioned, the Early Pennsylvanian was affected by the dynamic glaciation of the late Paleozoic ice age (Isbell et al, 2003; Blakey, 2008; Fielding et al, 2008; Rygel et al, 2008; Bishop et al, 2010). The recognition of multiple ice sheets requires high resolution glacioeustatic records from this time period to resolve the evolution of Late Paleozoic paleoclimate. In addition, Early Pennsylvanian strata such as the Smithwick provide insight into a significant gap in the sedimentological record due to the mid-Carboniferous unconformity (Blake and Beuthin, 2008).

The Walker D-1-1 and Potter core-sites were situated about 5-10° south of the paleoequator at the beginning of the Pennsylvanian and moved northward with the advancing Ouachita thrust belt (Scotese, pers. comm.) (**figure 4.4**). According to the Scotese paleogeographic reconstruction and paleoclimate zones (Scotese, PALEOMAP Project), the FWB was located in a tropical zone in the Late Serpukhovian/Early Bashkirian, but bordered the

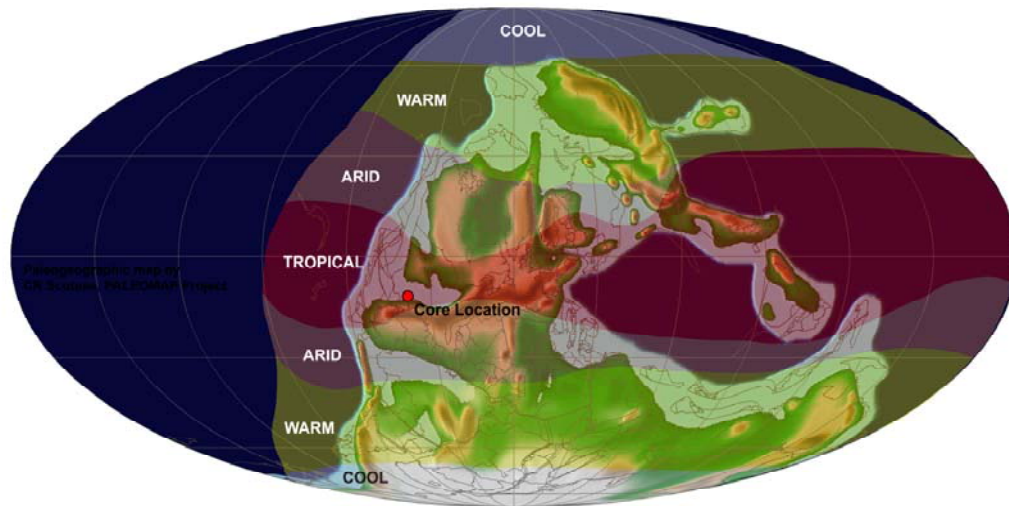


Figure 4.4 Paleogeographic map of 320 Ma showing paleoclimate zones based on paleogeographic locations of climate-indicative strata, i.e., bauxite, coal, calcrete, evaporate, kaolinite and tillite (C. R. Scotese, PALEOMAP Project).

arid zone. Assumptions in the constraints of the climatic zones, along with errors associated

with paleogeographic reconstruction and paleocoordinates, lead to a currently untestable degree of uncertainty. Furthermore, because of the oscillatory nature of the glacialclimate system, the potential existed for drastic shifts in the Early Pennsylvanian tropics, thus only a single time slice is depicted in **Figure 4.4**.

4.3.1 Potential Orbital Forcing and Glacioeustatic Changes

While a dearth of biostratigraphic information exists, the traditionally accepted timeframe for Smithwick-style deposition is considered to be from the Morrowan, through the Atokan, and possibly into the Desmoinesian (Bashkirian – Moscovian) (Plummer, 1947; McBride and Kimberly, 1963; Kier et al, 1979; Ng, 1979; Lovick et al, 1982; Thompson, 1982; Walper, 1982; Grayson et al, 1990; Pollastro et al, 2003; Erlich and Coleman, 2005). Given these accepted but largely untested constraints, the Smithwick could potentially represent 11.6 ± 1.0 m.y. (based on Gradstein et al, 2004). Thus, while the absolute timing of Smithwick deposition is not currently possible, an effort was made to assess the duration of time represented by the Smithwick in each core through defining chemostratigraphic cyclicity, assumed here to represent a regional climatic response to orbital cyclicity. Several studies have tied the occurrence of cyclical geochemistry of sediments to orbital (Milankovitch) cycling, which would have been an influence on late Paleozoic glaciation and eustasy (Anderson, 1996; Sageman et al, 1997; Sageman et al, 1998; Algeo et al, 2008). Pennsylvanian strata preserve well-documented high-frequency sea-level changes (Haq and Schutter, 2008), and the Early to Mid Pennsylvanian time period coincides with peak glacial conditions as hypothesized from the study of the Arrow Canyon successions (**figure 1.5**) (Bishop et al, 2010). The quasi-cyclical sedimentation pattern observed in the Si/Al and Ti/Al chemostratigraphies of the Smithwick in **Figures 3.13 and 3.14** potentially reflect sea-level changes due to orbital forcing. Specifically, if it is assumed that quasi-cyclical detrital signatures of the Smithwick samples are indicative of the 400 k.y. eccentricity cycle, then the 21 shaded cycles defined in the Smithwick section of the

Walker core, and the 8 shaded cycles defined in the Smithwick section of the Petty core represent depositional durations of 8.4 and 3.2 million years, respectively.

The orbitally-estimated durations for Smithwick deposition are shorter than the traditionally accepted timeframe of 11.6 million years. Several reasons for this discrepancy exist. The duration of Smithwick deposition could ultimately be found to be shorter in duration with appropriate time constraints. Alternatively, the Smithwick was deposited in an evolving basin that was continually migrating westward in the Early Pennsylvanian (Walper, 1982). Since drill core represents a particular point in space, a shorter duration of accumulation will be preserved due to the westward progradation of the Smithwick (**figure 4.5**). If the cycles represent a specific time interval, then the period should be relatively equivalent for both cores; however, the Walker core has an average ft/cycle of 23 (7.0 m/cycle) while the Potter averages 17 ft/cycle (5.2 m/cycle). The 30% difference can be explained through the aforementioned difference in depositional environment of the Smithwick section preserved in the Walker core due to its location in a graben. The increase in accommodation space would have potentially promoted an increase in sedimentation rate. Using the previously mentioned 8.4 m.y. and 3.2 m.y. that resulted in 480 ft (145 m) and 135 ft (40 m) of Smithwick strata in the Walker and Potter cores, respectively, a compacted sedimentation rate could be calculated. In an eccentricity-driven model the compacted sedimentation rate for the Smithwick portion of the Walker core would be approximately 57 ft/m.y. (17.4 m/m.y.), while the Potter core would be 42 ft/m.y. (12.8m/m.y.). Other than faulting, tectonic activity could also be partially responsible for the variation in periodicity between individual cycles in both cores through variable uplift and subsidence, as well as differential compaction.

Similarly, tectonics, paleoclimate, or a combination thereof, could be responsible for the deposition of siderite-rich intervals (**figures 3.6 and 3.7**). The formation of siderite (FeCO_3) requires an Fe source and a bicarbonate source. The majority of siderite formed in marine environments is microbially mediated (Ellwood et al, 1988; Middleton and Nelson, 1996). This

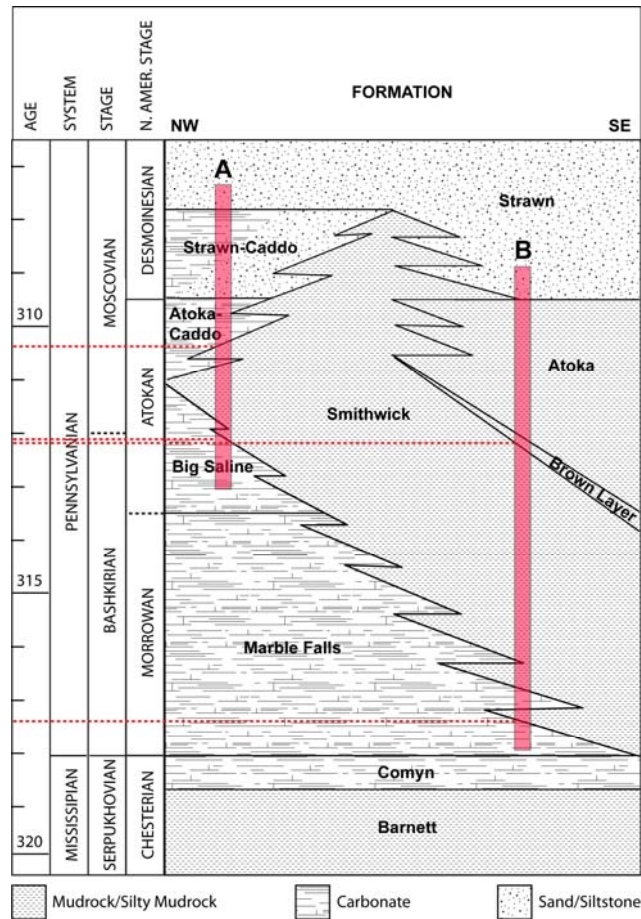


Figure 4.5 Illustration of possible drill core locations within the study area to demonstrate the various sedimentation durations preserved in the core based on their location within the basin. Time scale after Gradstein et al (2004).

process reduces ferric iron and provides a bicarbonate bi-product, but does not explain the origin of the Fe. Because of its largely insoluble nature in well-oxygenated environments and well-drained soils, iron is abundant in terrigenous material, but averages 2 ppb concentration in seawater (Li, 1982). Two main processes exist for the transport of abundant Fe into the ocean: 1) eolian, and 2) fluvial transport. The elevated Ouachita Orogeny to the south and east of the FWB basin could have provided wind-blown, Fe-enriched sediment, or direct contributions from rivers and tributaries could have brought Fe into the basin under a more seasonal climate regime. Either of the two scenarios is possible considering the uncertainty of the FWB's climate

during the Early to Mid Pennsylvanian. Two studies within reasonable proximity of the FWB are the Arrow Canyon, NV, study by Bishop et al (2010) and the Maritimes Basin, Canada, study by Gibling and Rygel (2008) (**figure 4.6**). The Arrow Canyon study hypothesizes that a sub-humid climate existed in the Late Mississippian which gradually evolved into a more seasonal climate in the Early Pennsylvanian, followed by aridification in the late Pennsylvanian (Bishop et al, 2010). In contrast, the Maritimes Basin is hypothesized to have experienced an arid climate in the mid-Mississippian and pronounced humidity

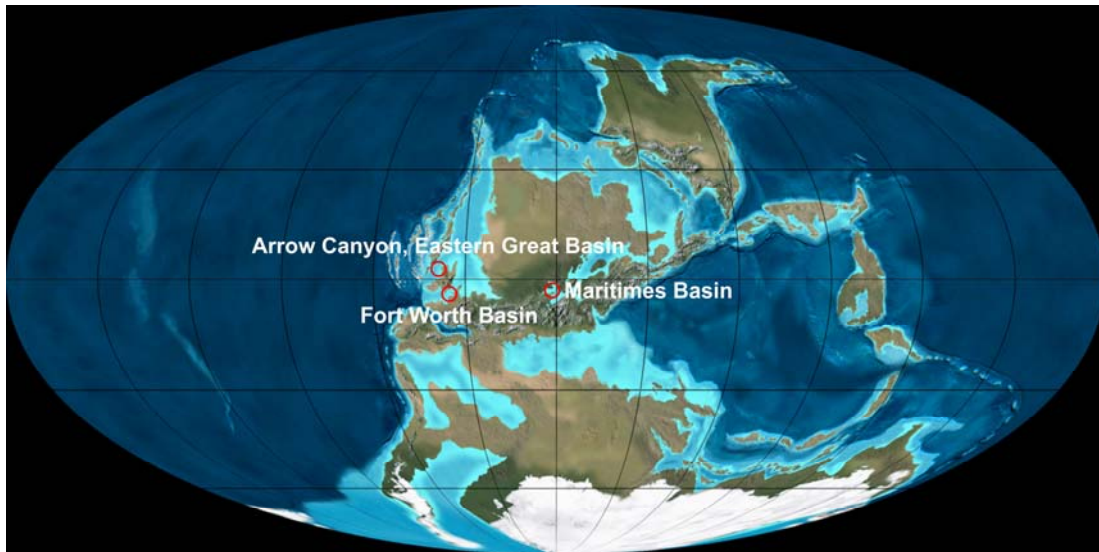


Figure 4.6 Late Pennsylvanian (300 Ma) paleogeographic map depicting the relative locations of Arrow Canyon, FWB, and the Maritimes Basin. Arrow Canyon paleolocation derived from Bishop et al (2010). Map by Ron Blakey, NAU Geology.

through the mid-Pennsylvanian (**Figure 4.7**) (Gibling and Rygel, 2008). The climate zone experienced during Smithwick deposition (**Figure 4.4**) largely coincides with that of the Maritimes Basin. The FWB basin site was paleogeographically further south in the Mississippian and moved progressively closer to the paleoequator during the Pennsylvanian. The Al-rich kaolinite layer stratigraphically above the Smithwick could indicate a shift toward intensified tropical weathering of the source and a subsequently higher detrital input of kaolinite into the

FWB (Griffin et al, 1968; Wignall and Ruffell, 1990). However, the large land mass (Laurussia) between the FWB and the Maritimes Basin would certainly have created differences between the paleoclimate conditions of the two regions. For instance, levels of precipitation would have been different since the two basins were on opposite sides of the greater Appalachian-Ouachita-Marathon system. In addition, there is evidence from the last glacial period to show that the tropics dried significantly (Liu, K. and Colinvaux, P.A., 1988). Glaciation on a large enough scale to affect sea-level at Arrow Canyon would most likely have also affected a location $\sim 10^\circ$ south and $\sim 4^\circ$ east. The inferred peak glaciation during the Pennsylvanian

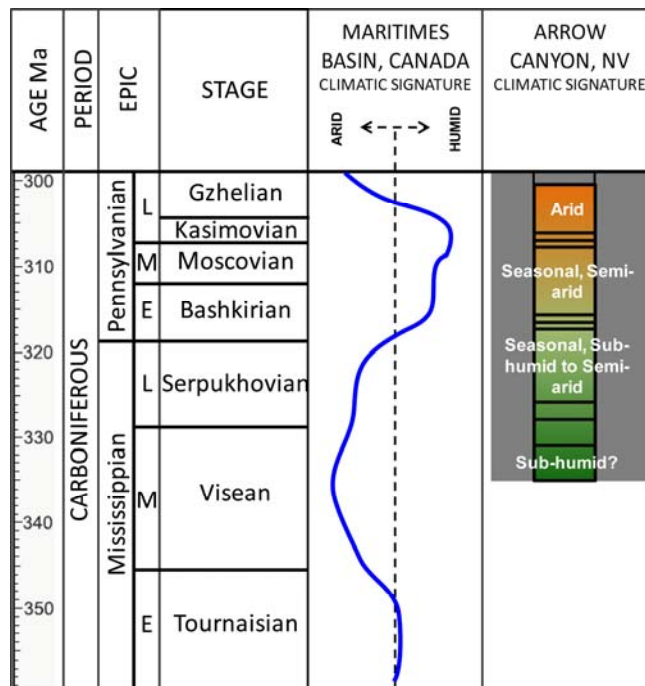


Figure 4.7 Comparison of climatic signatures from the Maritimes Basin redrawn from Gibling and Rygel (2008) and Arrow Canyon, Nevada redrawn from Bishop and others (2010). Time scale after Gradstein and others (2004).

recorded at Arrow Canyon could indicate that there was intense glaciation which also affected the FWB. The glaciation would effectively cool and increase wind in the vicinity, thereby increasing eolian transport of Fe-rich sediment. The kaolinite layer could also be explained by

weathering during subaerial exposure during a time of maximum glaciation when at least local sea-level was significantly lower than previously, and possibly enhanced by subsidence; however, this is unlikely due to the lack of significant bicarbonate that would be present in such a scenario to precipitate the numerous siderite-rich intervals through this layer (**figures 3.6 and 3.7**). Kaolinite is a common clay mineral around equatorial regions that can form on land from the chemical weathering associated with a humid climate, and later be transported to the marine environment with subsequent aridification (Griffin et al, 1968). The siderite-rich intervals decrease in the Atoka compared to the Smithwick and brown layer. They reappear again in the Potter core during the deposition of the upper Caddo facies. The climate conditions producing the siderite-rich intervals are uncertain, but their presence and absence potentially represent climatic shifts in the FWB.

CHAPTER 5

CONCLUSIONS

5.1 Summary of Smithwick

The Smithwick formation was deposited in the Fort Worth Basin (FWB) in Early to Early Mid Pennsylvanian (Ng, 1979; Lovick et al, 1982; Walper, 1982; Grayson et al, 1990; Erlich and Coleman, 2005). During the collision of Gondwana and Laurussia, the FWB developed in front of the advancing Ouachita thrust belt (Wickham et al, 1976; Lovick et al, 1982; Walper, 1982; Grayson et al, 1990; McKinzie and McLeod, 2003; Erlich and Coleman, 2005). Coupled with cratonic disturbances initiated by the Alleghanian orogeny in eastern North America (Walper, 1982), the Fort Worth Basin was tectonically active during the Early Pennsylvanian (Lovick et al, 1982; Denison, 1989; Grayson et al, 1990). The stratigraphic upward decrease in %Si and the rapidly decreased abundance of fossils preserved in the Smithwick indicate that it represents a transgressive unit associated with increased basin subsidence. The geochemical composition of the mudrock matrix of the Smithwick is largely invariant, supporting a singular sediment source, probably from the Ouachita thrust belt. The occurrence of siderite-rich intervals and minor fluctuations in the chemostratigraphy is potentially the result of episodic uplift of the Ouachita thrust belt, but could also reflect paleoenvironmental changes due to climate processes.

The onset of the Late Paleozoic ice age (LPIA) began in the Mississippian, continued through the Pennsylvanian, and into the Permian (Garzanti and Sciunnach, 1997; Mii et al, 1999; Bishop, 2010). Gondwanan glaciation is hypothesized to have been dynamic, involving multiple ice sheets instead of a single expanse of ice (Isbell et al, 2003; Blakey, 2008; Fielding et al, 2008; Rygel et al, 2008; Bishop et al, 2010). The waxing and waning of Gondwanan glaciation is responsible for global sea-level changes (Heckel, 1990, 1998, 2008; Isbell et al, 2003; Fielding et al, 2008; Rygel et al, 2008; Bishop et al, 2010). At present, the records of

Early Pennsylvanian glaciation do not possess sufficiently robust chronological constraints to support an in-depth correlation, especially when comparing Gondwanan records with tropical/subtropical records for Laurussia. Unfortunately, much of the midcontinental record for North America has been eroded by the mid-Carboniferous unconformity (Veevers and Powell, 1987; Gradstein, 2004; Blake and Beuthin, 2008; Rygel et al, 2008). Presently, the oscillations in the Al-normalized detrital chemostratigraphy of the Smithwick could, at best, represent orbitally forced eustatic changes providing an important Early Pennsylvanian North American record. Further biostratigraphic work on the Smithwick and correlative units may help develop a more robust timeframe for understanding low-latitude responses to Gondwanan glaciation.

In addition to sea-level fluctuations, glaciation affects the global climate. The paleogeographic location of the FWB places it ~5-10° south of the paleoequator, in a tropical zone (Scotese, PALEOMAP Project). Siderite-rich layers are intermittent throughout the Smithwick and represent Fe enrichment in the basin either through intensified precipitation and fluvial transport, typical of a tropical climate, or sea-level drop coupled with increased cooling and aeolian transport caused by glaciation. Determining the transport mechanism could aid in the development of a local climate curve based on the stratigraphy of siderite-rich intervals. Determining whether the siderite-rich intervals are laterally extensive, and whether there is a potential for correlation, is essential for the development of a climate model. The Atoka and brown layer also contain siderites, thus the record could be expanded into those lithologies.

The Atoka mudrock (Kier, 1980; Walper, 1982) and the thinner (20-35 ft/5-9 m), Al-rich brown layer overlie the Smithwick. Underlying the Smithwick in the southwest edge of the basin is the carbonate-rich Marble Falls (Kier, 1980; Lovick et al, 1982; Walper, 1982; Grayson et al, 1990) and the carbonate Big Saline (Lovick et al, 1982; Walper, 1982) further north. The gradational boundary between the Marble Falls and the Smithwick contains fossil and lithologic evidence to suggest a deepening of the basin. The Marble Falls and Big Saline represent carbonate shelf depositional environments, and the Smithwick is a basin facies that

transgressed the lower carbonate units. The combination of reduced Fe that formed siderite instead of pyrite, the low enrichments of trace metals in the sediment, and the lack of preserved biota would suggest that the basin was primarily suboxic during Smithwick deposition. Most sulfate reduction occurred below the sediment-water interface, forming minor pyrite. The low abundance of pyrite could in part be due to the lack of metabolizable TOC. The average TOC for the Smithwick was 1.5%, and mostly consists of marine algal matter.

5.2 Future Work

The Smithwick has the potential to provide an important window into glacioeustacy, climate, and tectonics during a critical segment of the LPIA; however, the current “floating” record cannot be definitively contextualized without geochronological constraints. Comparison of other contemporaneous strata deposited globally depends on the accurate age-dating of the Smithwick (Haq and Schutter, 2008). A biostratigraphic study of microfossils would be the most effective method for improving temporal constraints on the Smithwick strata.

Biostratigraphy would also help to constrain insight that can be derived from additional siderite research. Mechanisms introducing Fe into the basin have the potential to provide information about the paleoclimate affecting the FWB. Within the basin, determining carbon isotopes for siderite-rich intervals may help determine the processes behind the bicarbonate source and, subsequently, the types of reactions in the basin during their formation (Middleton and Nelson, 1996). In addition, demagnetization of the bacterially produced siderite has the potential to yield important paleomagnetic data (Ellwood et al, 1988) that could help to resolve paleogeographic uncertainties surrounding the Ouachita thrust and associated terrain.

The FWB was a site of tectonic and paleoclimatic activity during the Pennsylvanian. A major challenge in determining the depositional conditions associated with the Smithwick is developing the ability both to analyze the affects of these elements and to determine their respective contributions. A regional well log study in combination with additional cores for chemostratigraphy would provide details concerning the impact of faulting on the Smithwick

unit, and would be necessary to evaluate the lateral extent of siderite-rich beds, the brown layer, and detrital oscillations. It is also important to relate the chemostratigraphy to well logs. The gamma ray log is a measure of radioactive K, U, and Th. Reproducing a chemical gamma ray based on the same parameters is ideal for comparison, but is difficult to do in strata such as the Smithwick which have very low U concentrations.

Finally, further work is necessary in the evaluation of the organic matter to determine its role in the redox conditions of the FWB, and to evaluate the Smithwick as an economic resource. The type of organic matter could be the limiting factor in sulfate-reduction in the basin (Berner, 1970). Hydrogen index (HI) values can be used to determine whether the organic matter present is hydrogen-rich or -poor, with the latter creating conditions that will not sustain sulfate-reducing bacteria (Dean and Arthur, 1989). Determining the type of organic matter based on HI values can also aid in the evaluation of the Smithwick's hydrocarbon potential. The Smithwick in the Walker core has an average TOC of 1.5%, but a regional study may help locate areas where the Smithwick has a higher TOC. Also, identifying the thermal maturity gradient through vitrinite reflectance studies would be essential in identifying the Smithwick's potential as a hydrocarbon resource.

REFERENCES

- Algeo, T., Rowe, H., Hower, J.C., Schwark, L., Herrmann, A., Heckel, P., 2008. Changes in ocean denitrification during Late Carboniferous glacial–interglacial cycles. *Nature geoscience*, v. 1; 709-714.
- Algeo, T.J., Heckel, P.H. 2008. The Late Pennsylvanian midcontinent sea of North America: a review. *Palaeogeography, Palaeoclimatology, Palaeoecology* 268; 205-221.
- Algeo, T.J., Lyons, T.W., Blakey, R.C., Over, D.J., 2007. Hydrographic conditions of the Devonian–Carboniferous Seaway inferred from sedimentary Mo-TOC relationships. *Paleogeography, Paleoclimatology, Paleocology* 256; 204-230.
- Algeo, T.J., Maynard, J.B., 2004. Trace-element behavior and redox facies in core shales of Upper Pennsylvanian Kansas-type cyclothems. *Chemical Geology*, v. 20; 289-318.
- Algeo, T.J., Maynard, J.B., 2008. Trace-metal covariation as a guide to water-mass conditions in ancient anoxic marine environments. *Geosphere*, v. 4, no. 5; 872-887.
- Algeo, T.J., Rowe, H.D., Hower, J.C., Schwark, L., Herrmann, A., Heckel, P. 2008. Changes in ocean denitrification during Late Carboniferous glacial-interglacial cycles. *Nature Geoscience*, v. 1; 709-714.
- Algeo, T.J., Tribouillard, N., 2009. Environmental Analysis of paleoceanographic systems based on molybdenum-uranium covariation. *Chemical geology* 268; 211-225.
- Anderson, R.Y. 1996. Seasonal sedimentation: a framework for reconstructing climatic and environmental change. Geological Society, London, Special Publications, v. 116; 1-15.
- Arthur, M.A., Sageman, B.B., 1994. Marine black shales: depositional mechanisms and environments of ancient deposition. *Annu. Rev. Earth Planet Sci*, 1994; 499-551.
- Barnes, V.E. 1948. Ouachita Facies in Central Texas. Bureau of Economic Geology, Report of Investigations No. 2; 1-12.

- Berner, R.A. 1970. Sedimentary pyrite formation. *American Journal of Science*, v. 268; 1-23.
- Berner, R.A., Raiswell, R. 1983. Burial of organic carbon and pyrite sulfur in sediments over Phanerozoic time: a new theory. *Geochimica et Cosmochimica Acta* 47; 855-862.
- Bishop, J.W., Montañez, I.P., Osleger, D.A. 2010. Dynamic Carboniferous climate change, Arrow Canyon, Nevada. *Geosphere*, Feb. 2010, v. 6, no. 1; 1-34.
- Boardman, D.R., Heckel, P.H. 1989. Glacial-eustatic sea-level curve for early Late Pennsylvanian sequence in north-central Texas and biostratigraphic correlation with curve for midcontinent North America. *Geology*, v. 17; 802-805.
- Brumsack, H.J. 1989. Geochemistry of recent TOC-rich sediments from the Gulf of California and the Black Sea. *Geologische Rundschau* 78/3; 851-882.
- Cavaroc Jr., V.V., Ferm, J.C. 1968. Siliceous spiculites as shoreline indicators in deltaic sequences. *Geological Society of America Bulletin* 79; 263-272.
- Cruse, A.M., Lyons, T.W., 2004. Trace metal records of regional paleoenvironmental variability in Pennsylvanian (Upper Carboniferous) black shales. *Chemical Geology* 206; 319-345.
- Cruse, A.M., Lyons, T.W., 2004. Trace metal records of regional paleoenvironmental variability in Pennsylvanian (Upper Carboniferous) black shales. *Chemical Geology* 206; 319-345.
- Dean, W.E., and Arthur, M.A. 1989. Iron-sulfur-carbon relationships in organic-carbon-rich sequences I: Cretaceous Western Interior Seaway. *American Journal of Science*, v. 289; 708-743.
- Ellwood, B.B., Chrzanowski, T.H., Hrouda, F., Long, G.J., Buhl, M.L. 1988. Siderite formation in anoxic deep-sea sediments: A synergetic bacterially controlled process with important implications in paleomagnetism. *Geology*, v. 16; 980-982.
- Engleman, E.E., Jackson, L.L., Norton, D.R. and Fischer, A. G., 1985, Determination of carbonate carbon in geological materials by coulometric titration: *Chemical Geology*, v. 53; 125-128.

- Erlich, R.N., Coleman Jr., J.L., 2005. Drowning of the Upper Marble Falls carbonate platform (Pennsylvanian), central Texas: A case of conflicting "signals?" *Sedimentary Geology* 175; 479-499.
- Folk, R. L. 1980. *Petrology of sedimentary rocks*. Hemphill Publishing Co., Austin, Texas (182 p).
- Garzanti, E., Sciunnach, D. 1997. Early Carboniferous onset of Gondwanian glaciation and Neo-tethyan rifting in South Tibet. *Earth and Planetary Science Letters* 148; 359-365.
- Grayson, Jr., R.C., Pranter, M.J., Lambert, L.K., Merrill, G.K. 1990. Carboniferous geology and tectonic history of the southern Fort Worth (foreland) Basin and Concho Platform, Texas. Geological Society of America, 1990 Annual Meeting, Field Trip #20 Guidebook; 1-62.
- Griffin, J.J., Windom, H., Goldberg, E.D. 1968. The distribution of clay minerals in the World Ocean. *Deep-Sea Research*, v. 15; 433-459.
- Haq, B.U., Schutter, S.R., 2008. A chronology of Paleozoic sea-level changes. *Science*, v. 322; 64-68.
- Heckel, P.H. 1990. Evidence for global (glacial-eustatic) control over upper Carboniferous (Pennsylvanian) cyclothems in midcontinent North America. In: Hardman, R.F.P. & Brooks, J. (eds.), 1990, *Tectonic Events Responsible for Britain's Oil and Gas Reserves*, Geological Society Special Publication No. 55; 35-47.
- Heckel, P.H., Gibling, M.R., King, N.R. 1998. Stratigraphic Model for glacial-eustatic Pennsylvanian cyclothems in highstand nearshore detrital regimes. *The Journal of Geology*, v. 106; 373-383.
- Isbell, J.L., Miller, M.F., Wolfe, K.L., Lenaker, P.A. 2003. Timing of late Paleozoic glaciation in Gondwana: Was glaciation responsible for the development of the Northern Hemisphere cyclothems? In: Chan, M.A., Archer, A.W. (eds.) *Extreme Depositional*

- Environments: Mega End Members in Geologic Time, Geological Society of America, Special Paper 370; 5-24.
- Jarvie, D.M., Hill, R.J., Ruble, T.E., Pollastro, R.M. 2007. Unconventional shale-gas systems: The Mississippian Barnett Shale of north-central Texas as one model for thermogenic shale-gas assessment. AAPG Bulletin, v. 91, no. 4; 475-499.
- Kier, R.S. 1980. Depositional history of the Marble Falls Formation of the Llano Region, Central Texas. West Texas Geological Society, Geology of the Llano Region, Central Texas Guidebook, Pub. no. 80-73; 59-75.
- Kier, R.S., Brown Jr., L.F., McBride, E.F., 1979. The Mississippian and Pennsylvanian (Carboniferous) Systems in the United States – Texas. Geological Survey Professional Paper 1110-S.
- Li, Y. 1982. A brief discussion on the mean oceanic residence time of elements. *Geochimica et Cosmochimica Acta*, v. 46; 2671-2675.
- Liu, K., Colinvaux, P.A., 1988. A 5200-year history of Amazon rain forest. *Journal of Biogeography* 15, 231-248.
- Lovick, G.P., Mazzine, C.G., Kotila, D.A. 1982. Atokan clastics – Depositional environments in a foreland basin. Dallas Geological Society; 193-211.
- Lyons, T.W., Severmann, S. 2006. A critical look at iron paleoredox proxies: new insights from modern euxinic marine basins. *Geochimica et Cosmochimica Acta* 70; 5698-5722.
- McBride, E.F., Kimberly, J.E., 1963. Sedimentology of Smithwick Shale (Pennsylvanian), Eastern Llano Region, Texas. AAPG Bulletin, v. 47, no. 10; 1840-1854.
- McKinzie, M., McLeod, J. 2003. Pennsylvanian Fossils of North Texas. Occasional Papers of the Dallas Paleontological Society, v. 6; 1-154.
- Meyers, P.A. 1997. Organic geochemical proxies of the paleoceanographic, paleolimnologic, and paleoclimatic processes. *Organic Geochemistry*, v. 27, no. 5/6; 213-250.

- Meyers, S.R., Sageman, B.B., Pagani, M. 2008. Resolving Milankovitch: Consideration of signal and noise. *American Journal of Science*, v. 308; 770-786.
- Middleton, H.A., Nelson, C.S. 1996. Origin and timing of siderite and calcite concretions in late Palaeogene non- to marginal –marine facies of the Te Kuiti Group, New Zealand. *Sedimentary Geology* 103; 93-115.
- Mii, H., Grossman, E.L., Yancey, T.E. 1999. Carboniferous isotope stratigraphies of North America: Implications for Carboniferous paleoceanography and Mississippian glaciation. *Geological Society of America Bulletin*, v. 111, no. 7; 960-973.
- Murphy, J.B., Keppie, J.D., Nance, R.D., Dostal, J. 2010. Comparative evolution of the Iapetus and Rheic Oceans: A North America perspective. *Gondwana Research* 17; 483-499.
- Ng, D.T.W., 1979. Subsurface of Atoka (Lower Pennsylvanian) clastic rocks in parts of Jack, Palo Pinto, Parker, and Wise Counties, North-Central Texas. *AAPG Bulletin*, v. 63, no. 1; 50-66.
- Ogg, J.G., Ogg, J.M., Gradstein, F.M. 2008. *The Concise Geologic Time Scale*. Cambridge University Press, Cambridge; 1-178.
- Passey, Q.R., Creaney, S., Kulla, J.B., Moretti, F.J., Stroud, J.D. 1990. A practical model for organic richness from porosity and resistivity logs. *AAPG Bulletin*, V. 74, no. 12; 1777-1794.
- Piper, D.Z., Calvert, S.E., 2009. A marine biogeochemical perspective on black shale deposition. *Earth-Science Reviews* 95; 63-96.
- Piper, D.Z. 1994. Seawater as the source of minor elements in black shales, phosphorites and other sedimentary rocks. *Chemical Geology* 114; 95-114.
- Piper, D.Z., Perkins, R.B. 2004. A modern vs. Permian black shale – the hydrography, primary productivity, and water-column chemistry of deposition. *Chemical Geology* 206; 177-197.

- Piper, D.Z., Perkins, R.B., 2004. A modern vs. Permian black shale – the hydrography, primary productivity, and water-column chemistry of deposition. *Chemical Geology* 206; 177-197.
- Plummer, F.B., 1947. Lower Pennsylvanian Strata of the Llano Region: Summary of classification. *Journal of Paleontology*, v. 21, no. 2; 142-146.
- Pollastro, R.M., Hill, R.J., Jarvie, D.M., Henry, M.E. 2003. Assessing undiscovered resources of the Barnett-Paleozoic Total Petroleum System, Bend Arch – Fort Worth Basin Province, Texas. Online adaptation of presentation at AAPG Southwest Section Meeting, Fort Worth, TX, March 2003; 1-17.
- Pollastro, R.M., Jarvie, D.M., Hill, R.J., Adams, C.W., 2007. Geologic framework of the Mississippian Barnett Shale, Barnett-Paleozoic total petroleum system, Bend arch-Fort Worth Basin, Texas. *AAPG Bulletin*, v. 91, no. 4; 405-436.
- Potter, P.E., Maynard, J.B., Pryor, W.A. 1984. *Sedimentology of Shale: Study Guide and Reference Source*. Springer-Verlag, New York; 306 p.
- Raiswell, R., Berner, R.A. 1986. Pyrite and organic matter in Phanerozoic normal marine shales. *Geochimica et Cosmochimica Acta*, v. 50; 1967-1976.
- Raiswell, R., Buckley, F., Berner, R.A., Anderson, T.F. 1988. Degree of pyritization of iron as a paleoenvironmental indicator of bottom-water oxygenation. *Journal of Sedimentary Petrology* 58; 812-819.
- Rimmer, S.M. 2004. Geochemical paleoredox indicators in Devonian-Mississippian black shales, Central Appalachian Basin (USA). *Chemical Geology* 206; 373-391.
- Rimmer, S.M., 2004. Geochemical paleoredox indicators in Devonian-Mississippian black shales, Central Appalachian Basin (USA). *Chemical Geology* 206; 373-391.
- Rowe, H.D., Loucks, R.G., Ruppel, S.C., Rimmer, S.M. 2008. Mississippian Barnett Formation, Fort Worth Basin, Texas: bulk geochemical inferences and Mo-TOC constraints on the severity of hydrographic restriction. *Chemical Geology* 257; 16-25.

- Rowe, H.D., Loucks, R.G., Ruppel, S.C., Rimmer, S.M., 2008. Mississippian Barnett Formation, Fort Worth Basin, Texas: Bulk geochemical inferences and Mo-TOC constraints on the severity of hydrographic restriction. *Chemical Geology* 257; 16-25.
- Rygel, M.C., Fielding, C.R., Frank, T.D., Birgenheier, L.P. 2008. The magnitude of Late Paleozoic glacioeustatic fluctuations: A synthesis. *Journal of Sedimentary Research*, v. 78; 500-511.
- Sageman, B.B., Rich, J., Arthur, M.A., Birchfield, G.E., Dean, W.E. 1997. Evidence for Milankovitch Periodicities in Cenomanian-Turonian lithologic and geochemical cycles, western interior, U.S.A. *Journal of Sedimentary Research*, v. 67; 286-302.
- Sageman, B.B., Rich, J., Arthur, M.A., Dean, W.E., Savrda, C.E., Bralower, T.J. 1998. Multiple Milankovitch Cycles in the Bridge Creek Limestone (Cenomanian-Turonian), In: *Western Interior Basin. Stratigraphy and Paleoenvironments of the Cretaceous Western Interior Seaway, USA, SEPM Concepts in Sedimentology and Paleontology* no. 6; 153-171.
- Schieber, J., and W. Zimmerle, 1998, Introduction and overview: The history and promise of shale research, In: J. Schieber, W. Zimmerle, and P. Sethi (eds.), *Shales and Mudstones I: Stuttgart, Germany, E. Schweizerbart'sche Verlagsbuchhandlung*; 1-10.
- Scotese, C.R., 2004. A continental drift flipbook. *The Journal of Geology*. v.n112 no. 6; 729-741.
- Sigman, D.M., Altabet, M.A., François, R., McCorkle, D.C., Gaillard, J.-F. 1999. The isotopic composition of diatom-bound nitrogen in Southern Ocean sediments. *Paleoceanography*, v. 14; 118-134.
- Taboada, T., Cortizas, A.M., García, C., García-Rodeja, E. 2006. Particle-size fractionation of titanium and zirconium during weathering and pedogenesis of granitic rocks in NW Spain. *Geoderma*, v. 131; 218-236.
- Thompson, D.M., 1982. Atoka Group (Lower to Middle Pennsylvanian), Northern Fort Worth Basin, Texas: Terrigenous depositional systems, diagenesis, and reservoir distribution

- and quality. Bureau of Economic Geology, The University of Texas at Austin, Report of Investigations No. 125.
- Tissot, B.P., Welte, D.H. 1984. Petroleum formation and occurrence. New York, Springer-Verlag; 699 p.
- Tribouillard, N., Algeo, T.J., Lyons, T., Riboulleau, A., 2006. Trace metals as paleoredox and paleoproductivity proxies: An update. *Chemical Geology* 232; 12-32.
- Veevers, J.J., Powell, C.M. 1987. Late Paleozoic glacial episodes in Gondwanaland reflected in transgressive-regressive depositional sequences in Euramerica: *Geological Society of America, Bulletin*, v. 98; 475-487.
- Viele, G.W., Thomas, W.A. 1989. Tectonic synthesis of the Ouachita orogenic belt. In: Hatcher Jr., R.D., Thomas, W.A., Viele, G.W. (Eds.) *DNAG: The Appalachian-Ouachita orogen in the United States, Geology of North America*, v. F-2, The Geological Society of America, Boulder, CO; 695-728.
- Walper, J.L. 1982. Plate Tectonic Evolution of the Fort Worth Basin. *Petroleum Geology of the Fort Worth Basin and Bend Arch Area*, Dallas Geological Society; 237-251.
- Wedepohl, K.H., 1971. Environmental influences on the chemical composition of shales and clays. In: Ahrens, L.H., Press, F., Runcorn, S.K., Urey, H.C. (Eds.), *Physics and Chemistry of the Earth*. Pergamon, Oxford; 305-333.
- Wickham, J., Roeder, D., Briggs, G. 1976. Plate tectonics models for the Ouachita foldbelt. *Geology*; 173-176.
- Wignall, P.B., Ruffell, A.H. 1990. The influence of a sudden climatic change on marine deposition in the Kimmeridgian of northwest Europe. *Journal of the Geological Society*, London, v. 147; 365-371.

BIOGRAPHICAL INFORMATION

Elisha Nichole Hughes (Niki) graduated with her B.S. in geology-engineering option from the University of Texas at Arlington. At the time of her graduation in December, 2008, she was impressed by the curriculum and knowledge of the geology professors and made the decision to stay for a Master's. Her focus was in inorganic geochemistry under the direction of Dr. Harold Rowe. With the growing interest of mudrocks for economic exploitation, her research dealt with this still poorly understood lithology in the hopes of obtaining a career in the petroleum industry. Niki Hughes will receive her M.S. in Geology in May, 2011 and is currently employed as a geologist in her desired industry. Sadly, however, the geology program she was so fond of is being cut due to funding. Environmental earth science and geology are not the same field, and so Miss Hughes would like to dedicate her thesis to the dying geology program at the University of Texas Arlington. Hopefully the incredibly knowledgeable professors currently (2006-2010) teaching physical and historical geology, structural geology, sedimentology and stratigraphy, geomorphology, petrology and mineralogy, geochemistry, paleontology, seismic, and paleogeography are able to sustain the geology portions of the proposed program long enough for a resurrection of the geology degree at the University of Texas Arlington.